NASA Contractor Report 165711

Research on Graphite Reinforced Glass Matrix Composites

K.M. Prewo
E.R. Thompson

UNITED TECHNOLOGIES RESEARCH CENTER
East Hartford, Ct. 06108

Contract NAS1-14346

May 1981

National Aeronautics and Space Administration

Langley Research Center
Hampton, Virginia 23665

Date 11-16-81

To: Micrographics Division, Office of Publications.

From: Special Reproduction Unit, NTIS.

Please process the attached document, ACCESSION NUMBER N81-24181, as circled below:

1. Fiche for file.
   Return document to Special Reprcduction Unit, NTIS

2. Fiche for file.
   Fill orders.
   Return document to Special Reproduction Unit, NTIS

(3.) Fiche for file.
   Return document to Special Reproduction Unit, NTIS,
   ATTN: JM.

4. Fiche for file.
   Return document to Special Reproduction Unit, NTIS,
   ATTN: _____.
   Printing requests are pending.

To: Special Reproduction Unit, NTIS.

From: Micrographics Division, Office of Publications.

The attached document has been _____.

MICROFICHE

(mj-Oct. 73)

N81-24181

RESEARCH ON GRAPHITE REINFORCED GLASS MATRIX COMPOSITES (FINAL REPORT)

K. M. Prewo, et al

United Technologies Research Center
East Hartford, CT

MAY 81

NASA Contractor Report 165711

Research on Graphite Reinforced Glass Matrix Composites

K.M. Prewo
E.R. Thompson

UNITED TECHNOLOGIES RESEARCH CENTER
East Hartford, Ct. 06108

Contract NAS1-14346

May 1981

National Aeronautics and Space Administration

Langley Research Center
Hampton, Virginia 23665

1. Report No.	2. Government Accession No.	3. Recipient's Catalog No.
NASA CR-165711		

4. Title and Subtitle	5. Report Date
RESEARCH ON GRAPHITE REINFORCED GLASS MATRIX COMPOSITES	May 1981
	6. Performing Organization Code

7. Author(s)	8. Performing Organization Report No.
K. M. Prewo and E. R. Thompson	R81-912545-61
	10. Work Unit No.

9. Performing Organization Name and Address	11. Contract or Grant No.
United Technologies Research Center East Hartford, CT 06108	NAS1-14346
	13. Type of Report and Period Covered Final Report March 1976 - February 1981

12. Sponsoring Agency Name and Address	14. Sponsoring Agency Code
National Aeronautics & Space Administration Washington, DC 20546	

15. Supplementary Notes

Project Manager, Dennis Dicus, NASA Langley Research Center, Hampton, VA 23365

16. Abstract The herein described program has succeeded in demonstrating the exceptional potential of graphite fiber reinforced glass matrix composites for structural and nonstructural applications. Combinations of properties have been achieved which are unrivaled by any other fiber reinforced composite system. Low density, high strength, high stiffness, dimensional stability and retention of performance up to high temperatures have all been achieved in a manner not possible in resin or metal matrix composite technology. The following points summarize some of the more important accomplishments of the program.

- A broad group of fibers and matrices have been combined to create a wide range of composite properties.
- Primary material fabrication procedures have been developed which readily permit the fabrication of flat plate and shaped composites.
- Composite mechanical properties were measured under a wide range of test conditions. Tensile, flexure mechanical fatigue, thermal fatigue, fracture toughness, and fatigue crack growth resistance were all evaluated.
- Selected fiber-matrix combinations were shown to maintain their strength at up to 1300 K when tested in an inert atmosphere.
- Composite high temperature mechanical properties were shown to be limited primarily by the oxidation resistance of the graphite fibers.
- Composite thermal dimensional stability was measured and found to be excellent.

17. Key Words (Suggested by Author(s))		18. Distribution Statement
Composite	Graphite-Glass	Unclassified - Unlimited
Fiber Reinforced Glass	Graphite Fiber Reinforced	
Glass Matrix Composite	Thermal Expansion	
Ceramic Matrix Composite		

19. Security Classif. (of this report)	20. Security Classif. (of this page)	21. No. of Pages	22. Price*
Unclassified	Unclassified	135	

* For sale by the National Technical Information Service, Springfield, Virginia 22151

NOTICE

THIS DOCUMENT HAS BEEN REPRODUCED FROM THE BEST COPY FURNISHED US BY THE SPONSORING AGENCY. ALTHOUGH IT IS RECOGNIZED THAT CERTAIN PORTIONS ARE ILLEGIBLE, IT IS BEING RELEASED IN THE INTEREST OF MAKING AVAILABLE AS MUCH INFORMATION AS POSSIBLE.

UNITED TECHNOLOGIES
RESEARCH CENTER

East Hartford, Connecticut 06108

NASA CR-165711

Research on Graphite Reinforced Glass Matrix Composites

K. M. Prewo
E. R. Thompson

FINAL REPORT
Contract NAS1-14346

May 1981

i-b
i-a

Research on Graphite Reinforced Glass Matrix Composites

TABLE OF CONTENTS

TABLE OF CONTENTS (Cont'd)

LIST OF TABLES

LIST OF TABLES (Cont'd)

LIST OF ILLUSTRATIONS

LIST OF ILLUSTRATIONS (Cont'd)

LIST OF ILLUSTRATIONS (Cont'd)

LIST OF ILLUSTRATIONS (Cont'd)

LIST OF ILLUSTRATIONS (Cont'd)

LIST OF ILLUSTRATIONS (Cont'd)

LIST OF ILLUSTRATIONS (Cont'd)

I. INTRODUCTION

This report describes progress made in the fabrication and characterization of a fiber reinforced composite material which adds a new dimension to the already well known family of resin and metal matrix composite materials. Through the use of glass as a matrix, it will be shown that it has been possible to develop a series of graphite fiber reinforced composites which exhibit unique properties. They combine the attributes of low density, high strength and stiffness, high toughness, mechanical and thermal fatigue resistance, and exceptional dimensional stability over a temperature range well beyond that of resin matrix composites. In addition, the combination of low density and environmental stability has not been achieved by any metal matrix composite system.

The use of glass as a matrix for fiber reinforcement is a consequence of the increasing need for higher temperature, stable, low density composites. This constitutes a direct outgrowth from the already well developed technology of resin matrix composites in that the matrix can be caused to flow and encapsulate the reinforcing fibers without damage to fiber integrity. Also, as in the case of resin and metal matrix composites, the elastic modulus of the fibers exceeds that of the matrix sufficiently to provide an effective reinforcement. References to formative studies which demonstrated the viability of the concept of fiber reinforced glasses can be found in the literature (Refs. 1-4), while the development of the fabrication procedures and technology which have led to the herein reported data can be traced through the previous three interim technical reports of this program (Refs. 5-7) and several summary publications (Refs. 8,9). The current report summarizes the most important aspects of this work and includes a summary of the most recently developed composites and their properties. Of particular note is the development of composites which maintain high levels of strength to temperatures in excess of 1200 K.

Use of commercial products or names of manufacturers in this report does not constitute official endorsement of such products or manufacturers, either expressed or implied, by the National Aeronautics and Space Administration.

The authors would like to thank Mr. Dennis Dicus, the NASA Langley contract monitor, and Mr. M. L. Duhl, AFWAL-Materials Laboratory contract monitor, for their helpful comments. The contributions of Mr. J. F. Bacon, now retired from United Technologies Research Center, are also greatly appreciated. Mr. Bacon was a major contributor to the early phases of the overall program.

II. EXPERIMENTAL

A. Materials

Although a wide variety of glass matrix compositions and carbon fiber types were initially investigated (Ref. 5), only several combinations were investigated in great detail. The constituent materials for these systems are described below.

1. Graphite Fibers

The seven most important types of graphite fibers used are summarized in Table I. They varied in character from a low elastic modulus PAN based carbon (T-300) to an extremely high elastic modulus (Thornel pitch based) fiber and thus provided a wide variation of fiber properties for composite performance assessment. Six fibers were utilized in their continuous strand form and the Celion 6000 fiber was also used in a chopped fiber paper form with an average fiber length of 2×10^{-2} m as was a higher modulus discontinuous graphite, Fortafil 5.

2. Glass Compositions

The Corning Glass Works (CGW) borosilicate glass 7740 was the major composition used throughout the performance of this program. Its characteristics, Table I, have been shown to be particularly well suited to the fabrication of carbon fiber reinforced composites due to its combination of low thermal expansion and relatively low working point. The rather low value of coefficient of thermal expansion (CTE) permits composite fabrication without generating large networks of cracks on cool down from the required hot pressing temperature while the viscosity characteristics of the glass, Fig. 1, permit composite densification at temperatures lower than those required for some of the more refractory glasses such as 96% SiO_2. The viscosity vs temperature curves and other physical characteristics are compared in Fig. 1 and Table I for several of the glasses used during this program.

3. Slurry Composition

As will be discussed below, the composite fabrication process developed entails the use of a glass powder slurry through which the carbon fibers are passed to achieve glass particulate infiltration of the fiber bundles. During the earliest stages of this work a variety of slurry compositions was explored (Refs. 5,6); however, one was determined to be most successful for use with the borosilicate (7740) glass.

Table I

Graphite Fiber Properties

	Celion 6000	HTS	Thornel 300	Fortafil 5	HMS	GY-70	Thornel Pitch Type VS0054-0
Fiber Diameter (microns)	7.1	7.6	7.0	-	7.3	8.4	11.0
Filaments Per Tow	6000	10,000	1000	-	10,000	384	2000
Density, kg/m^3	1760	1658	1760	1770	1800	1960	2100
Elastic Modulus, GPa	234	256	234	330	350	516	654
Tensile Strength, MPa	2758	2830	2930	2756	2700	1860	2070

Glass Properties

	CGW 7740	CGW 1723	CGW 7940	CGW 7900
Glass Type	Borosilicate	Aluminosilicate	Pure Silica	96% SiO_2
Density, kg/m^3	2230	2640	2200	2180
Elastic Modulus, GPa	63	88	72	67
Coeff. Thermal Expansion, 10^{-7}.m/mK	32.5	46	3.5	5.0
Strain Point K	783	938	1229	1093
Anneal Point K	833	983	1357	1183
Softening Point K	1093	1141	1853	1723
Working Point K	1525	1181	-	-

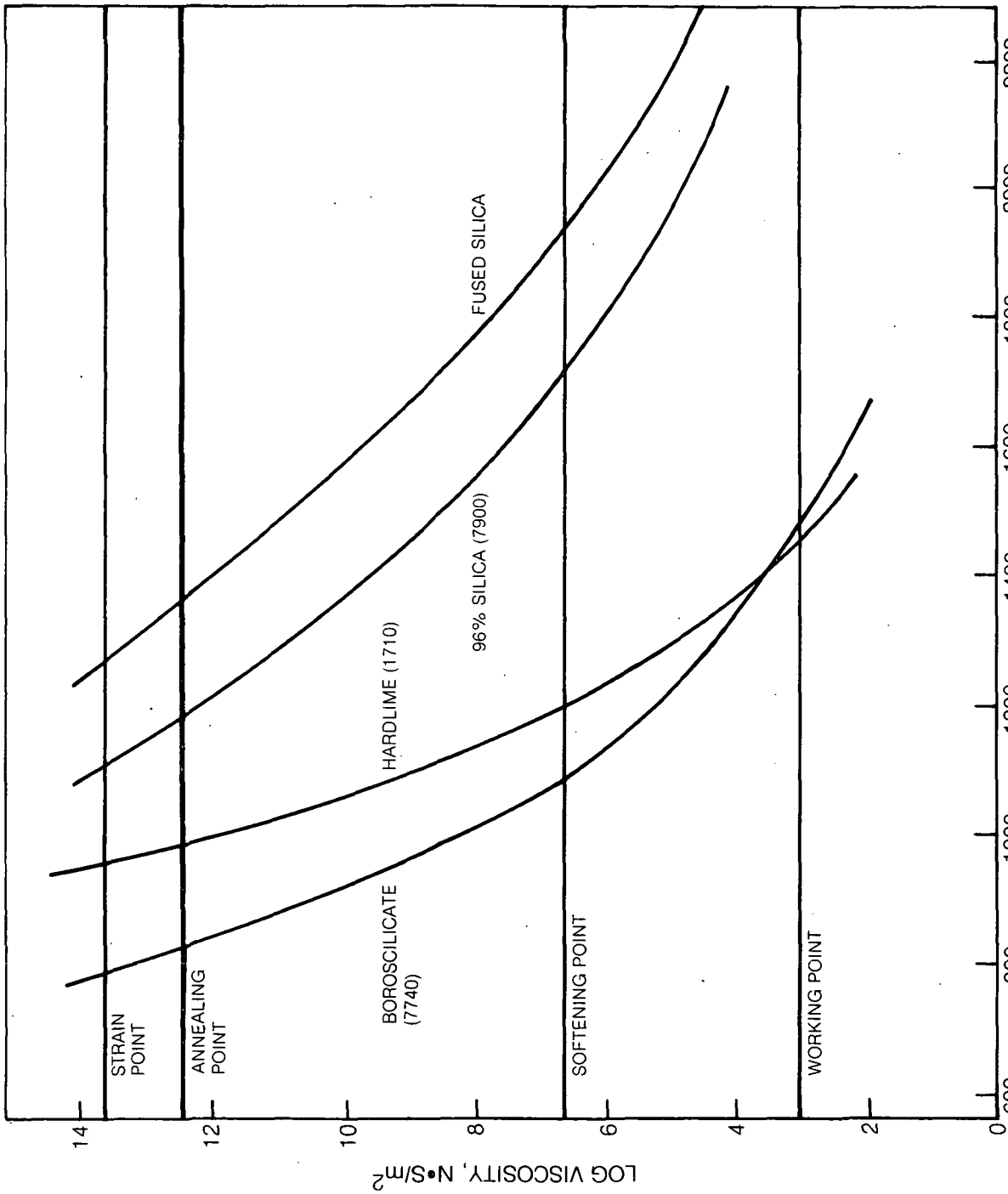

Fig. 1. Vicosity — Temperature Curves

81–2–100–1

This slurry consisted of 85 grams of glass in 0.26 liters of isopropyl alcohol with 24 grams of polyethylene glycol, 6 grams of DuPont Ludox H.S. 30 plus 5 drops of wetting agent. After composite hot press consolidation was completed, this mixture results in a matrix of 7740 glass that contains an additional 2% SiO_2 obtained from the Ludox. For the remainder of this report this matrix will simply be referred to as 774M glass; it is understood that this includes the 2% SiO_2 addition.

B. Composite Fabrication Procedures

Composite fabrication consisted, in all cases, of first making a precursor tape consisting of fiber and dispersed glass powder. This tape was then cut into segments and placed in graphite dies for hot press consolidation into composite panels. The various stages of this overall process are described below.

1. Precursor Tape Fabrication

Three different types of fiber plus glass powder tapes were produced during the course of the program. They are described below.

a. Continuous fiber reinforced tape is made by unwinding fiber from its spool, pulling it through the agitated slurry (composition described above) of glass powder particles, and rewinding it onto a mandrel at a controlled spacing to produce a collimated array of glass coated fiber tows. The schematic in Fig. 2 illustrates this process which results in a tape that can then be removed from the mandrel, cut into segments and stacked in a die for hot pressing.

b. Discontinuous fiber reinforced tapes employing chopped fiber paper were prepared using the same type of agitated slurry; however, in this case strips of paper were dipped into the slurry and then dried. The chopped fiber paper was used with an unimpregnated areal density of 0.027 kg/m^2 and an average fiber length of 1.9 cm.

c. Tapes were fabricated using both continuous and discontinuous fiber paper where the paper was used as a support scrim for the continuous fiber tape. This scrim addition was achieved by first cutting a strip of scrim from a larger roll of chopped fiber paper. This was generally equal in size to the width and length of the intended tape, i.e. the length is equivalent to the circumference of the mandrel used for tape winding. The scrim was then wrapped onto the mandrel forming a single layer around its circumference. Infiltrated fiber was wrapped, in a controlled manner, over this scrim covered mandrel. The fiber was applied with a controlled spacing just as in the above tape winding procedures. The scrim plus fiber tape was then cut from the mandrel and handled in the same manner as any other tape.

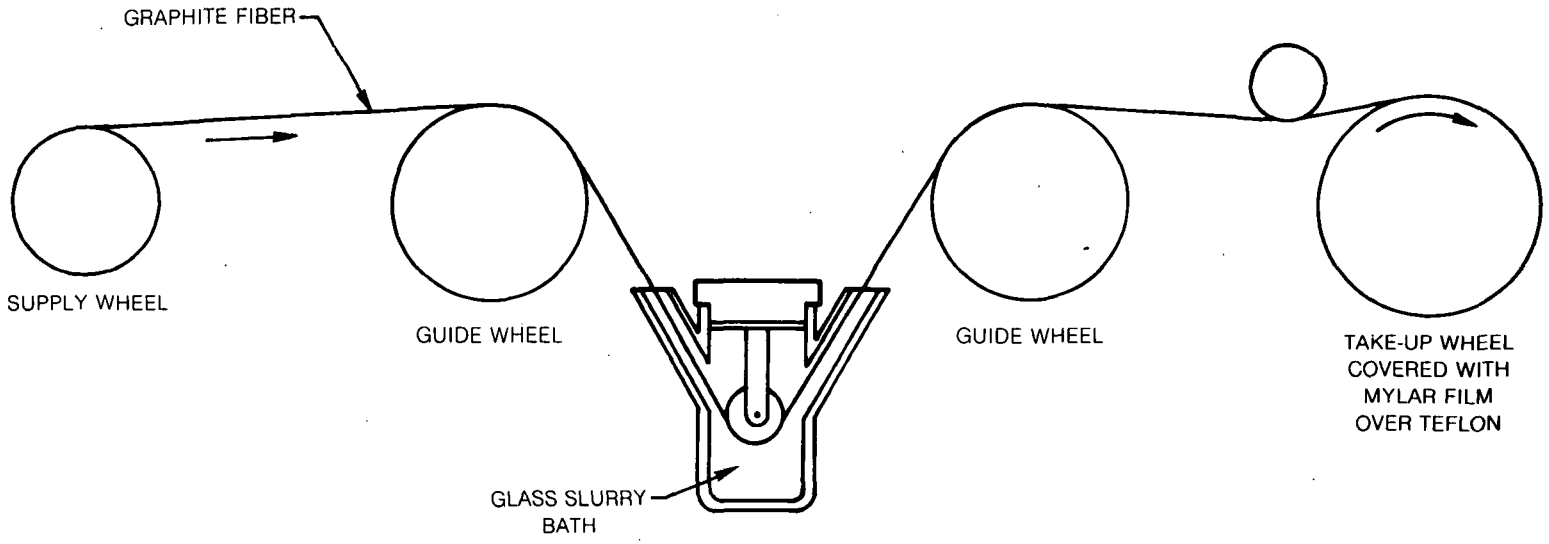

Fig. 2. Slurry Method of Coating Continuous Graphite Fiber

2. Hot Press Consolidation of Flat Plates

After drying in air, the precursor tapes were cut into segments of the desired size and orientation and placed in graphite dies. Thin BN coated molybdenum foils were placed on both sides of this ply lay-up to act as die release agents. Most frequently, composite panels measuring 7.5 cm square were fabricated; however, in some cases 10 cm square panels were also produced. The loaded dies were then placed in the hot press which was subsequently evacuated to achieve an initial vacuum atmosphere. Thereafter, if desired, controlled gases could be flowed through the press or a vacuum maintained for heat-up and hot pressing. In general, 774M matrix composites were consolidated using the conditions found to be superior in the previous phase of this program (Refs. 5,6), i.e. at a temperature of 1723 K, with a pressure of 6.89 MPa maintained for 1 hr, and an atmosphere of argon. After consolidation the pressure was held during cool down until the temperature dropped below 973 K.

3. Hot Press Consolidation of Hat Sections

One of the objectives of this program is to demonstrate that simple shapes can be fabricated using the current state-of-the art glass matrix composite technology. The fabrication of several composite hat section beam segments using two different techniques is an example of this technology. The hat section beam shape was chosen because of its applicability to many structural elements as well as the fact that it represents a three dimensional structure, as compared to the essentially two dimensional flat plates produced for test specimens.

A matched set of graphite tools was designed which could produce a hat section with a uniform section thickness of 0.38 cm, a total length of 10 cm, and a total span of 7.5 cm. The two fabrication procedures used to fabricate hat sections are described below. In each case the material used consisted of HMS fibers in a 774M glass matrix. Composite plys were oriented in a 0/90 alternating ply sequence.

Process #1 - Hot Press Consolidation Directly to Final Shape

In this process the starting material is unconsolidated fiber plus glass powder tape plys which are laid directly into the die cavity in a 0°/90° sequence. The overall ply dimensions are 10 cm x 10 cm which correspond to the dimensions of the total surface area of the hat section. The total ply lay-up is then hot pressed using standard conditions developed in this program for flat plates. A resultant hat section (GC 514), pressed at 1623 K, is shown in Fig. 3. The surface discolorations are due to the BN die release coating. During pressing, one portion of the hot pressing die fractured causing a nonuniformity in resultant hat section thickness; however, this was the only major imperfection resulting from this procedure. One additional, less important, problem was that the molybdenum foil on the convex side of the hat section wrinkled during pressing causing imprints of these wrinkles along the length of the top surface.

Process #2 - Hot Forming of a Preconsolidated Composite Plate

The second procedure utilized preconsolidated 0/90 reinforced flat plates of composite which have been fully processed using standard bonding procedures. These flat plates were cut to a dimension of 10 cm x 7.5 cm so that they would fit into the open die cavity. It was recognized that this would not permit the fabrication of specimens with full flange width ; a wider die opening would have to be used to achieve the same size flange as resulted from Process #1 above. Each flat plate was individually formed to final shape by placing it between the matched die halves, heating to a desired temperature, and then applying pressure. Several pressings were made and it was soon found that component shaping could take place rapidly and at relatively low pressure. The details of three such hot forming operations are given in Table II and the resultant hat sections are shown in Fig. 4 along with the component made by Process #1. The most important point to be noted in Table II is that it was possible to complete a forming operation in 1 min. This is the time during which pressure was applied and material deformation took place. It was not determined whether forming could have taken place even faster; however, this is quite likely and points to the possibility of developing a very low cost fabrication procedure which utilizes flat plate stock as the starting material. In addition, the maximum pressure required to achieve this rapid rate of deformation was only 1.6 MPa.

A significant problem uncovered during these secondary forming operations was that the molybdenum foil wrinkled on the convex sides of the formed parts. These wrinkles consisted of two longitudinal folds that ran the length of each of the completed hat sections and left their imprints in the composite surfaces. In further experiments, it was shown that this problem could be overcome through the use of highly polished carbon tools which did not bond to the glass and thus did not require the use of Mo foils as a bond release agent.

C. Composite Joining Procedures

Several experiments were performed to ascertain whether graphite fiber reinforced glass matrix composites can be joined using secondary bonding procedures. The following three different techniques were used to join composite plates consisting of 0/90 HMS reinforced 774M and also chopped Celion 6000 fiber reinforced 774M.

- Metallic soldering in which both composite plate faces to be joined were coated, by sputtering, with layers of first chromium and then gold. The solder consisted of an 80% Au-20% Sn alloy foil.

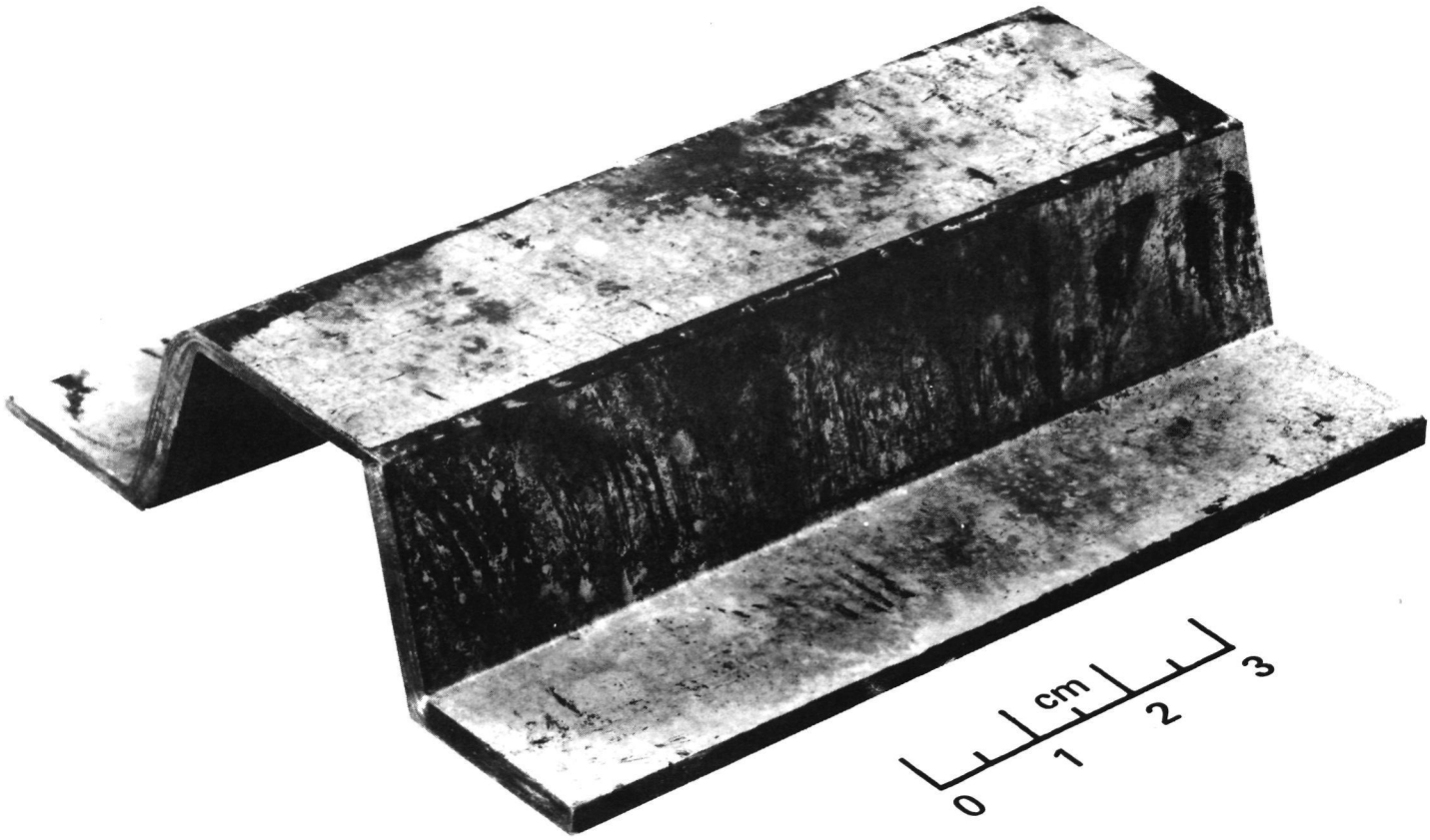

Fig. 3. 0/90 — HMS Reinforced 7740M Hat Section Fabricated Using Process No. 1

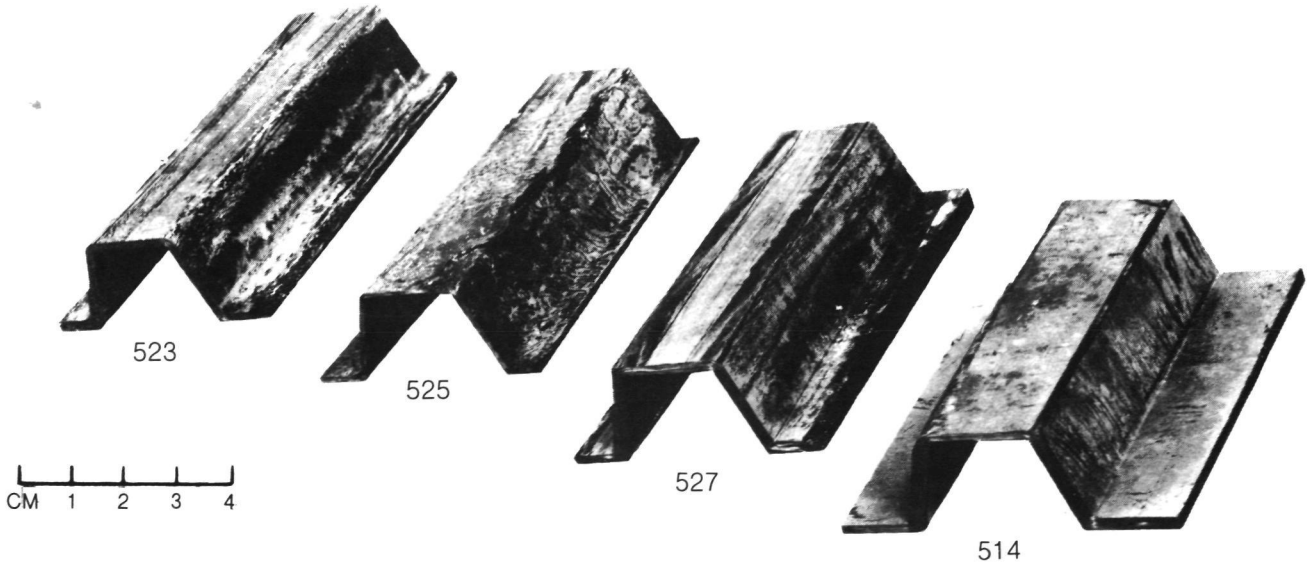

Fig. 4: 0/90 — HMS Reinforced 774M Hat Sections Fabricated Using a Variety of Conditions

Table II

Hot Forming of Preconsolidated Composite Plates

Maximum Temp(K)	Maximum Pressure(MPa)	Total Forming Time(min)	Comments
1173	3.35	10	•Cracks formed at the bend radii •Moly foil wrinkled on convex side •Free edges became ragged
1473	3.35	5	•Basic shape excellent •No cracks •Moly foil wrinkled on convex side •Free edges became ragged
1473	1.6	1	•Basic shape excellent •No cracks •Moly foil wrinkled on convex side •Free edges became ragged

- Glass soldering in which various slurry compositions were synthesized by mixing glass powders in isopropyl alcohol and painting them onto the surfaces to be bonded.

- Field assisted bonding in which highly polished surfaces of composite were sandwiched together with either thin molybdenum or glass foils between them. Application of a very large electric potential across the bond line and simultaneously raising the temperature to 773 K proved insufficient to form any sort of bond.

The detailed procedures and results of the above experiments are presented in Ref. 7. It was found that the two soldering procedures were quite successful in generating bonds with shear strengths in excess of 55 MPa at room temperature. The microstructures of two of these joints are shown in Figs. 5 and 6.

D. Composite Characterization Procedures

1. Analysis of Fiber Content

A procedure was developed and verified for the determination of composite fiber content, matrix content and porosity.

The procedure consists of the following steps.

(1) Measure the density of the total composite specimen (ρ_c). This is done either on the full composite plate after hot pressing, or by using a smaller mechanical test specimen.

(2) Weigh the composite specimen prior to oxidation and obtain its total weight (W_c).

(3) Expose the specimen to 1073 K for 12 hrs in air. The graphite fiber is oxidized completely by this procedure, leaving no char or residue.

(4) Weigh the specimen after oxidation to obtain the weight of the remaining glass (W_g).

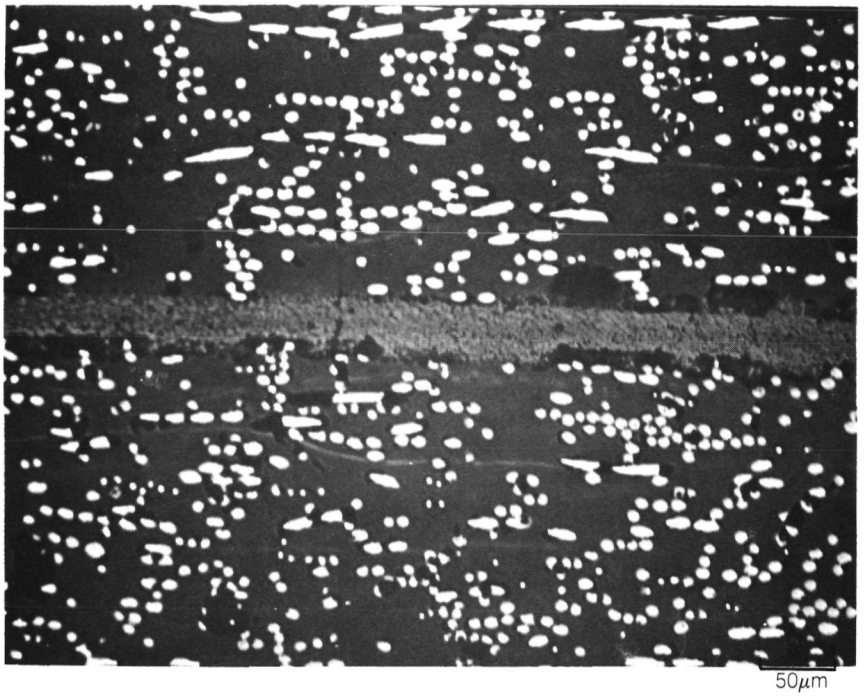

Fig. 5. Bond Region for Glass Soldered Composite GC658

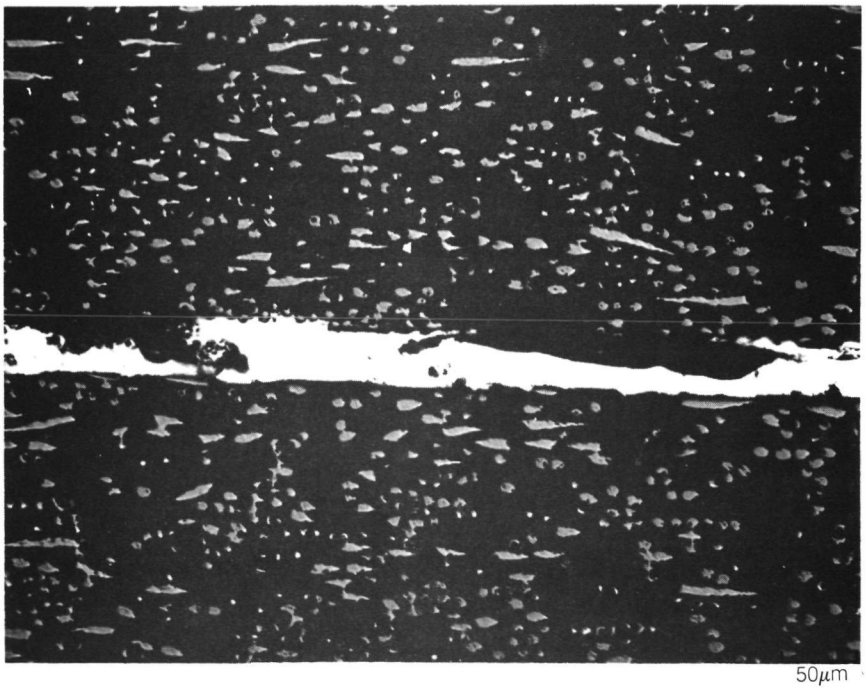

Fig. 6. Bond Region for Metal Soldered Composite GC658

(5) Using the known quantities

density of glass - ρ_g
density of fiber - ρ_f

calculate the following:

(a) Weight of fibers in specimen	$W_f = W_c - W_g$
(b) Volume of composite specimen	$V_c = W_c/\rho_c$
(c) Volume of glass in specimen	$V_g = W_g/\rho_g$
(d) Volume of fiber in specimen	$V_f = W_f/\rho_f$
(e) Volume of porosity in specimen	$V_p = V_c - V_f - V_g$
(f) Volume percent glass in specimen	v/o G = V_g/V_c x 100%
(g) Volume percent fiber in specimen	v/o F = V_f/V_c x 100%
(h) Volume percent porosity in specimen	v/o P = V_p/V_c x 100%

A confirmation of the procedure's accuracy was obtained by determining the fiber content of an HMS/774M composite by two methods, i.e. oxidation and dissolution of the matrix in acid. The comparative data, Table III, indicate that both methods provide equivalent values.

2. Three Point Flexural Strength

Three-point bend tests were performed on specimens of several thicknesses using a range of testing spans to provide a wide spectrum of span-to-depth ratios. In each case the specimens were 0.5 cm wide and 7.7 cm in overall length with all surfaces ground prior to testing. The majority of tests were performed in air with applied load vs mid-span deflection traces taken using a deflectometer attached to the crosshead of the loading machine. Tests were performed over the temperature range of 300 K to 973 K.

3. Three Point Flexural Creep

Standard three-point bend specimens (0.2 cm x 0.5 cm x 7.7 cm) were cut and surface ground in preparation for test. All tests were performed in three-point bend with a span of 5 cm and in an air atmosphere. In each case the mid-span deflection of the specimen was monitored continuously with an LVDT to provide a recording of deformation vs time. Tests were halted either due to specimen fracture or when the time of test exceeded 200 hrs.

Table III

Determination of Composite Fiber Content

Specimen	Method		Fiber v/o F	Glass v/o G	Porosity v/o P
GC 414A-1	Oxidation		62.2	36.8	1.0
-4	"		61.6	38.0	0.3
-6	"		62.2	36.7	1.1
-8	"		63.8	35.9	0.3
		Avg	62.5	36.9	0.7
-3	Acid Leach		62.1	37.1	0.8
-7	"		61.3	37.8	0.9
-9	"		62.9	36.4	0.7
		Avg	62.1	37.1	0.8

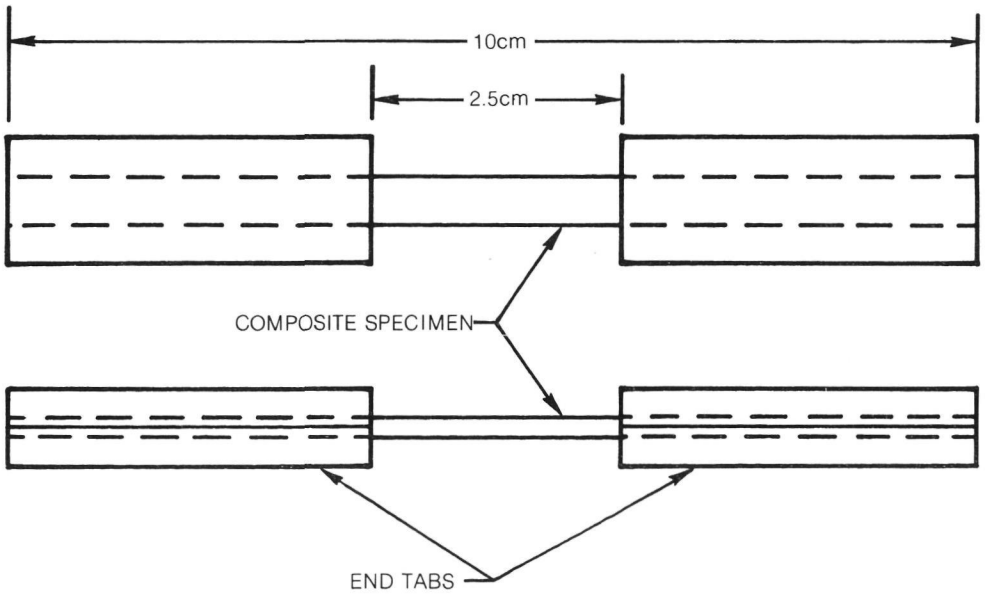

Fig. 7 Tensile Specimen Configuration

4. Three Point Flexural Fatigue

Standard three-point bend specimens (0.2 cm x 0.5 cm x 7.7 cm) were cut and surface ground in preparation for test. All testing was performed in three-point bend with a span-to-depth ratio of 25 at a frequency of three cycles per second in an atmosphere of air. Tests were run at 300 K and 703 K with several unfatigued quality control specimens tested to fracture at 300 K from each test group. All fatigue tests were run with a ratio of minimum to maximum applied flexural stress of 0.1 (R = 0.1).

5. Tension Test

The tensile testing of several different types of graphite fiber reinforced glass composites was performed. Specimens with a total length of 10 cm were cut from 10 cm x 10 cm panels fabricated in the standard manner. The specimens were parallel sided and bonded into glass fiber reinforced resin tabs leaving a 2.5 cm free gauge length, Fig. 7. The specimen thickness and width were approximately 0.18 cm and 0.5 cm respectively. The doublers were slotted to accept these specimen dimensions, and all specimens were strain gauged prior to test. Tensile testing was performed at a crosshead rate of 0.25 mm per minute.

6. Thermal Exposure and Thermal Fatigue

Samples were machined for air oxidation in the dimensions 0.2 cm x 0.5 cm x 7.7 cm. All specimens had their major flat surfaces ground to expose the graphite fibers and several specimens, to be exposed at each temperature, were trimmed at the ends to remove excess glass. This was done to ensure uniformity of structure throughout the specimens and remove any protective layer which might inhibit oxidation. Mass and dimensional measurements were made prior to and after exposure and cycling. Stainless steel wire baskets vertically supported the samples to prevent contact with the center of the sample and ensure that the samples remained in a relatively unstressed condition.

7. Crack Growth Resistance

Prenotched three point bend specimens were tested to measure composite crack growth resistance under monotonic and fatigue loading conditions. The test geometry shown in Fig. 8 with two notch tip configurations typical of the specimens used. The sharpened notch was used originally (Refs. 5,6) but was then replaced in the later phases of the program with a straight notch due to difficulties in properly locating the sharpened tip in the center of the larger groove. The data from the two test configurations, however, should be directly comparable since the configuration at the tip of the notch is of greatest significance and this was nearly identical in both tests.

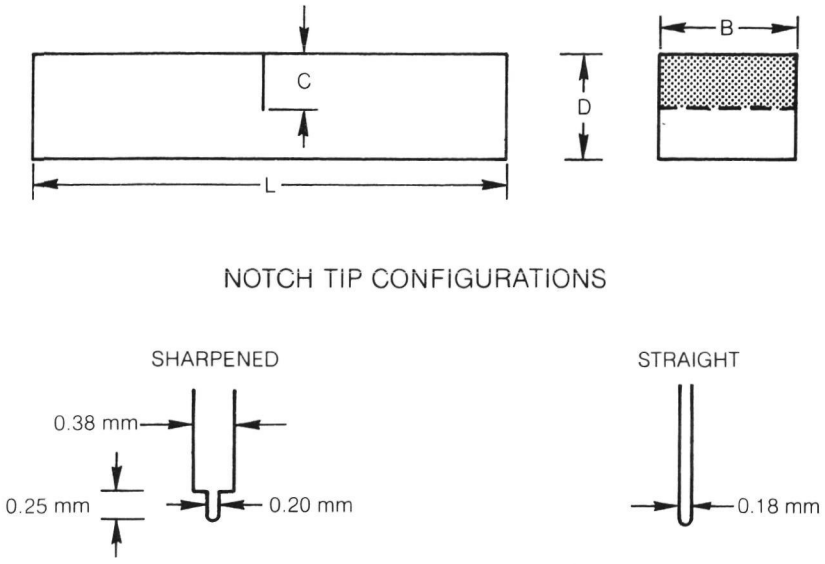

Fig. 8. Fracture Toughness Specimen

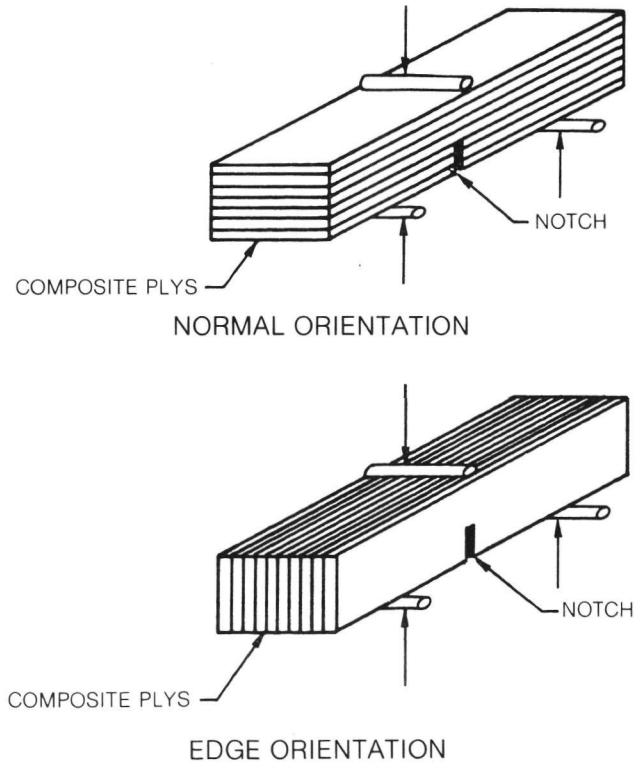

Fig. 9. Three Point Bend Configurations Tested for 0/90 Reinforced Specimens

Both unidirectionally reinforced and 0/90 cross ply reinforced composite specimens were tested in the notched configuration with the 0/90 oriented specimens also tested in two different crack growth directions as shown in Fig. 9. In the "normal" orientation the prenotch direction is normal to the ply planes while in the "edge" configuration the notch is placed so that crack growth can proceed in a direction parallel to the ply planes with the plys on edge during the test.

8. Thermal Expansion

Thermal expansion measurements were made in a Theta Industries differential dilatometer which was operated in a horizontal mode. The composite specimens consisted of 0.62 cm x 0.62 cm x 2.5 cm long parallel sided blocks of material which were individually placed in series with instrument silica push rods and holders. The comparative specimen consisted of a Corning 7971 (SiO_2-TiO_2) glass sample of nearly the same dimensions which was located in a similar arrangement, but in parallel with, the graphite reinforced glass specimen. The 7971 standard had previously been calibrated by both the University of Arizona and Corning Glass over a temperature range of 73 K to 873 K. The actual operative procedure consisted of thermally stabilizing the specimen in the instrument, by holding at room temperature for 5 hrs, followed by heating at a rate of 2 K per minute to the maximum desired temperature. Thereafter the specimen was cooled at a rate determined by the rate of heat loss of the instrument, which was somewhat less than the 2 K per minute heating rate. The differential length change (difference between standard and composite) was then analyzed by computer and plotted as a change in length of the composite. Thus, the thermal strain was taken to be the change in length divided by the original length, referred back to the starting room temperature condition. Testing was performed in air.

III. RESULTS AND DISCUSSION - BOROSILICATE GLASS MATRIX COMPOSITES

A. Composite Fabrication Studies

The fabrication procedure described in the Experimental section of this report resulted in a wide variety of composite microstructures. In almost every case it was possible to fabricate composites that contain little or no porosity and a wide range of fiber volume fractions and fiber orientations. The composite microstructure depicted in Fig. 10 is that of a unidirectional, continuous HMS fiber reinforced 774M matrix composite that contains (by volume) approximately 66% fiber, 34% glass, and less than 1% porosity. The overall structure of this composite is such that each fiber is surrounded by glass and that there is only a slight residual "memory" of the location of the individual fiber tows. Some of the glass rich areas noticeable in the figure correspond to these inter-tow regions. By orienting the individual tape plys to produce a 0/90 cross ply structure, the microstructure shown in Fig. 11 was developed.

1. Effects of Scrim

The use of a thin discontinuous graphite fiber scrim in precursor tape fabrication significantly increased the handleability of the tapes and also markedly altered composite microstructure and performance. An example of the change in composite structure produced can be found in Figs. 12 and 13 where unidirectional Thornel 300 fiber reinforced composite microstructures are compared with and without the presence of the thin scrim layer in each ply. The addition of the thin discontinuous fiber layers has resulted in a stratified structure with distinctly glass rich areas corresponding to the regions of the scrim. In these regions, which occupy 25% of the total composite structure, the discontinuous graphite fibers constitute only 30% by volume of the structure while in the larger continuous fiber reinforced regions the microstructure consists of 60% graphite fibers.

The effects of the presence of this scrim on overall composite performance were assessed by the fabrication of a series of composite panels wherein varying percentages of discontinuous fiber scrim were introduced into the overall composite structure. These panels, which received their primary reinforcement from the presence of Thornel 300 graphite fibers oriented in the 0° direction, were then tested in three point flexure to measure both 0° and 90° performance. The resultant data are presented in Fig. 14 where composite fleuxral strength is plotted as a function of scrim reinforced glass content. This refers to the fraction of the overall composite microstructure which is comprised of discontinuous graphite fiber reinforced glass. In Fig. 14 it is clearly seen that composite transverse flexural strength increases with scrim content. The data point for the 100% scrim composite was obtained for composite specimens tested

Fig. 10. Microstructure of HMS Fiber Reinforced 774 M

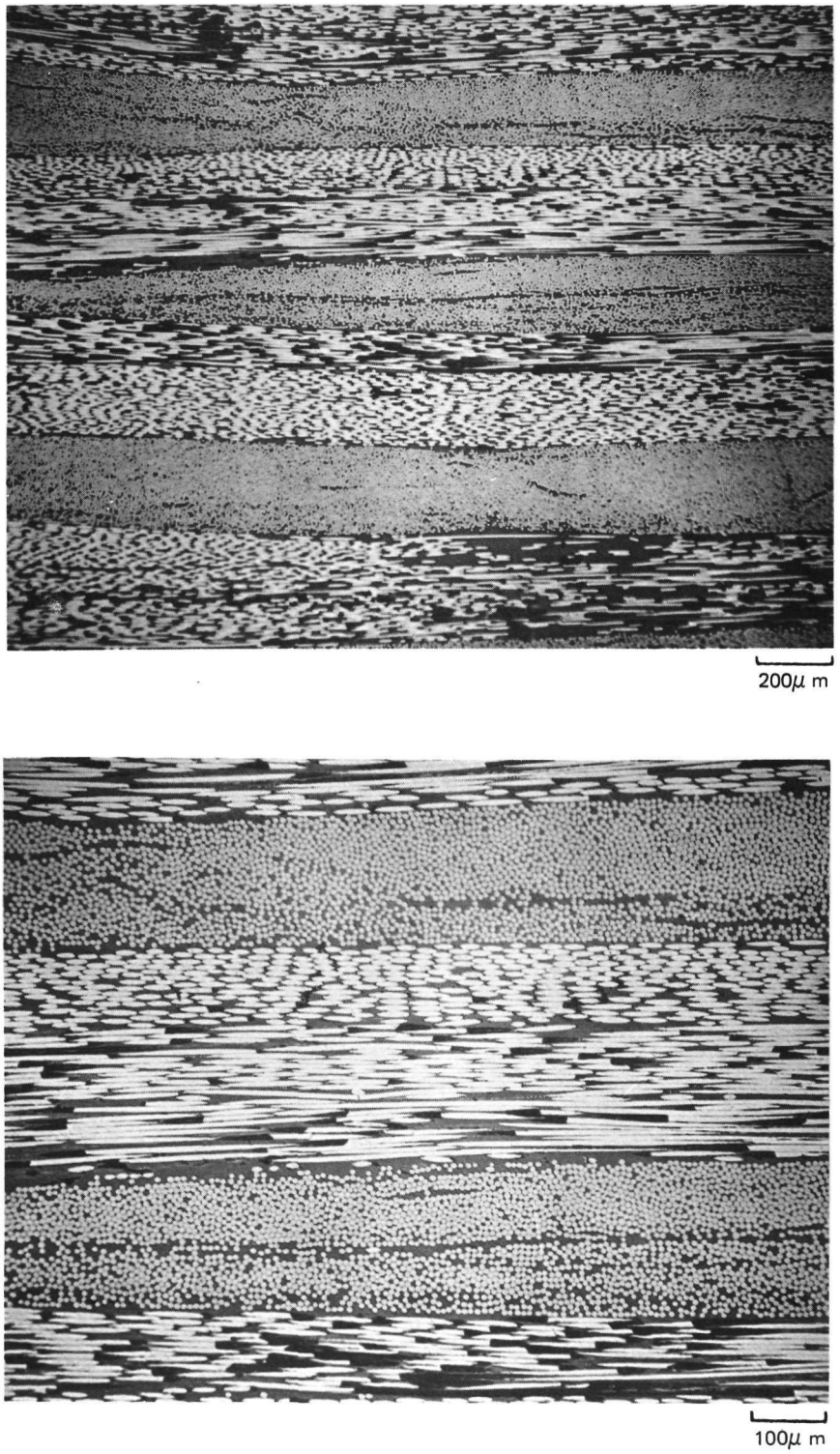

Fig. 11. Microstructure of HMS Reinforced 774M $[(0/90)_4]_S$

78–06–208–8

Fig. 12. Microstructure of Thornel 300 Fiber Reinforced 774M without Scrim

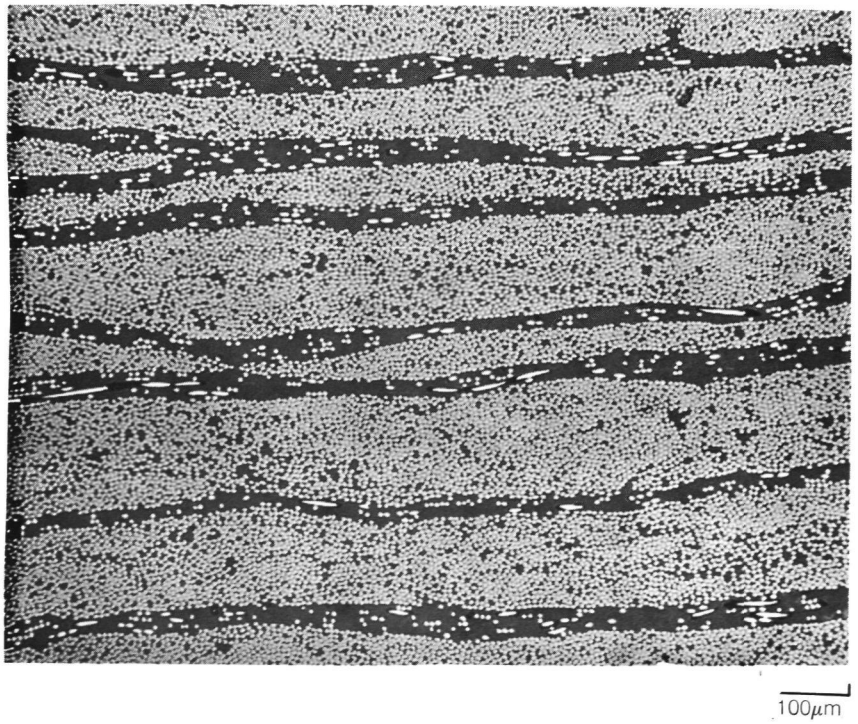

Fig. 13. Microstructure of Thornel 300 Fiber Reinforced 774M with Thin Scrim

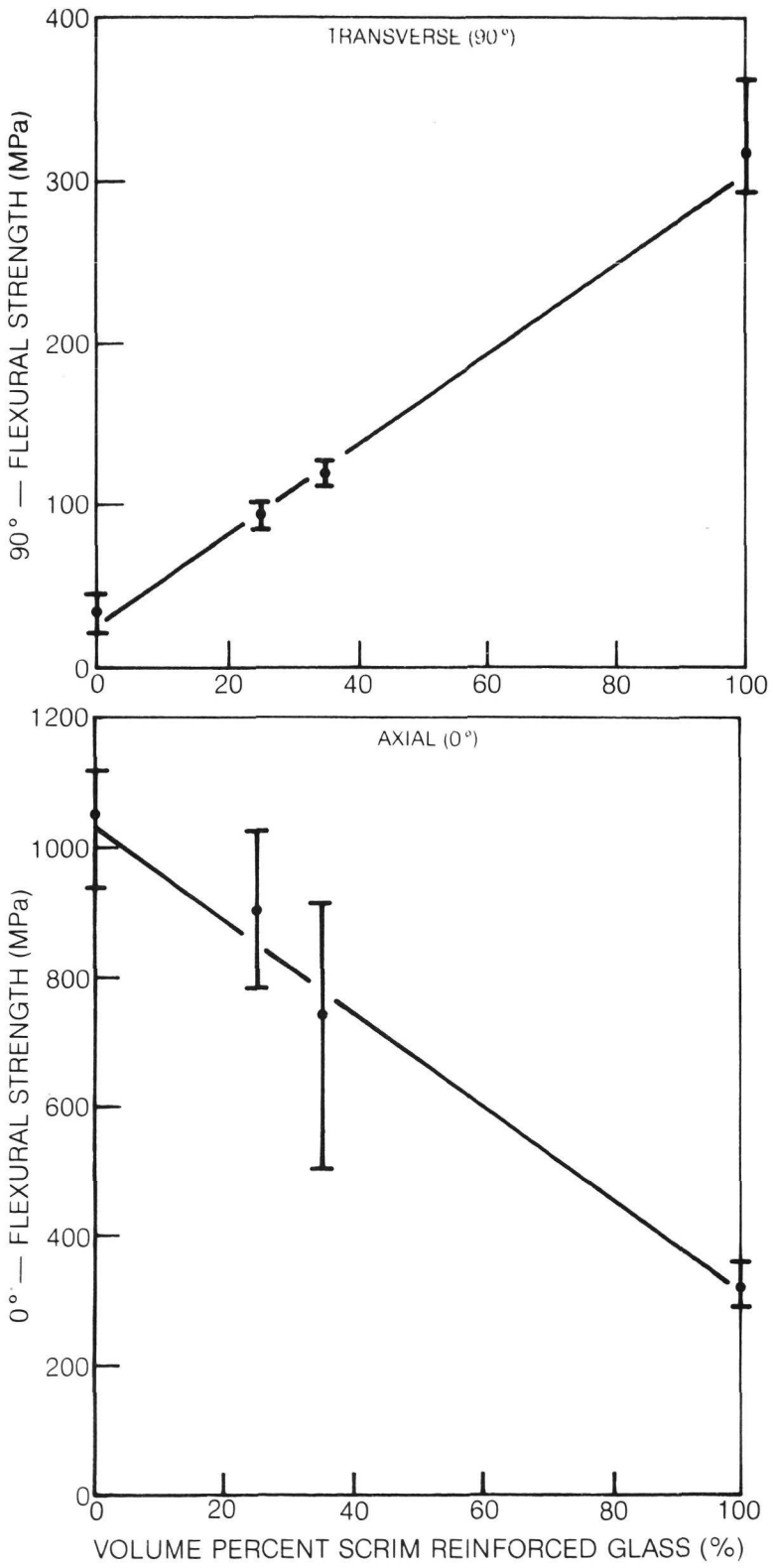

Fig. 14. Flexural Strength of Thornel 300 Reinforced 774M Containing Chopped Fiber Scrim

previously (Ref. 7), wherein the only graphite reinforcement is due to the presence of the discontinuous two dimensional array of graphite fibers. A nearly linear dependence of strength on scrim content is noted, with the transverse flexural strength of the composites containing 0% scrim equal to 35 MPa.

Axial composite flexural strength was also strongly affected, Fig. 14, with once again a linear dependence of strength on scrim content noted. In this case the change in strength is a decrease with increasing scrim content.

From the above it can be seen that the modification of composite performance by the presence of the scrim can be readily explained in terms of its effects on the volume percent of reinforcing phases present. Depending on structural performance and handling requirements, a composite can be designed with the desired amount of scrim. By decreasing the thickness of the scrim, or increasing the number of fiber tows in each ply, it would be possible to decrease the amount of scrim in the Thornel 300 reinforced specimens to below 25% and still retain transverse integrity. At a scrim content of 15% the axial strength would still exceed 900 MPa while the transverse strength would have been raised to 70 MPa.

The use of scrim was also demonstrated for the case of HMS fiber reinforcement where the addition of 15% by volume of scrim containing glass resulted in a composite transverse flexural strength of 41 MPa. Without the presence of any scrim the 90° composite transverse flexural strength was measured to be 10-15 MPa (Ref. 6). A significant penalty in axial strength, however, accompanied this 90° reinforcement improvement. The 0° flexural strength dropped from 708 MPa for HMS fiber reinforced specimens with no scrim to 492 MPa for the specimens containing 15% scrim. The microstructure of the scrim containing specimens is shown in Fig. 15.

2. Effect of Hot Pressing Conditions

As described in the experimental section, a hot pressing temperature of 1723 K was found, in Ref. 6, to be the optimum bonding temperature when the matrix of 774M is hot pressed using a starting slurry which contains a small addition of silica. The hot press diffusion bonding of unidirectional continuous HMS fiber reinforced composites illustrated this point. A series of composite panels was hot pressed using a pressure of 6.9 MPa and pressing time of 60 min over a temperature range of 1473 to 1773 K. Resultant composite density and three point flexural strength were measured and the data are presented in Fig. 16 where it can be seen that highest strength is achieved using the pressing temperature of 1723 K. Previous studies (Refs. 5,6) had demonstrated that a matrix of pure 7740 glass could be well densified at 1473 K; however, as shown in Fig. 16, the addition of only 2% silica caused a major change in hot pressing character and a need for the 250 K increase in temperature. This increased temperature, however, also was accompanied by the development of a flexural strength in excess of 1000 MPa which was substantially greater than flexural strengths obtained previously with 7740 only of approximately 600 MPa.

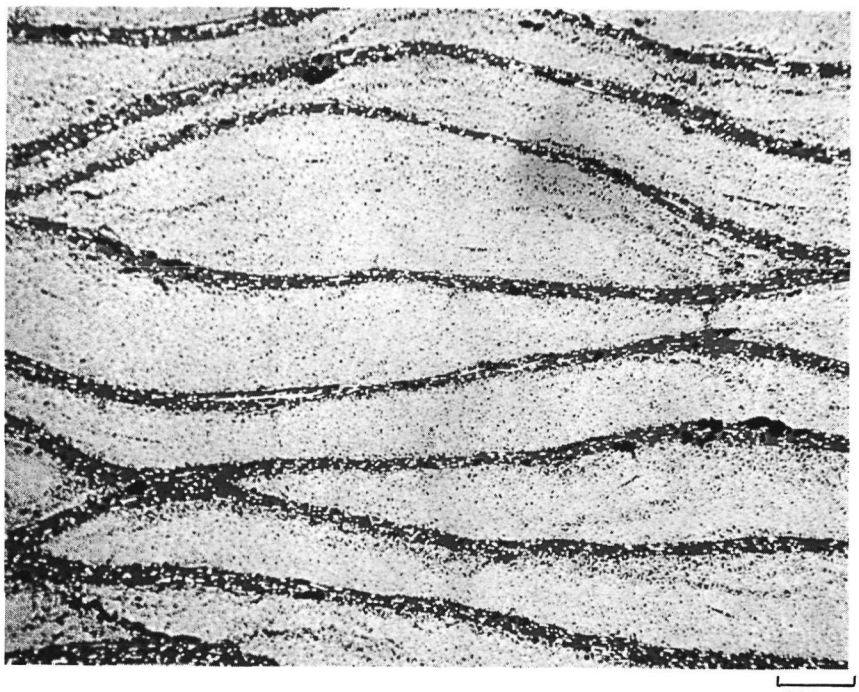

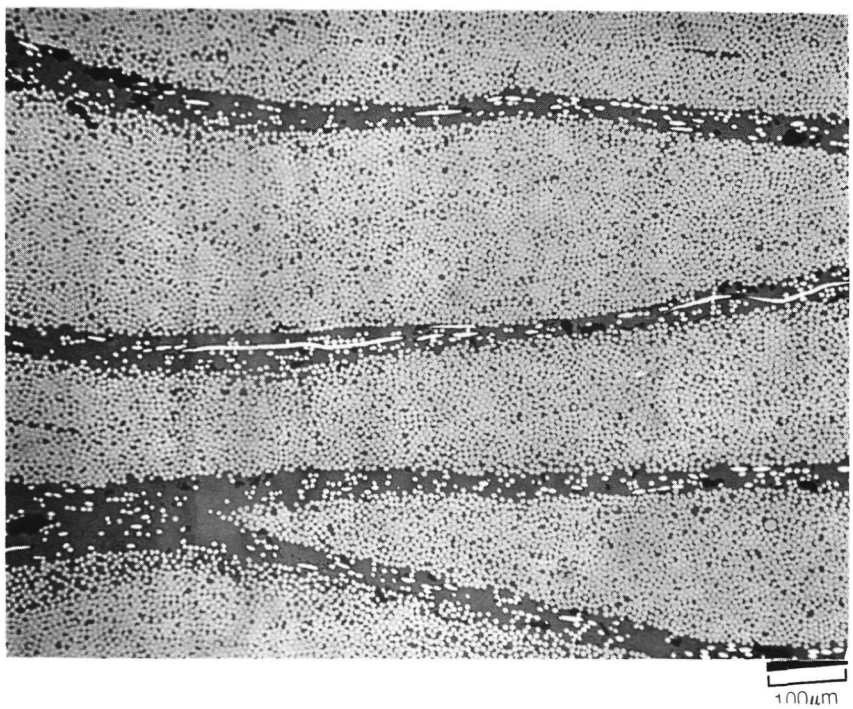

Fig. 15. Microstructure of HMS Fiber Reinforced 774 M with Thin Scrim (GC 738)

80–3–141–4

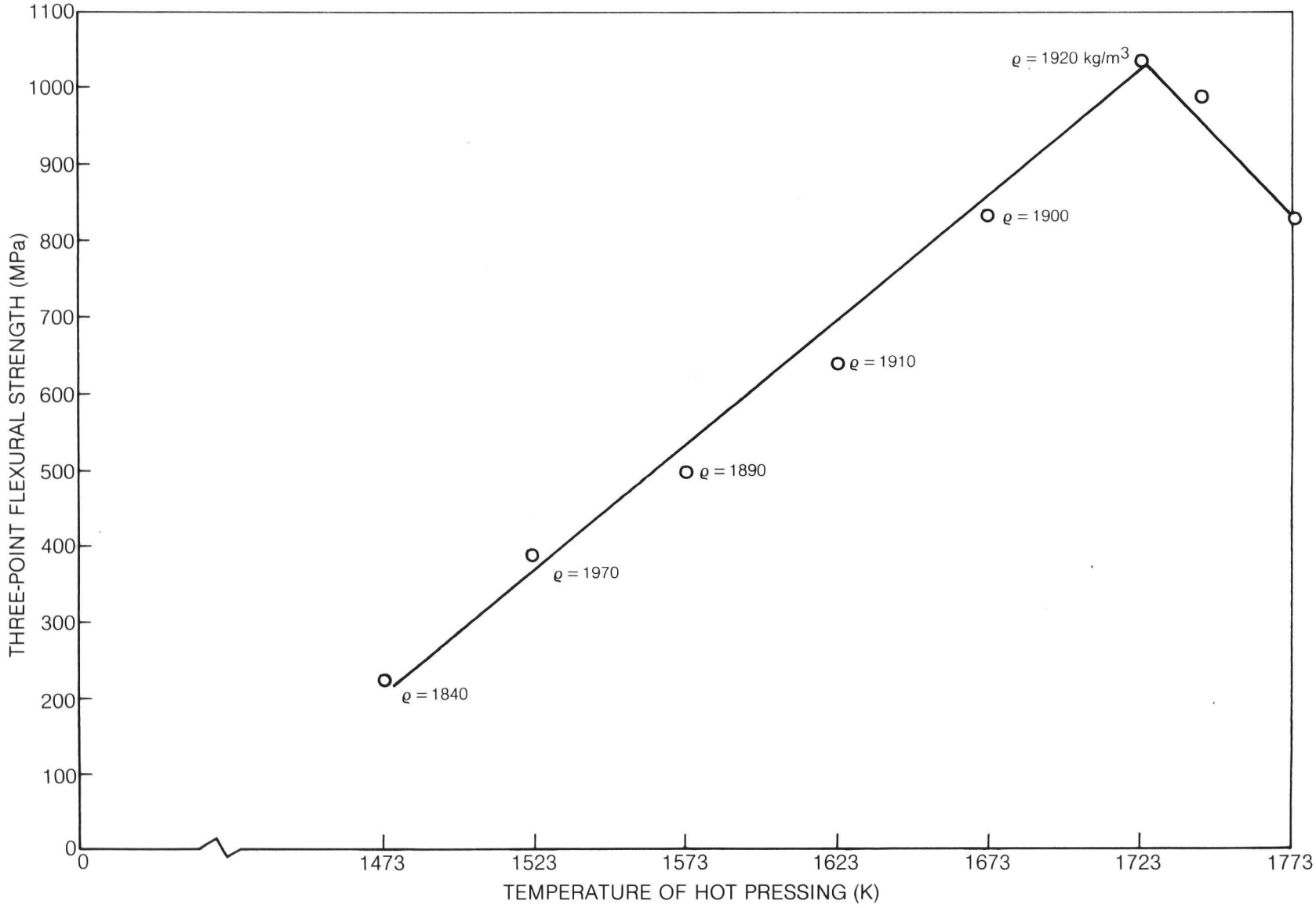

Fig. 16. Relationship of Three-Point Flexural Strength of HMS-774M Composite to Temperature at which Composite is Hot Pressed

81-2-100-6

To further demonstrate the importance of fabrication parameters, a series of unidirectionally reinforced Thornel 300/774M composites, with nominally 35% scrim reinforced glass, were fabricated using a variety of hot pressing conditions. Changes in hot pressing atmosphere, pressure and time were made while holding the hot pressing temperature of 1723 K constant. The resultant data are presented in Table IV where it should be noted that the negative percentage porosity values probably reflect some inconsistencies in fiber density value used, as well as some lack of accuracy in experimental technique. The Thornel 300 fiber density used was 1.75 gm/cm^3; however, this number was taken from the manufacturer's general literature and not measured for the particular batch of fiber used. For the purpose of this investigation the data are precise enough, however, since it is trends in the data which are of greatest concern in this brief parametric fabrication study.

The base line composite is the one fabricated using the conditions of 60 min, 6.9 MPa, vacuum-argon. Its average 0° flexural strength was determined to be 902 MPa. This strength value is particularly significant when it is also noted that the specimens did not fracture into separate pieces after crack initiation at the maximum load. Instead, the crack was diverted within the composite microstructure so that each specimen still possessed exceptional residual strength. This ability to blunt cracks seems to have been accentuated by the presence of the chopped fiber scrim in each ply. The range of 0° strength values of this specimen set was 746 to 1039 MPa. The 90° base line composite data are also rather outstanding. An average transverse flexural strength of 193 MPa is very competitive with many resin and even metal matrix composites. The range of 90° strengths for this specimen set was 172 to 230 MPa. Also of importance was the observation that for the 90° specimens the applied load vs measured specimen mid-span deflection curves were rather nonlinear and exhibited large deflections to failure. The following importance of hot pressing parameters was noted.

Atmosphere - Changes in the hot pressing atmosphere appeared to cause a significant alteration in axial strength. The standard procedure used consists of heat up in vacuum to remove any volatile or adsorbed gases from the glass powder and fiber, followed by a change to argon at 1173 K which is the atmosphere retained through the remainder of the cycle. Because of the expense involved in the use of argon, "all-vacuum" and a substitution of less expensive nitrogen were both tried. In the latter case there was no deleterious effect due to the nitrogen used while the all-vacuum cycle did result in a definite reduction in axial flexural strength. The reason for this decrease in 0° strength was not accompanied by any other significant change in composite characteristic and remains unexplained.

Pressure - The use of a much lower bonding pressure (1.7 MPa) caused a decrease in composite fiber content and an increase in the amount of porosity. Both of these factors contributed to a decrease in 0° flexural strength.

Table IV

Effect of Hot Pressing Conditions on Th-300 Fiber Reinforced 774M (with scrim) Composite Performance

Hot Pressing Conditions			Composite Flexural Strength*		Composite Composition		
Time (min)	Pressure MPa	Atmosphere	0° Axial MPa	90° Transverse MPa	v/o Fiber	v/o Glass	v/o Porosity
60	6.9	Vac/Argon	902	193	54	47	-1
60	6.9	Vac/Vac	708	214	57	43	0
60	6.9	Vac/Nitrogen	1000	214	56	46	-2
60	1.7	Vac/Argon	774	232	42	56	2
15**	6.9	Vac/Argon	797	223	49	52	-1
15**	1.7	Vac/Argon	580	129	40	60	0

*Six 0° and three 90° specimens tested for each condition

**For these short hot pressing times the composite was held at temperature for 10 min prior to pressure application

Time - A major reduction of time under pressure to 15 min also caused a measurable decrease in strength and fiber content, although in this case the maintenance of the high (6.9 MPa) bonding pressure eliminated the generation of porosity.

Time and Pressure - Finally, the decrease of both pressure and time resulted in the lowest fiber content and hence also lowest axial flexural strength. In this case composite transverse strength was also significantly degraded.

3. Effects of Defects and Procedural Variations

A series of 0° HMS fiber reinforced 774M matrix composites was fabricated using a variety of procedures to investigate the sensitivity of composite performance to procedural variations. The data are summarized in Table V where data were also obtained using standard fabrication procedures. The other composite data represent the following.

Bent Fibers - Composite plys were cut from tape such that the ply length (0° dimension) was approximately 10% longer than was necessary to fill the hot press die cavity. Thus, the fibers were necessarily bent to fit in the cavity. This would represent an error that might occur in lay-up and resulted in a composite where the fibers were bent sufficient to be noticed by visual observation. This defect caused a marked reduction in specimen flexural strength and was also accompanied by a reduction in fiber content.

Fiber Angle - A composite was hot pressed using the standard procedures; however, specimen cutting was performed so that the specimen edges were misaligned by 3° from the 0° fiber direction. Both composite strength and elastic modulus were decreased to 80% of the standard values. It should be noted that the fiber content was decreased by 6% from the standard.

Volume Percent Fiber - A composite was hot pressed with mechanical stops and additional glass to achieve a lower percentage of fiber reinforcement. In comparison with the standard composite, a 20% reduction in fiber content was achieved which resulted in a 25% decrease in flexural strength and 30% decrease in elastic modulus. An attempt to fabricate a composite with still lower fiber content was unsuccessful in that excess porosity resulted.

Glass Powder Size - A composite was fabricated using 774M powder which was given an additional ball milling operation for 100 hrs. This was intended to decrease the average glass particle size prior to tape making and hot pressing. The resultant composite contained a lower volume percentage of fiber (as did the starting tape) and also exhibited significantly lower strength and elastic modulus than the standard composite.

Table V

The Effect of Fabrication Procedures on the Performance of Unidirectionally Reinforced HMS/774M

Fabrication Condition	v/o Fiber	v/o Glass	v/o Porosity	Flex. Strength* (MPa) Avg.	Flex. Strength* (MPa) Std Dev.	Flex. Modulus* (GPa) Avg.	Flex. Modulus* (GPa) Std Dev.
Standard Procedure	71	29	0	1165	101	230	18
Bent Fibers	51	49	0	560	107	133	10
3° Off Axis	67	33	0	910	90	185	4.6
Volume Percent Fiber	58	42	0	867	61	164	5.8
Ball Milled Matrix Powder	54	46	0	780	108	174	7.0

*9 specimens tested for each condition

In all of the above cases, except in the case of fiber orientation, it would appear that fiber content was the most important factor in determining composite axial strength and modulus.

B. Composite Strength and Elastic Modulus

Composite strength and elastic modulus were measured both in tension and three point flexure with the strain in the tensile tests recorded through the use of strain gauges. The following sections will illustrate that composite performance was strongly influenced by both material composition and test technique.

1. Continuous and Discontinuous Fiber Reinforced Composites

The tensile strength, elastic modulus and strain to failure obtained for composites reinforced with continuous or discontinuous fibers are presented in Table VI. In the case of continuous fiber reinforcement, the data are primarily for unidirectionally reinforced specimens tested in the 0° direction. Specimens were not tested in the 90° direction because of the very low transverse strength of these unidirectionally reinforced specimens. One 0/90 cross ply specimen of the HMS fiber reinforced system was also tested. Each of the systems tested will be described in turn below.

a. HMS Fiber Reinforced 774M - Composites GC 628, 594 and 593

The tensile stress vs strain curve for one of the 0° specimens is shown in Fig. 17. It should be noted that these HMS reinforced specimens contain a lower fiber content than those reported elsewhere in this report. Although the curve appears to be quite linear, it actually is composed of two nearly linear portions that transition at a stress level of approximately 75 MPa. The specimen fracture surface is quite flat with no signs of fiber pull out or gross delamination.

The 0/90 cross ply reinforced specimens were considerably weaker than their all 0° counterparts and fracture occurred in only one case completely within the test gauge length. The overall composite failure strain, Fig. 18, however, was similar to that achieved with the 0° material.

b. HTS Fiber Reinforced 774M - Composite GC 629

The stress-strain curve for this 0° composite, Fig. 19, was essentially linear to the point of failure. This system exhibited the highest strength and failure strain combination of any of those tested. It also contained the highest percentage of fiber reinforcement. The composite fracture surface was markedly different from that of the HMS specimen. In this case it was very fibrous with the entire gage length of the specimen taking on a brush-like appearance after fracture.

Table VI

Tensile Test Data (300 K Test)
for 774M Matrix Composites

Specimen	Fiber	v/o F	v/o G	v/o P	Orientation	UTS MPa	E GPa	ε_f (%)	Fracture Location
GC 594-14	HMS	54	46	0	0^o	412	195	0.20	Gage
-15	HMS	-	-	-	0^o	398	193	0.20	Gage
GC 628-4	HMS	48	52	0	0^o	342	195	0.17	Dbl. Edge
-6	HMS				0^o	354	173	0.20	Dbl. Edge
-8	HMS				0^o	349	-		Dbl. Edge
GC 593-3	HMS	46	56	-	$0^o/90^o$	137	60.1	0.27	Gage*
-4	HMS	-	-	-	$0^o/90^o$	126	67.8	0.20	Dbl. Edge*
GC 629-4	HTS	67	32	1	0^o	572	151	0.36	Gage
-6	HTS				0^o	658	153	0.41	Gage
-8	HTS				0^o	613	-	-	Gage
GC 630-4	Pitch	54	46	0	0^o	616	338	0.22	Gage
-6	Pitch				0^o	511	329	0.16	Gage
-8	Pitch				0^o	534	-	-	Gage
GC 631-4	Th 300	39	60	1	0^o	359	126	0.32	Gage + Dbl.
-6	Th 300				0^o	460	121	0.40	Gage + Dbl.
-8	Th 300				0^o	386	-	-	Dbl. Edge
GC 632-4	GY-70	58	42	0	0^o	424	293	0.14	Gage
-6	GY-70				0^o	362	273	0.12	Gage
-8	GY-70				0^o	Failed prior to loading			
GC 633-4	Cel				0^o	447	117	0.32	Gage
-6	6000				0^o	395	110	0.40	Gage
-8	"				0^o	432	-	-	Gage
GC 576-2	Cel	27	67	6	Paper	157	55.2	0.65	In Dbl.
	6000	-	-	-	0^o	142	48.4	0.61	In Dbl.
	Paper								

*Specimens were not surface ground prior to test. All other specimens were surface ground prior to test.

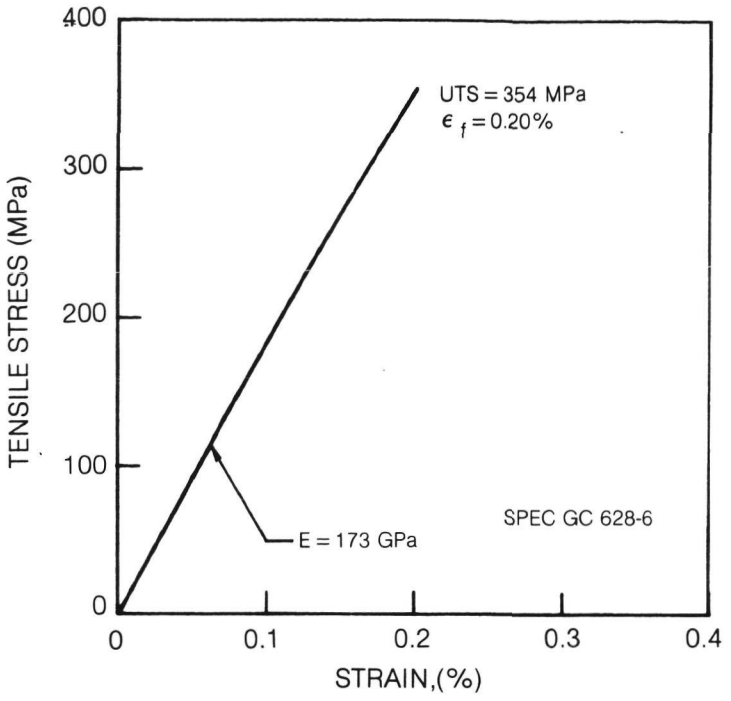

Fig. 17. Axial Tensile Stress — Strain Curve for 0° — HMS/774M at 300K

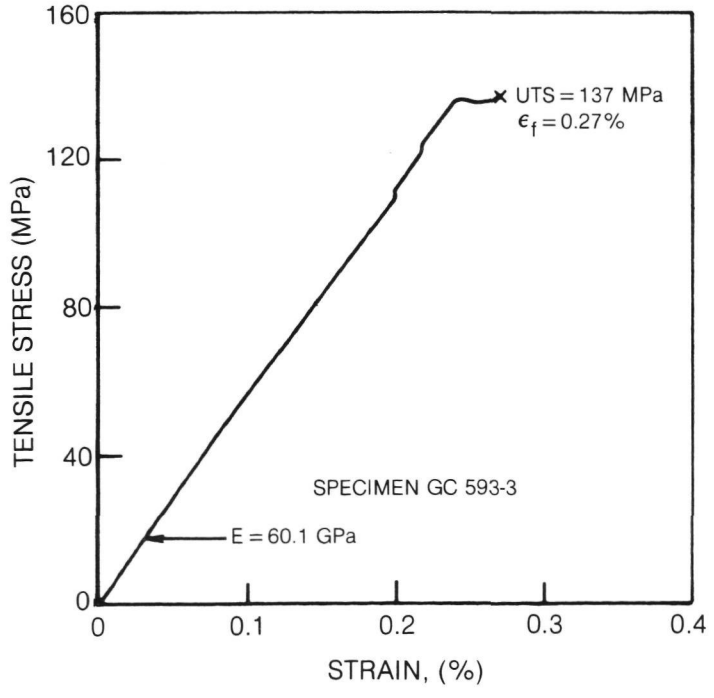

Fig. 18. Transverse Tensile Stress — Strain Curve for 0/90 — HMS/774M at 300K

80–5–82–12

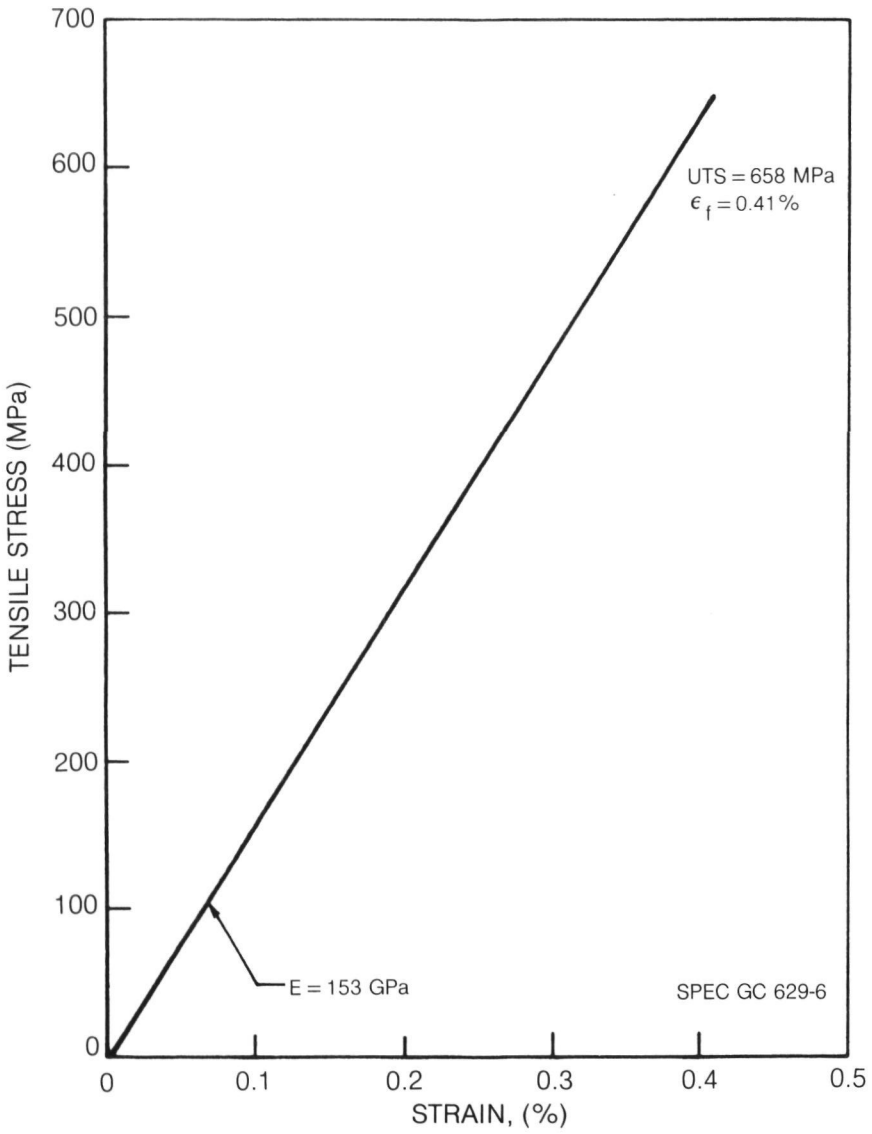

Fig. 19. Axial Tensile Stress — Strain Curve for 0° — HTS/774M at 300K

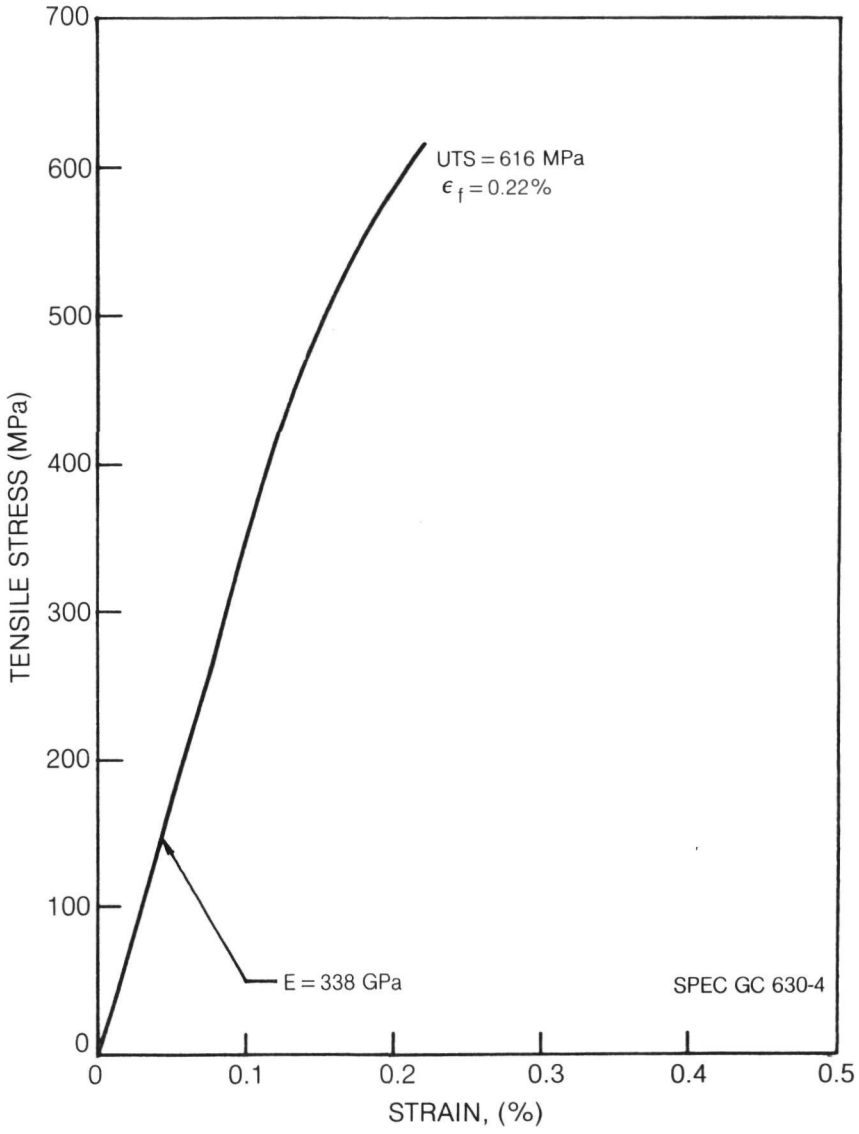

Fig. 20. Axial Tensile Stress-Strain Curve for 0° — Thornel Pitch (VS0054-0)/774M at 300K

80-5-82-16

c. Thornel Pitch Fiber Reinforced 774M - Composite GC 630

The 0° stress vs strain curve, Fig. 20, was linear up to about 65% of the UTS, after which it became very nonlinear. This latter behavior was probably due to the formation of large longitudinal shear cracks which were a prominent feature of the fractured specimens. No fiber-matrix debonding or pullout, however, accompanied these cracks. The very high elastic modulus obtained is a major aspect of this composite and hence, even though the composite tensile strength was relatively high, the final failure strain was low.

d. Thornel 300 Fiber Reinforced 774M - Composite GC 631

The 0° stress vs strain curve, Fig. 21, is bi-linear with the decrease in slope occurring at approximately 100 MPa. Although the composite tensile strength is relatively low, the failure strain is quite high due to the low elastic modulus of both fiber and composite. The slight nonlinearity in the curve near the UTS is probably associable with the formation of large longitudinal shear cracks, some of which followed an interlaminar path. Again, as in the case of the Pitch based fiber, no fiber-matrix debonding or pullout occurred.

e. GY70 Fiber Reinforced 774M - Composite GC 632

The stress vs strain curve for this composite, Fig. 22, was totally linear to the point of fracture and the resultant composite fracture surface appeared relatively featureless. The fracture plane was flat and no signs of pullout or shear cracking were evident.

f. Continuous Celion 6000 Fiber Reinforced 774M - Composite GC 633

The stress vs strain curve for this 0° material was the most nonlinear of all of the 0° continuous fiber reinforced specimens tested, Fig. 23. An initial decrease in slope occurred at about 100 MPa followed by a major nonlinear portion of the curve at approximately 85% of the UTS. This latter feature contributed to raising the ultimate composite failure strain to approximately 0.50% and is probably associated with the extensive fiber-matrix debonding characteristic of the final fracture. The entire gage section turned into a "brush" of graphite fibers after fracture.

g. Discontinuous Celion 6000 Fiber Reinforced 774M - Composite GC 576

The stress-strain behavior, Fig. 24, of the Celion 6000 discontinuous fiber reinforced glass matrix composites differed significantly from that of the above materials. In this case the specimen exhibited a major decrease in slope

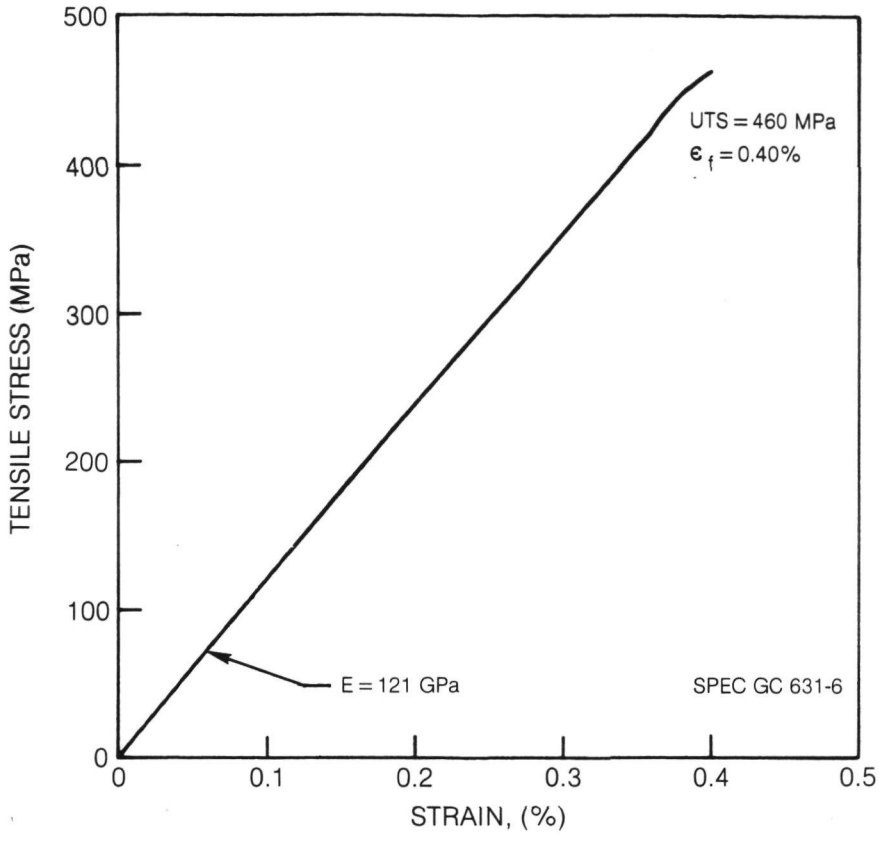

Fig. 21. Axial Tensile Stress — Strain Curve for 0° — Thornel 300/774M at 300K

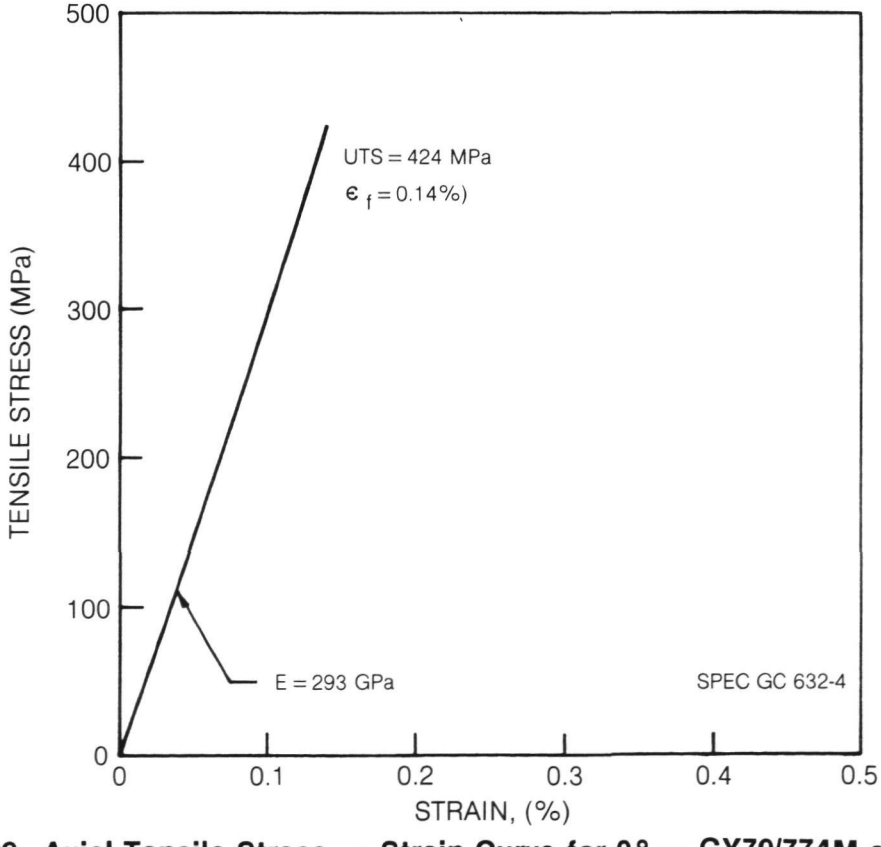

Fig. 22. Axial Tensile Stress — Strain Curve for 0° — GY70/774M at 300K

80–5–82–13

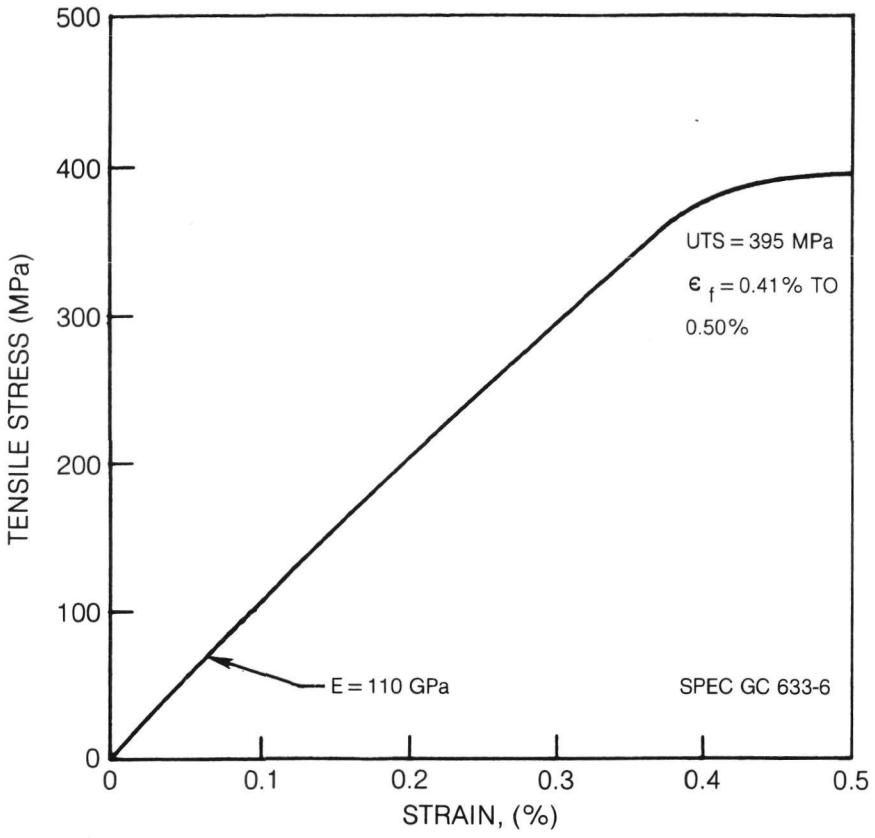

Fig. 23. Axial Tensile Stress — Strain Curve for 0° — Celion 6000/774M at 300K

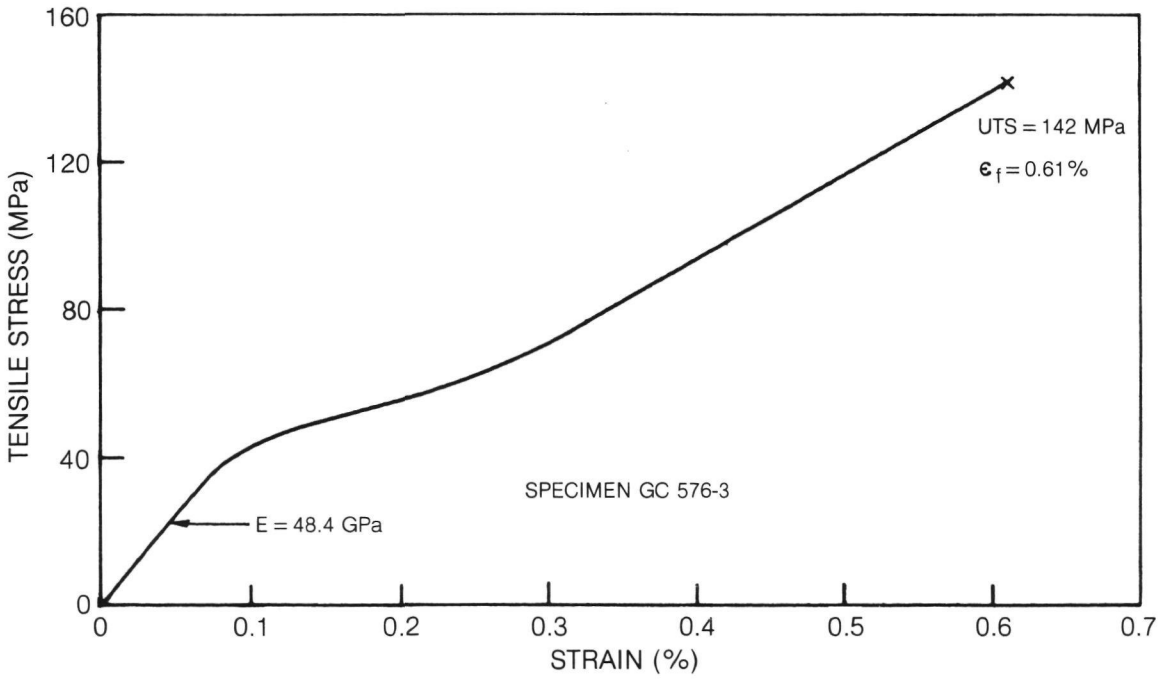

Fig. 24. Tensile Stress — Strain Curve for Discontinuous Celion 6000 — 774M Tested at 300K

80–5–82–14

at an applied stress of 40 MPa, which was then followed by an increase in slope and final failure at approximately 0.6% strain. This unique behavior is probably related to the occurrence of matrix cracking at the 40 MPa stress level and the extreme difficulty for crack propagation through the specimen cross section. The resultant high level of failure strain is highly desirable for most applications; however, the low level of overall strength, compared to the unidirectionally reinforced material, would be unsatisfactory for many high performance situations.

A further comparison of composite properties is presented in Table VII where manufacturer's claimed fiber properties of strength and elastic modulus are used as a baseline. A simple rule-of-mixtures calculation of composite elastic modulus, using the tabulated values for fiber and 7740 glass matrix properties, indicates that all of the measured axial moduli fall below those expected. The level of agreement ranges from between 79% and 95%. Some of the inaccuracy may be related to the fact that the manufacturer's "typical" data are used rather than those for a particular spool. In addition, the use of the full matrix elastic modulus of 63 MPa may overestimate the matrix contribution. Matrix cracking may lower this value significantly.

Although it was expected that a "rule-of-mixtures" approach should yield relatively good agreement for the elastic modulus comparison, no such agreement should be expected for composite tensile strength. Even a simplified calculation, used in the table, which completely neglects any matrix contribution term, would not be expected to be very accurate since, at the very least, an effective bundle strength should be used for the fiber strength. However, the statistical data needed to determine the bundle strength are not available. The calculation presented in Table VII is used simply in a relative sense. The Pitch fiber reinforced composite came closest to achieving a large fraction of the fiber average strength, 49%, while all of the other composites were at a 27-36% level of achievement. Because of the relatively linear shapes of the stress vs strain curves, the levels of agreement in composite failure strain resemble those based on strength.

Three point flexural bend strengths (using a span-to-depth ratio of 30 to 1) were also determined for specimens taken from the same composite panels used to obtain the above described tensile data. A comparison between the average tensile and flexural strengths and elastic moduli is presented in Table VIII. It can be noted that composite elastic modulus is nearly identical as measured by either test while the composite flexural strength is substantially higher than the tensile strength in four out of eight cases. In the case of the HMS fiber reinforced specimens, the flexural strengths in this table are significantly lower than those reported earlier in this report, Fig. 16. This is primarily due to the lower percentage of fiber reinforcement present in the current specimens but may also relate to variations in starting fiber properties.

Table VII

Comparison of Measured and Simplified Rule of Mixtures 0° Properties
for Uniaxially Reinforced Specimens

Specimen	Type	Fiber			Composite Elastic Modulus			Composite UTS			Composite Failure Strain		
		E_f (GPa)	UTS_f (MPa)	v/o F	Calc* (GPa)	Meas (GPa)	Meas/Calc	Calc** (MPa)	Meas (MPa)	Meas/Calc	Calc*** %	Meas %	Meas/Calc
594	HMS	350	2700	54	218	194	0.89	1460	405	0.28	0.77	0.20	0.26
628	HMS	350	2700	48	200	184	0.92	1300	348	0.27	0.77	0.18	0.23
629	HTS	256	2830	67	192	152	0.79	1900	614	0.32	1.1	0.38	0.35
630	Th Pitch	654	2070	54	382	334	0.87	1120	554	0.49	0.32	0.19	0.60
631	Th 300	234	2930	39	130	124	0.95	1142	400	0.35	1.25	0.36	0.29
632	GY 70	537	1860	58	338	283	0.84	1080	395	0.36	0.35	0.13	0.37
633	Cel 6000	234	2760	-	-	113	-	-	425	-	1.18	0.36	0.30

*calculated using $E_c = (v/oF)\ E_f + (v/oG)\ (63\ GPa)$

**calculated using $UTS_c = (v/oF)\ (UTS_f)$

***calculated using $\varepsilon_f = UTS_f/E_f$

Table VIII

Comparison of Tensile and Flexure Data

Specimen	Fiber Type	Composite Flexural Properties		Composite Tensile Properties		Flex Strength/ Tensile Strength
		Strength (MPa)	Elastic Modulus (GPa)	Strength (MPa)	Elastic Modulus (GPa)	
594	0° HMS	620*	-	405	194	1.53
628	0° HMS	527**	180	348	184	1.51
593	0/90 HMS	325*	-	132	64	2.46
629	0° HTS	806**	155	614	152	1.31
630	0° Th. Pitch	683**	332	554	334	1.23
631	0° Th. 300	711**	127	400	124	1.78
632	0° GY70	432**	275	395	283	1.09
633	0° Cel 6000	388**	94	425	113	0.91
576	0° Cel 6000 paper	433*		150	52	2.88

* 5 specimens tested to obtain an average flexural strength
** 4 specimens tested to obtain an average flexural strength

The superiority of flexural strength was expected for several reasons. First, on a statistical basis it is expected that a higher flexural strength would result due to the smaller volume of material undergoing the maximum calculated beam stress. Second, the problems of alignment and gripping induced failure should be less for the flexural test. On the other hand, it is possible to measure a low flexural strength due to the occurrence of other failure modes such as shear or compression. Examination of the fractured continuous Celion 6000 fiber reinforced three point bend specimens did indeed indicate that they failed by an interlaminar shear mode rather than in tension. A very poor fiber-matrix bond existed and this was also reflected in the fractured tensile specimen character where the specimens appeared brush-like after testing. In the case of specimen set GC 632 consisting of GY70 reinforced glass, it was not possible to ascertain whether specimens failed in tension or compression by simply looking at the fractured specimens. Therefore, three additional specimens were tested from the same panels and again it was not possible to ascertain the exact mode of failure because of its very sudden nature and the rather brittle appearance of the fracture surfaces. In the cases of both the Thornel Pitch (GC 630) and HTS (GC 629) fiber reinforced specimens it was possible to note evidence for compression, rather than tensile, failure in the flexural test. This was particularly true for the Thornel Pitch reinforced composites which exhibited only compression failure.

The fracture surfaces of three types of tensile specimens were examined in the scanning electron microscope. The fracture surface of a 0^{o} HMS fiber reinforced 774M specimen, Fig. 25, is characterized by the presence of almost no fiber pull out from the matrix. However, large axial splits are observed which appear to occur primarily along fiber rich zones. These may correspond to regions of low transverse strength which, upon the sudden release of energy during tensile failure, fracture. The fracture of a $0^{o}/90^{o}$ HMS reinforced 774M composite, Fig. 26, includes the same above-mentioned features as well as transverse ply fracture which occurs primarily along fiber-matrix interfaces. Finally, the tensile fracture of chopped Celion 6000 fiber reinforced glass, Fig. 27, is characterized by extensive fiber pull out on a microscale. Fiber lengths of 300-500 microns in length are readily observed completely free of any surrounding matrix.

2. Continuous Fiber Reinforced Composites with Scrim

As described in the previous section, unidirectionally reinforced continuous fiber composites exhibited adequate values of 0° tensile strength, however, composite 90° strength was very low. This inadequacy in transverse performance can be alleviated through the use of the addition of small amounts of two dimensionally arrayed discontinuous fibers, or scrim, as described in the earlier sections of this report. Three different forms of continuous fiber reinforcement were used to obtain tensile test data which included ultimate

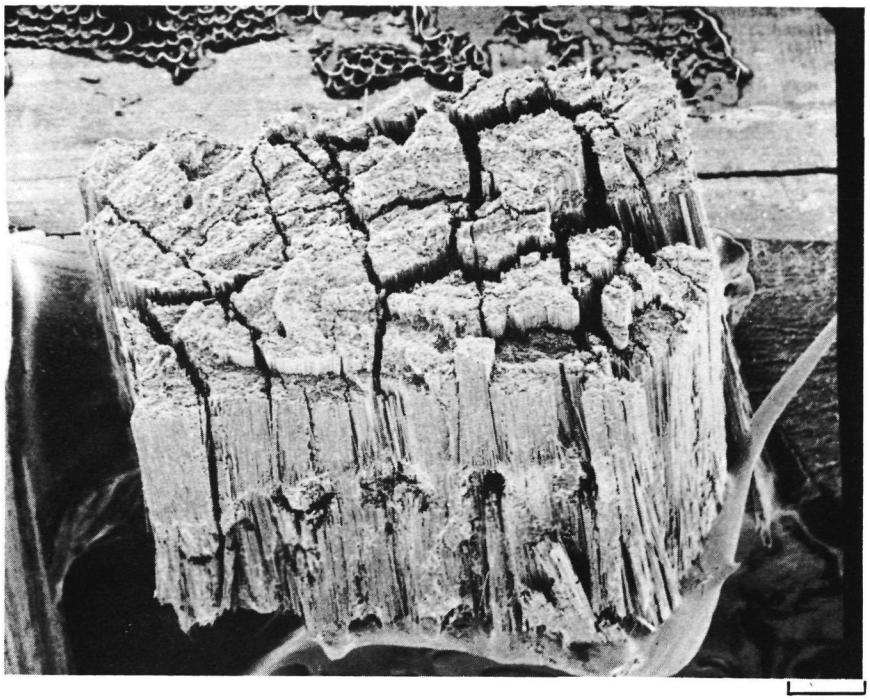

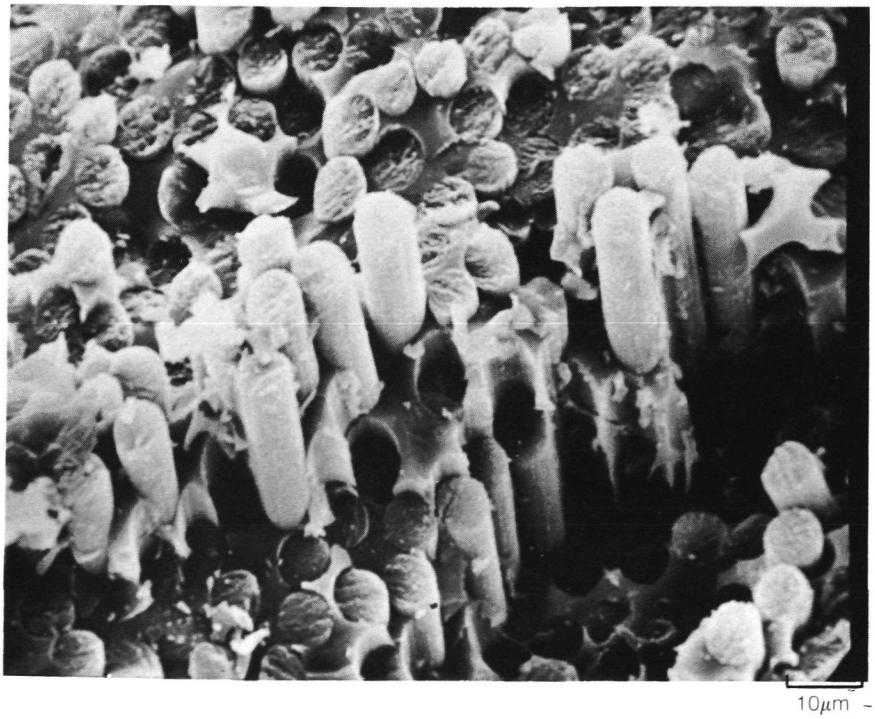

Fig. 25. Fracture Surface of 0° — HMS/774M Tensile Specimen GC 594-14

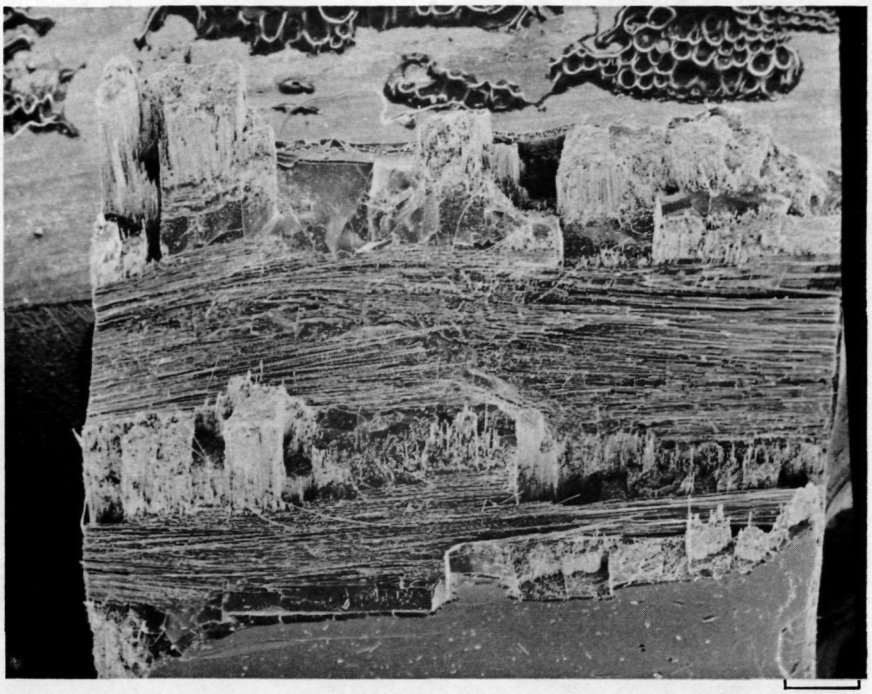

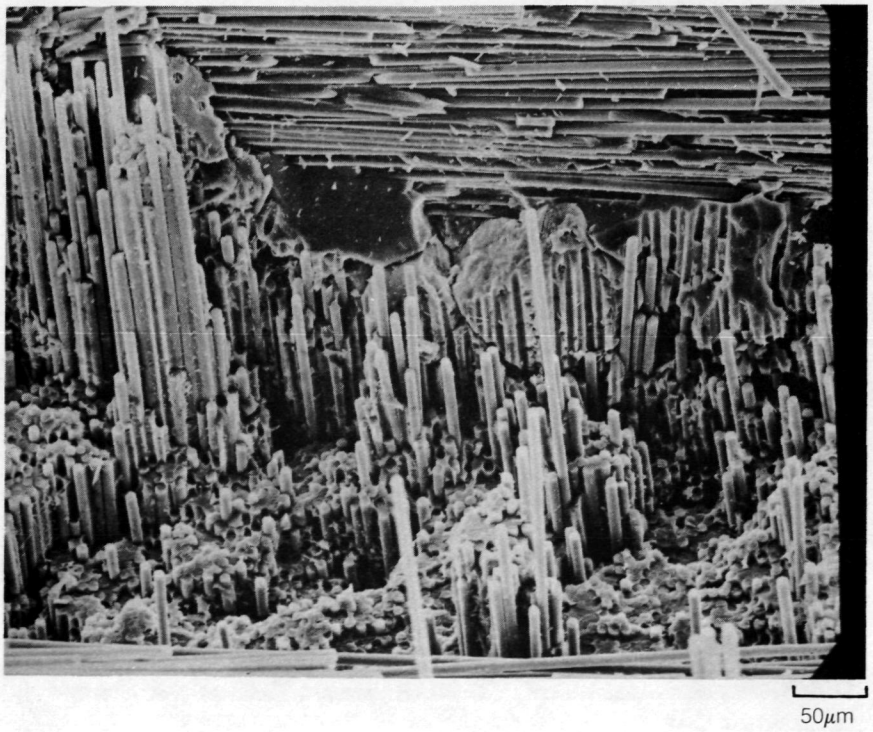

Fig. 26. Fracture Surface of 0/90 — HMS/774 M Tensile Specimen GC 593-3

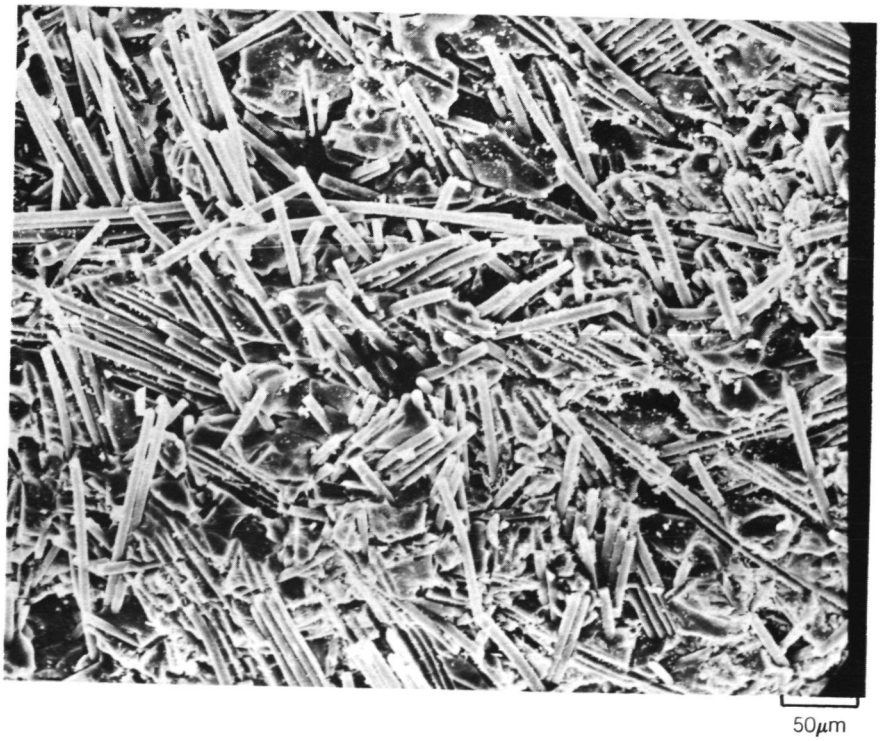

Fig. 27. Fracture Surface of Celion 6000 Paper/774M Tensile Specimen GC 594-14

strength, elastic modulus, failure strain and principal Poisson's ratio, Table IX. As can be seen from these data, it was possible to achieve significant transverse (90°) tensile strength, without reduction in axial tensile strength. This can be concluded by comparing the current data, Table XI, with those for specimens not containing scrim, Table VIII. The overall fiber volume fractions are not constant in this comparison so that detailed comparisons cannot be made. However, particularly in the case of the Thornel 300 fiber reinforced composites, the 0° strength of the scrim enhanced specimens was significantly greater. Only in the case of the Thornel Pitch fiber reinforced specimens was there a decrease in axial strength and that was 15%.

The tensile performance of the 0/90 cross ply specimens is summarized in Table X. As expected, strength and elastic modulus values are both reduced substantially while the failure strain values are, in many cases, equivalent to those obtained for the 0° specimens. This relates to the fact that the controlling failure mechanism for these 0/90 specimens is fracture of the 0° plys.

The Thornel 300 fiber reinforced composite system provided the best overall combination of axial and transverse tensile strength performance as well as translation of tensile performance into a 0/90 cross ply. A summary of overall composite performance for the Thornel 300 (with scrim) fiber reinforced system is given in Table XI. Figure 28 presents the tensile stress vs strain curves for several individual specimens of this material. One of the most interesting aspects of these curves is the relatively large transverse tensile failure strain. This is primarily due to the fact that approximately 25% of the composite material cross section consists of chopped fiber paper reinforced 774M glass. Reference to Fig. 24 illustrates that a composite consisting solely of chopped fiber paper in 774M exhibits a tensile failure strain of 0.6% and a tensile strength of 142 MPa. Also, as shown in Fig. 14, the presence of approximately 25% by volume of scrim (chopped fiber paper) reinforced glass provides a major increase in transverse strength, over that of composites without scrim. Thus even if the remainder of the composite microstructure fractures in 90° tension, the scrim reinforced glass carries the additional stress to the point of failure at the larger strain. An actual microstructure of this type of composite can be found in Fig. 13.

The stress-strain curves of the 0° and 0/90 composites, although appearing totally linear to nearly the point of fracture, are not. The arrows in Fig. 28 point to the positions where a decrease in slope occurs for both curves. Although in the figure it appears that this deviation from linearity occurs at the same strain of 0.06% for both orientation types, it varied from 0.05% to 0.1% for all of the specimens tested. The decrease in apparent elastic modulus, in both cases, is undoubtedly due to matrix cracking taking place; however, as would be expected, the ultimate composite failure strain is controlled by the fibers loaded in axial tension. Thus, the ultimate composite failure strain in both the 0° and 0/90 orientations is nearly the same.

Table IX

Tensile Test Data for Unidirectionally Reinforced Specimens Containing Scrim

Specimen	Fiber	Orientation	v/o Fiber	v/o Glass	v/o Porosity	UTS MPa	E GPa	ε_f %	ν
674	HMS	0°	66	31	3	402	230	0.18	-
			68	31	1	307	227	0.13	-
						411	210	0.20	-
						332	220	0.15	-
						314	-	-	-
						350	188	0.21	0.22
					Avg	352	215	0.17	
		90°				11.6	11.0	0.24	0.034
						12.8	9.5	0.29	0.010
					Avg	12.2	10.2	0.26	0.022
677	Th 300	0°	54	46	0	476	180	0.29	-
			54	46	0	538	169	0.33	-
						678	177	0.41	-
						603	170	0.36	-
						658	161	0.40	0.20
						532	156	0.34	0.22
					Avg	580	168	0.36	0.21
		90°				29.5	19.2	0.20	0.016
						31.7	15.0	0.65	0.008
						25.9	16.1	0.50	-
					Avg	29.0	16.8	0.45	0.012
681	Th Pitch	0°	54	43	3	550	318	0.22	-
			58	42	0	393	383	0.16	-
						498	341	0.15	-
						303	432	0.08	-
						591	-	-	-
						451	384	0.11	0.32
					Avg	464	372	0.14	
		90°				9.7	9.4	0.26	0.013
						6.8	-	-	-
						10.1	13.3	0.36	0.015
					Avg	8.9	11.4	0.31	0.014

Table X

Tensile Test Data for 0/90 Cross Ply
Reinforced Specimens Containing Scrim

Specimen	Fiber	v/o Fiber	v/o Glass	v/o Porosity	UTS MPa	E GPa	ε_f (%)	ν
675	HMS	67	31	2	93.9	65.0	0.15	
		67	30	3	90.0	115	0.08	
					75.3	-	-	
					75.8	91.2	0.08	
					109.0	-	0.16	
					109.0	-	0.12	
				Avg	92.2	90.4	0.12	
676	Th 300	60	40	0	199	68.0	0.29	
		60	40	0	251	84.8	0.31	
					229	71.0	0.33	
					209	77.2	0.31	
					216	73.6	0.30	
					284	55.4	0.20	0.04
					334	74.7	0.53	0.04
				Avg	246	72.1	0.32	0.04
690	Th Pitch	47	50	3	290	165	0.23	
		49	51	0	234	169	0.29	
					209	172	0.13	
					292	185	0.22	
				Avg	256	173	0.22	

Table XI

Thornel 300 Reinforced 774M*
(with scrim)

Unidirectional				0/90 Cross Ply	
E_{11}^T =	168 GPa	E_{22}^T =	16.8 GPa	E_{11}^T =	72.1 GPa
σ_{11}^T =	580 MPa	σ_{22}^T =	29.0 MPa	σ_{11}^T =	246 MPa
$\varepsilon_{f_{11}}^T$ =	0.36%	$\varepsilon_{f_{22}}^T$ =	0.45%	$\varepsilon_{f_{11}}^T$ =	0.32%
ν_{12}^T =	0.21	ν_{21}^T =	0.012	ν_{12}^T =	0.04
E_{11}^F =	124 GPa	E_{22}^F =	25.4 GPa		-
σ_{11}^F =	905 MPa	σ_{22}^F =	94 MPa		-

ρ = 2.0 gm/cm^3

*Superscript T denotes property measured in tension
Superscript F denotes property measured in three point flexure

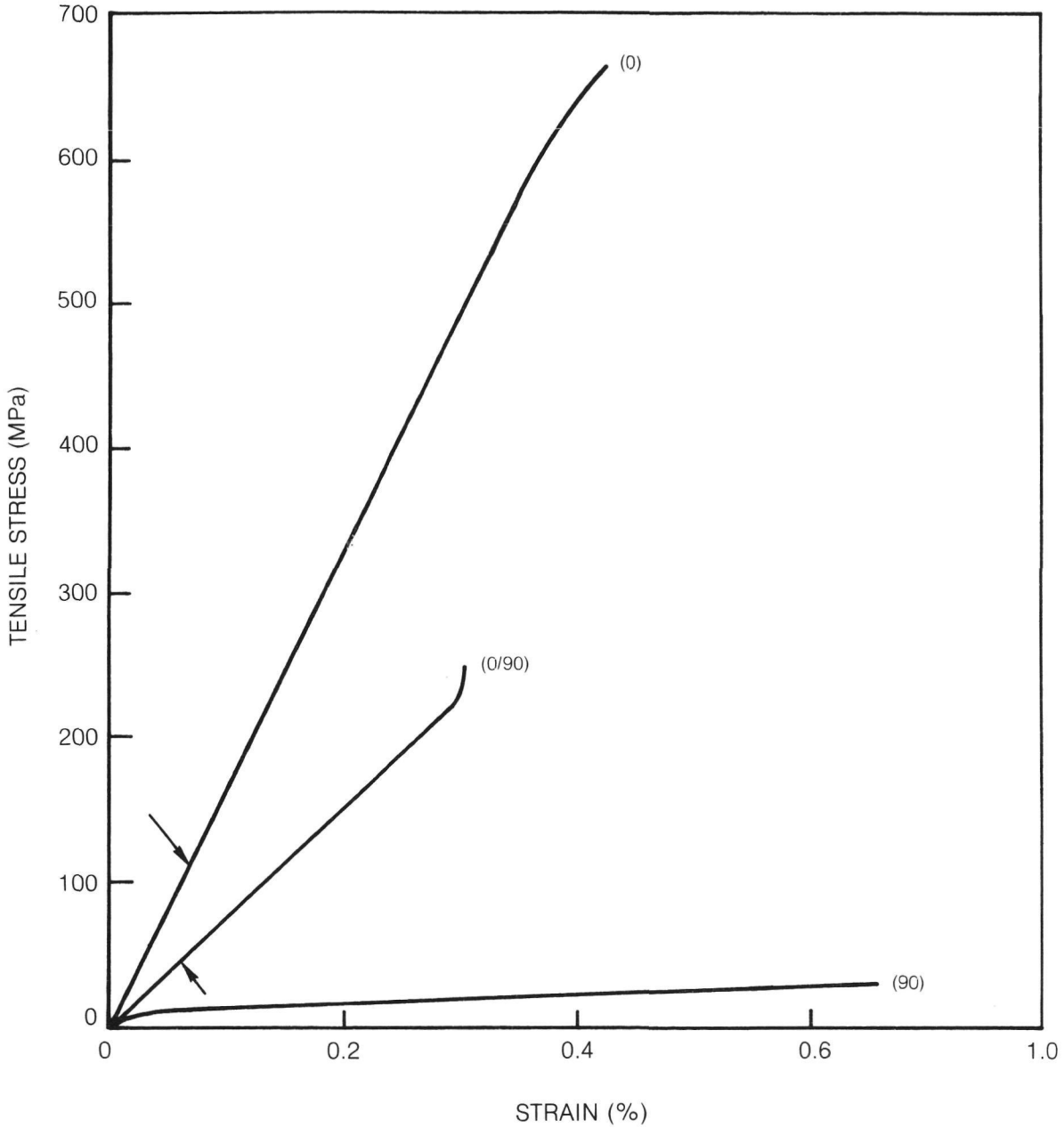

Fig. 28. Tensile Stress-Strain Curves for Th300 Fiber Reinforced 774M (with Scrim)

80–5–48–1

The fracture characteristics of the three different types of fiber reinforced composites were determined by both optical and scanning electron microscopy and the overall appearance of the axial tensile specimens is shown in Fig. 29. Closer examination of these fracture surfaces, Figs. 30-33, revealed that in all three cases regions of extensive fiber pullout, as well as regions of brittle fiber fracture on the primary crack plane, occurred. In the case of the HMS fiber reinforced specimens, Fig. 30, it appeared that major changes in fracture plane occurred at the ply boundaries due to the presence of the chopped fiber scrim in each layer, Fig. 30a. In the fractured plys themselves, however, many of the fibers fractured without any noticeable pullout, Fig. 30b. Also noticeable is the very precise replication of the fiber surface by the glass during hot pressing. Comparison with the fracture surface of an HMS fiber reinforced composite that did not have any scrim in it, Fig. 25, indicates that the presence of the scrim introduces the above mentioned ply boundary effect. It also, however, seems to have prevented the cracking of the composite along planes at right angles (but parallel to the fibers) to the plys.

The fracture surface features of the Thornel 300 fiber reinforced specimens, Fig. 31, are quite similar to those shown in Fig. 30. The overall fracture surface appears to have somewhat less overall fiber pullout; however, the interply crack diversion and exceptional fiber-matrix replication are both evident.

A major change in fracture appearance is noticeable for the Thornel pitch based fiber reinforced composite, Figs. 32 and 33, where it can be seen that the fracture is dominated by extensive fiber pullout and fiber-matrix debonding. The fracture surface also includes a large shear plane, Fig. 32a, which extends through the entire gage length of the specimen. It is also interesting to note that a small number of the fibers appeared to be degraded in appearance, Fig. 33b, while all of the fibers exhibited the very pronounced radial structure of pitch based graphite fibers, Figs. 33a and 33b.

3. Three Point Flexural Strength as a Function of Temperature and Test Geometry

The three-point flexural strengths obtained by testing 0°-HMS/774M (no scrim) over the temperature range of 300 to 973 K (in argon) are presented in Fig. 34. The specimens were tested at a span-to-depth ratio of 32 to 1. The average 300 K strength of 930 MPa agrees well with the high levels of strength reported

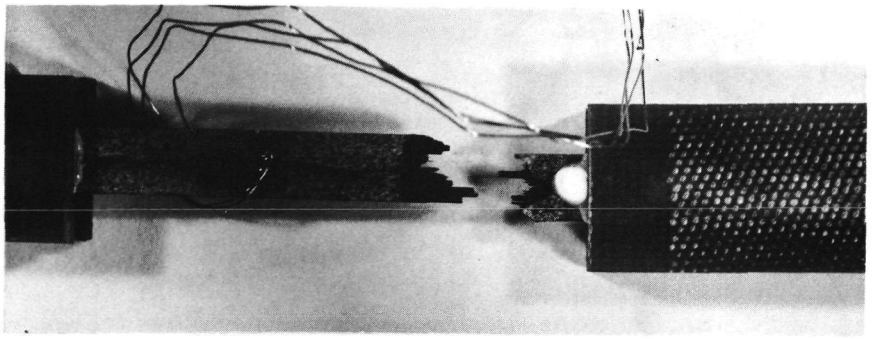

0° HMS REINFORCED 7740

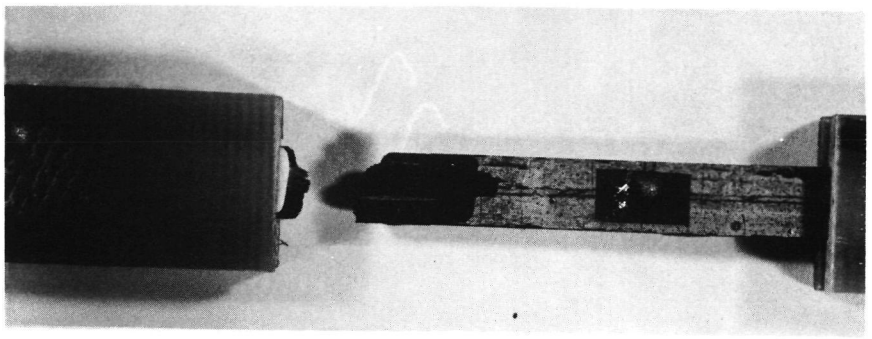

0° Th 300 REINFORCED 7740

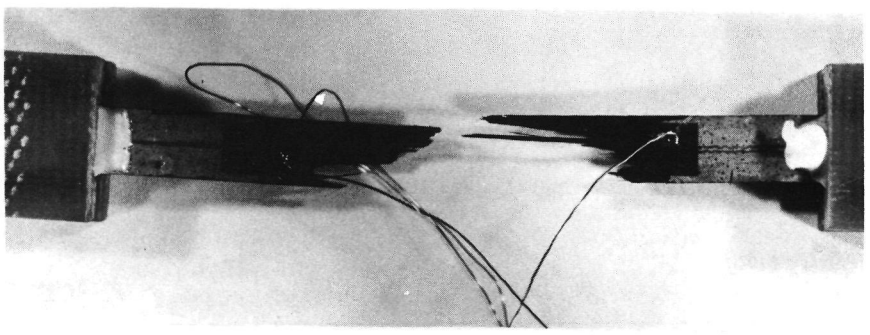

0° Th PITCH REINFORCED 7740

Fig. 29. Fracture 0° Tensile Specimens of Unidirectionally Reinforced Composite Specimens (with Scrim)

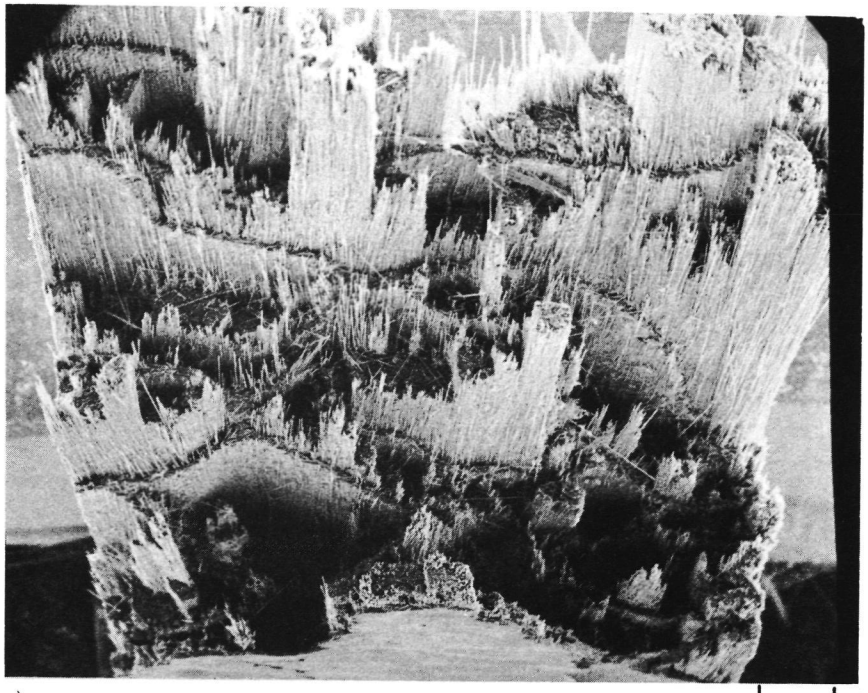

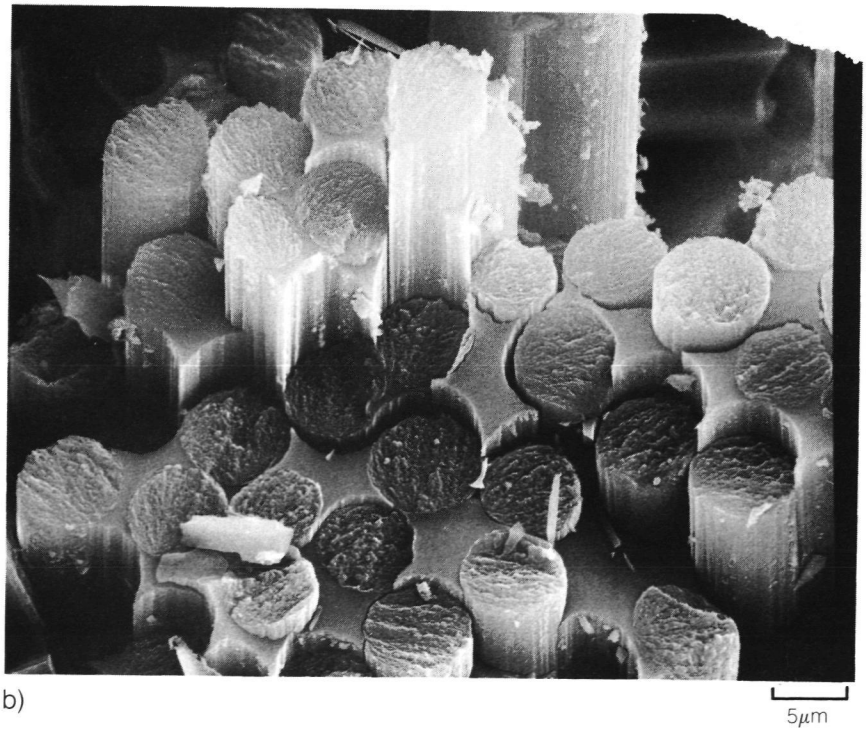

Fig. 30. Fracture Surface of HMS Fiber Reinforced 774M (with Scrim

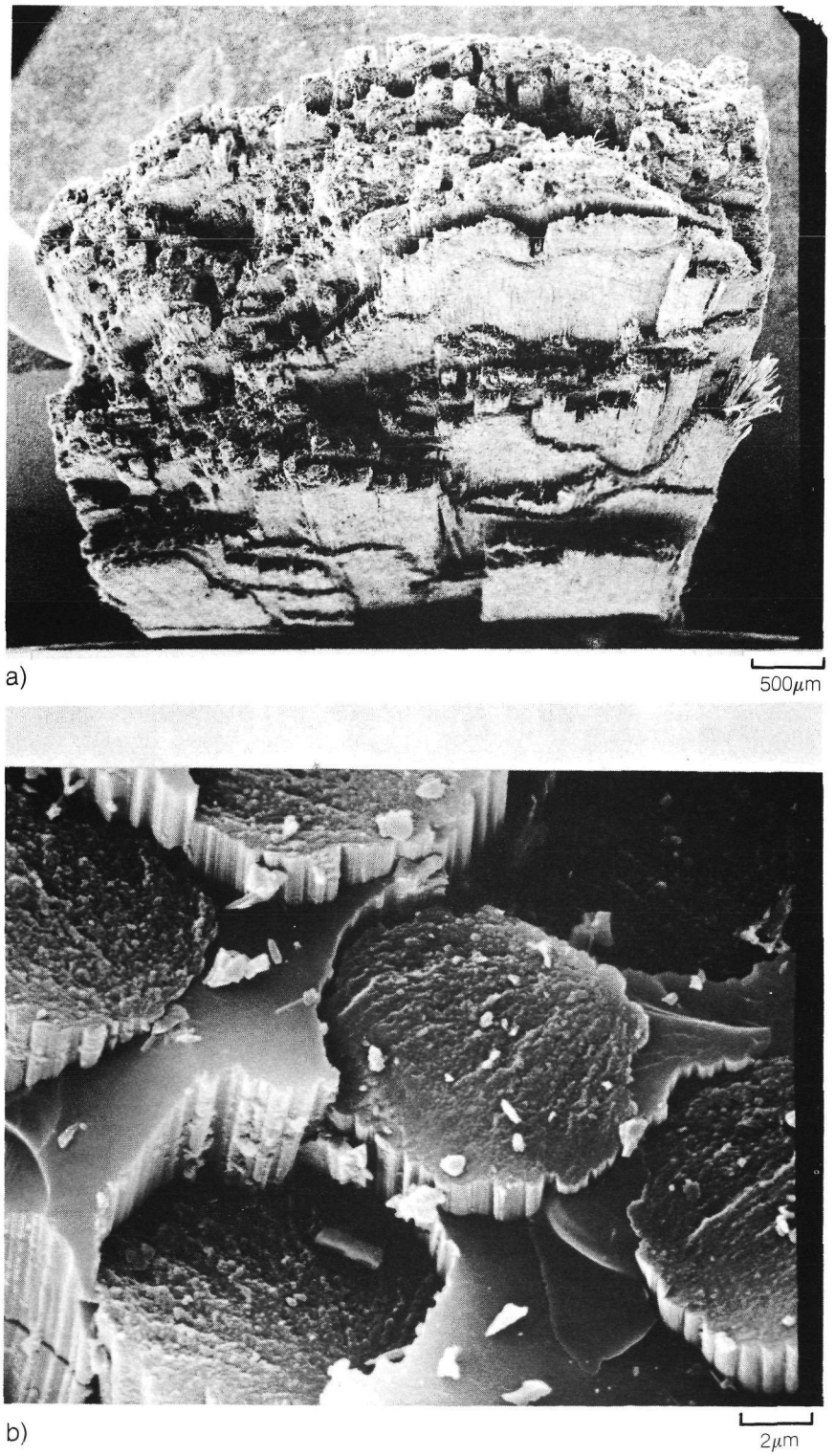

Fig. 31. Fracture Surface of Th300 Fiber Reinforced 774M (with Scrim)

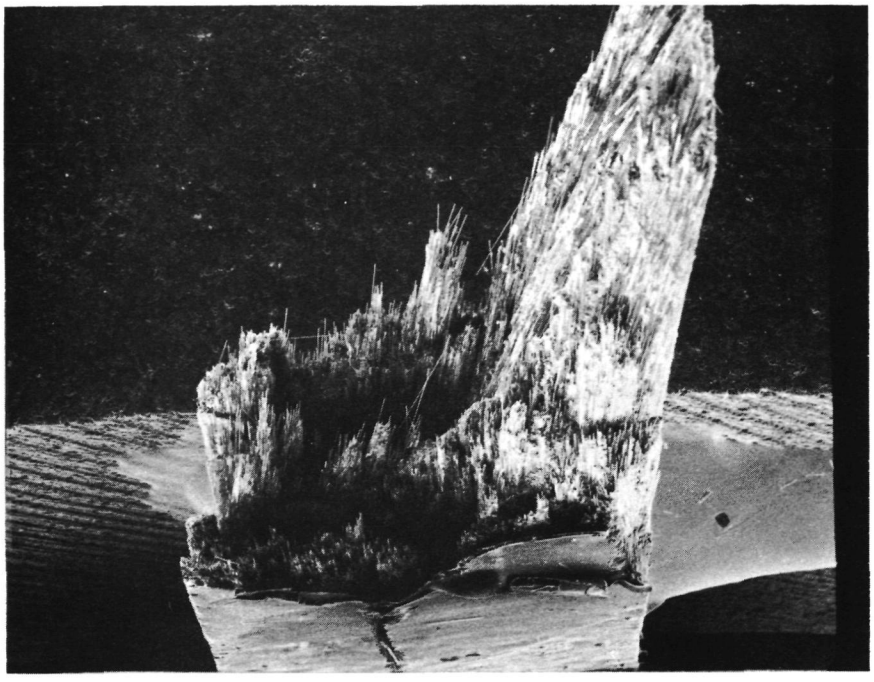

a)

1000μm

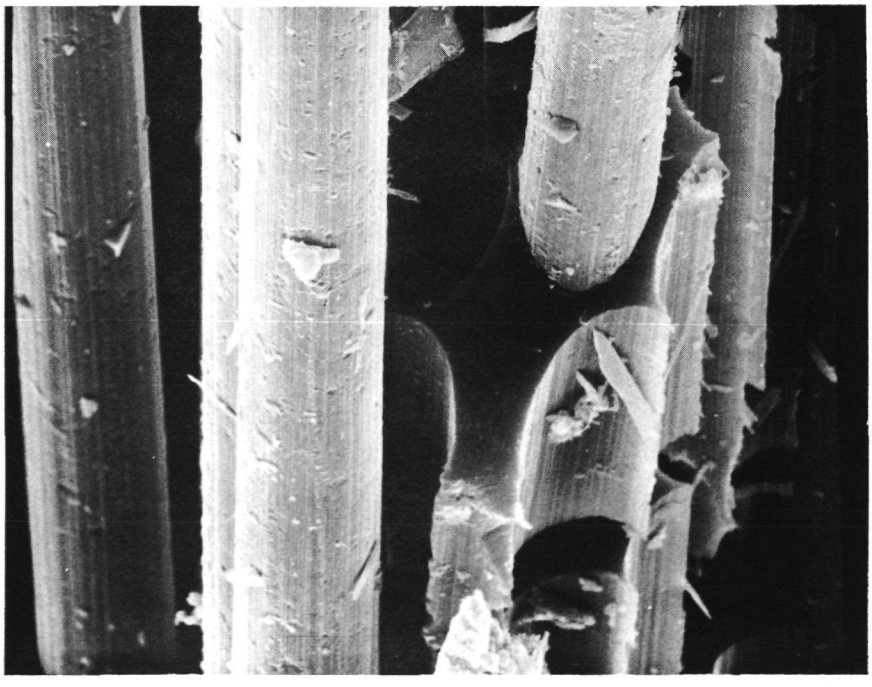

b)

5μm

Fig. 32. Fracture Surface of Th Pitch Fiber Reinforced 774 M (with Scrim)

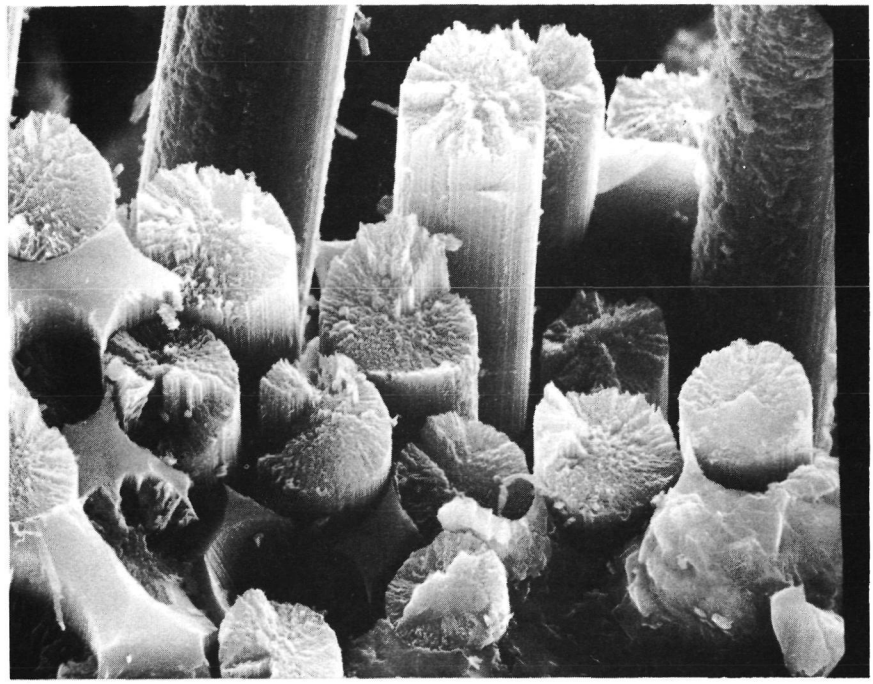

a)

5μm

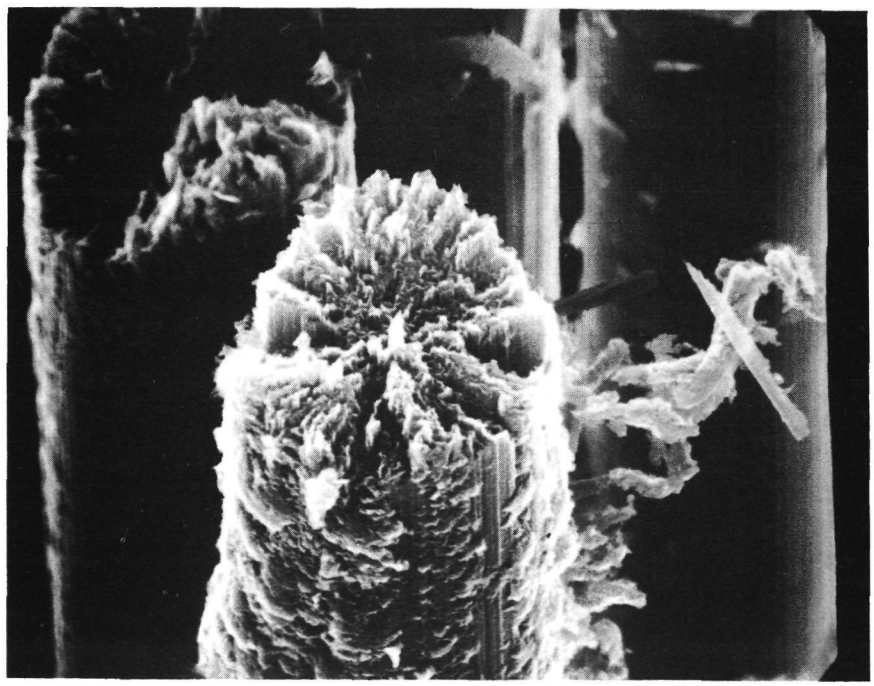

b)

2μm

Fig. 33. Fracture Surface of Th Pitch Fiber Reinforced 774M

80-4-121-5

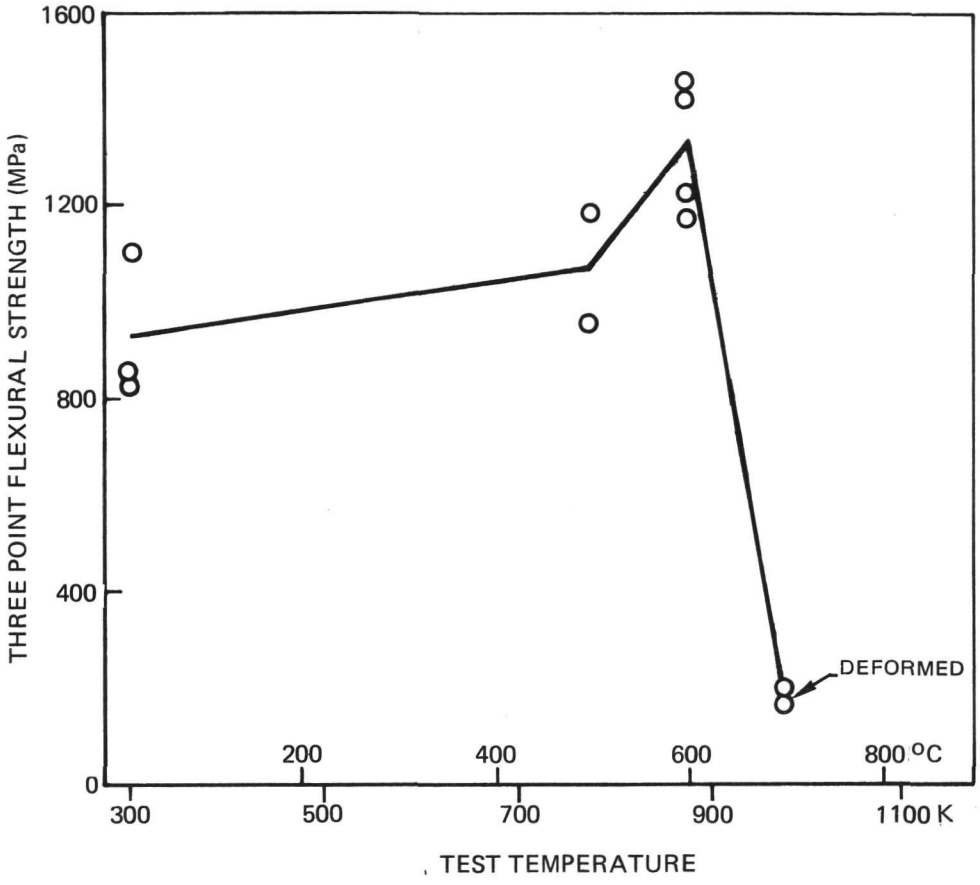

Fig. 34. Three Point Longitudinal Flexural Strength for HMS Reinforced 774M (No Scrim) as a Function of Test Temperature (Tested in Argon)

79-01-171-1

previously in Fig. 16 for composites fabricated at 1723 K. Analysis of this composite indicated that it contained 71% by volume fiber, 27% matrix glass and approximately 1-2% voids. The flexural strength increased with increasing temperature to a maximum average of 1324 MPa at 873 K and then decreased with increasing test temperature. This behavior was reported previously (Refs. 6,7) and is typical of borosilicate glass matrix composites. Up to the temperature of 873 K composite failure occurs by fiber and matrix rupture at the maximum applied load. However, at temperatures above 873 K specimen failure is due to extensive matrix deformation which permits the specimen to deform without fracturing. The data in the figure, for specimens tested at 973 K, are labeled "deformed" to indicate that the values reported do not correspond to composite strengths but are simply elastic calculations based on the maximum load achieved.

Composite three-point bend test data were also obtained over a wide range of span-to-depth ratios to better examine composite behavior. Because of both the complex stress state generated in a three-point bend test, and also because of multiple composite failure modes possible, the resultant test data are presented both as flexural strength and also shear strength values. In both cases the strength calculations were made using the following simple beam equations which determine the maximum flexural stress (σ_{max}) on the beam tensile surface, and the maximum shear stress (τ_{max}) which occurs at the beam mid plane.

$$\sigma_{max} = \frac{3}{2}\frac{PL}{bh^2} \qquad \tau_{max} = \frac{3}{4}\frac{P}{bh}$$

In these expressions P represents the load applied to the specimen mid span, L is the span, b and h are the specimen width and depth respectively. Thus, during any given test the ratio of maximum applied shear to flexural stresses depends on the specimen span-to-depth ratio (L/h). Since a given material can fail by either shear or tension, one of these failure modes will occur first depending on test configuration. For high longitudinal strength composites, the large ratio of tensile to shear strength causes these materials to deform by shear for test configurations having low values of (L/h) and to fracture in tension for high values of (L/h). In the figures to be described below, composite flexural and shear strengths are calculated for all specimens tested. It should be noted that actual composite strength does not vary with span-to-depth ratio. It is only the calculated values which vary due to the fact that an inappropriate failure mode is assumed. The first example below for 0^{o}-GY70/774M demonstrates this point clearly where it will be shown that the test data provide an accurate assessment of material flexural strength and an underestimate of material shear strength.

The data obtained for 0°-GY70/774M are presented in Figs. 35 and 36 as a function of test span-to-depth ratio. The flexural strength data, Fig. 35, exhibit little or no dependence on test geometry or temperature over the ranges of (L/h) and temperature investigated. For all specimens tested, the average strength is 630 MPa. In contrast, the calculated individual specimen 300 K shear strength data, Fig. 36, show a continuous decrease in strength with increasing (L/h). The line drawn through the data was obtained, not by fitting the data points, but by calculating an effective shear strength for each value of (L/h), based on the average 300 K flexural strength of 600 MPa. This correlation suggests that failure of all of the specimens was controlled by the flexural strength of the material and that true shear failure did not occur. Thus, the data plotted in Fig. 36 are simply the calculated maximum shear stresses acting on the beam mid-plane during test. The true shear strength of the material was not reached and thus it must exceed a value of 55-60 MPa as determined by this test technique. On the other hand, the true flexural strength appears to have been determined at 600 MPa.

Examination of the fractured bend specimens confirms the above. Even at the smallest value of L/h tested (5.4), the specimens failed without any sign of shear deformation. Instead, fracture propagated across the specimen after initiating on the tension side of each beam. This is characteristic of the GY70/774M system in which the fiber-matrix bond appears to be quite strong.

Another interesting aspect of this test is the value of elastic modulus obtained as a function of (L/h), Fig. 37. The modulus calculation was performed based on the assumption of no deformation due to shear taking place; however, as can be seen from the figure, this assumption is only good for very large (L/h) values. For small values of span-to-depth ratio, elastic shear deformation can be substantial because of the much lower shear modulus of the material, as compared to the true axial elastic modulus of approximately 325 GPa.

The similarly obtained data for 0^{o}-HMS/774M composites are presented in Figs. 38 and 39. Unlike the GY70 reinforced composites, the flexural strength was found to vary substantially with span-to-depth ratio. The significant decrease in calculated flexural strength in the low (L/h) region implies that some shear failure is taking place. This is in agreement with the observation that the specimens passed through the maximum in the load-deflection trace without the appearance of any visible cracking on the specimen tensile surfaces. The specimens were not, however, severely bent after testing; only a slight overall change in specimen shape was detected after test. The shear strength data, Fig. 39, do not indicate unambiguously that the value of approximately 60 MPa can be taken as the effective material shear strength. However, by virtue of the observed failure mode described above, it is highly probable that this is fairly close to the actual material value.

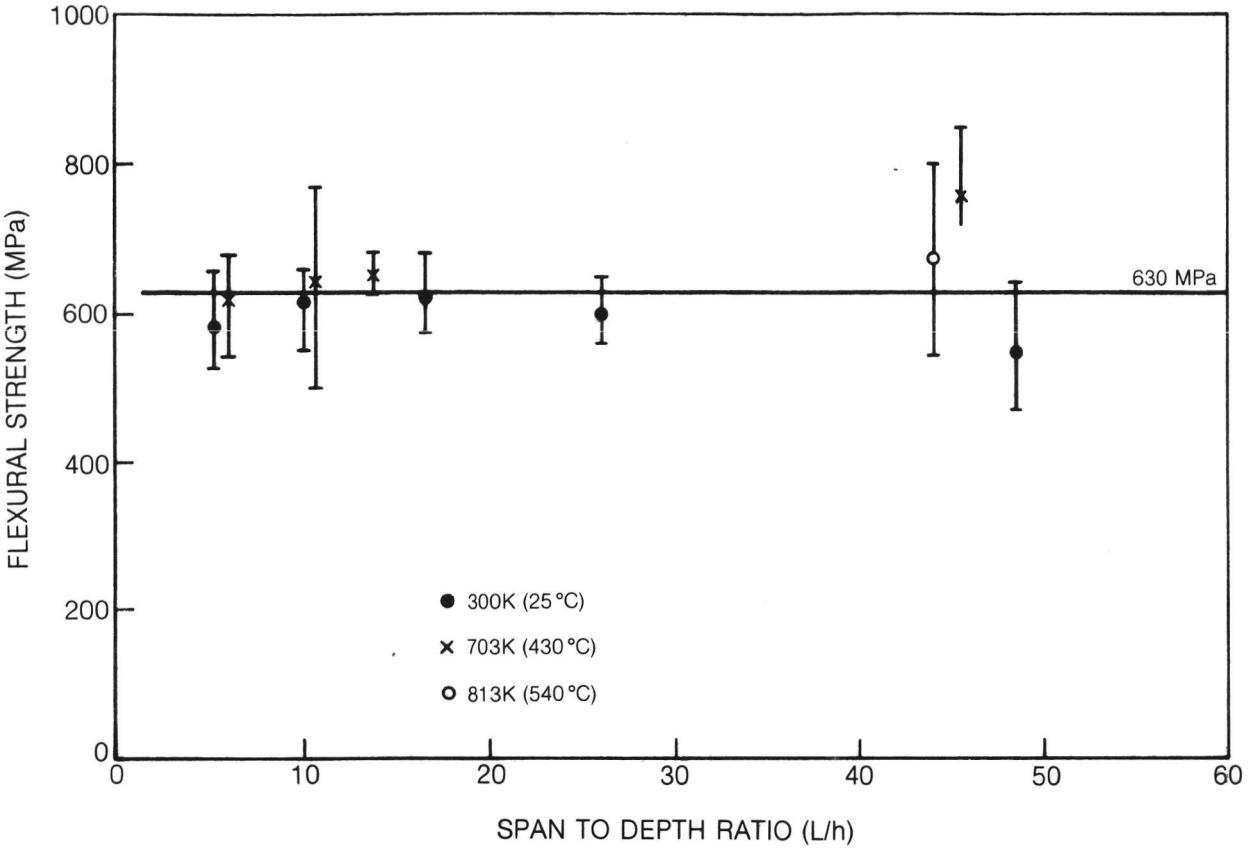

Fig. 35. Observed Flexural Strength as a Function of Span to Depth Ratio for 0° — GY70/774M (Tested in Air)

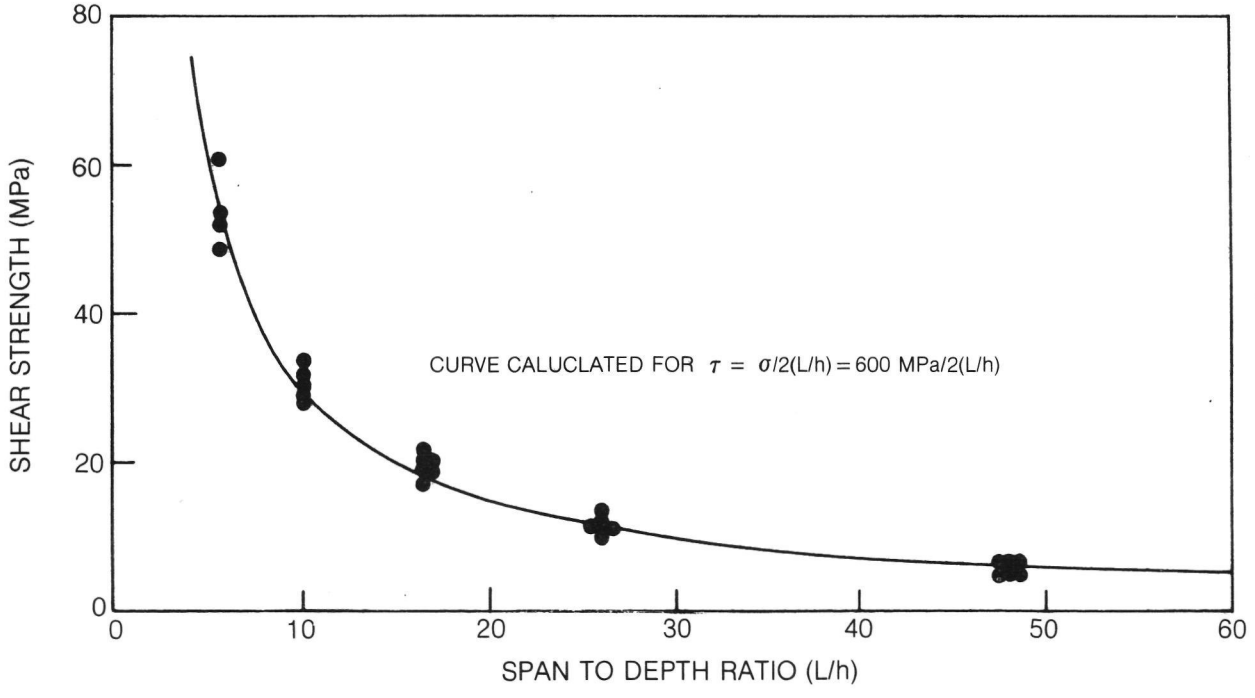

Fig. 36. Observed Shear Strength as a Function of Span to Depth Ratio for 0° — GY70/774M at 300K (Tested in Air)

80–5–82–3

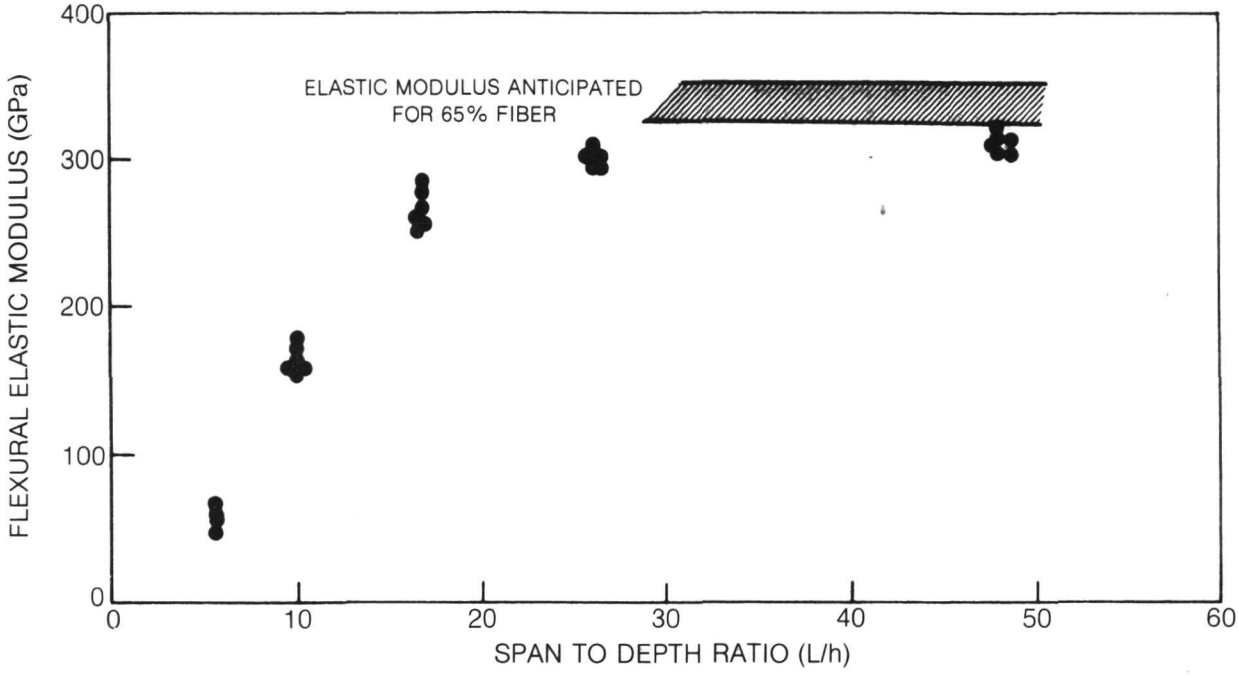

Fig. 37. Observed Flexural Elastic Modulus as a Function of Span to Depth Ratio for 0° — GY70/774M at 300K

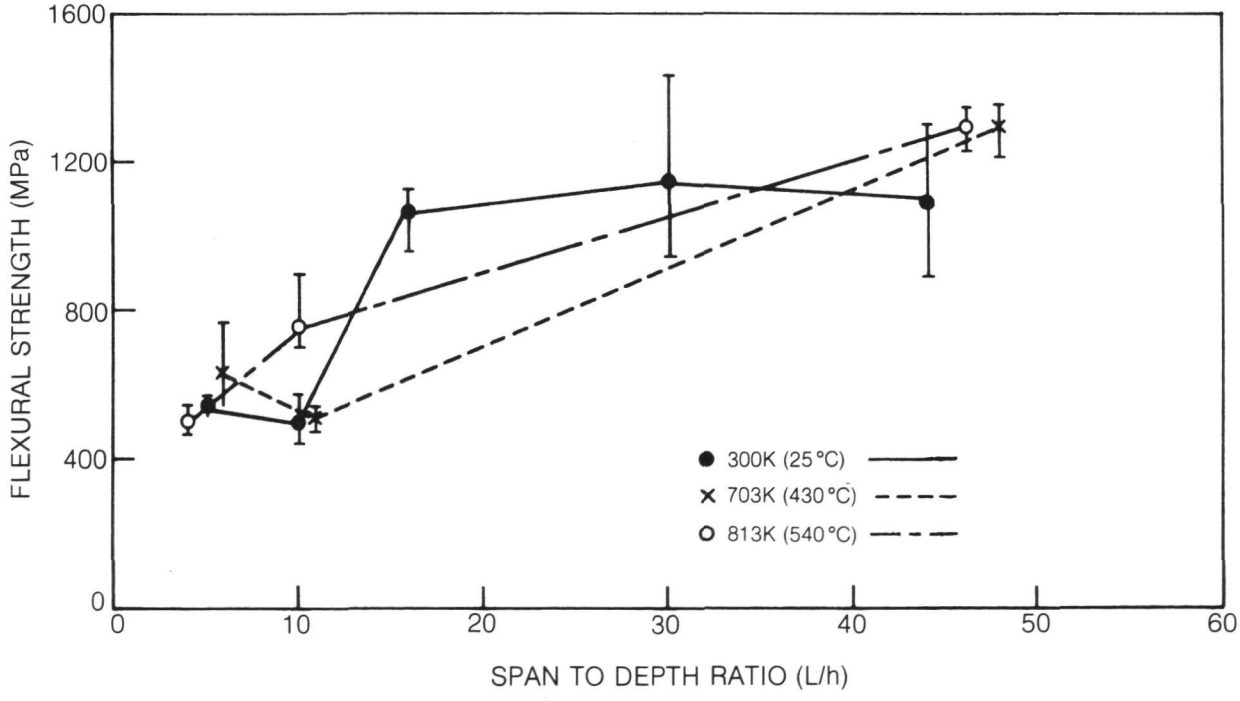

Fig. 38. Observed Flexural Strength as a Function of Span to Depth Ratio for 0° HMS/774M (Tested in Air)

80–5–82–4

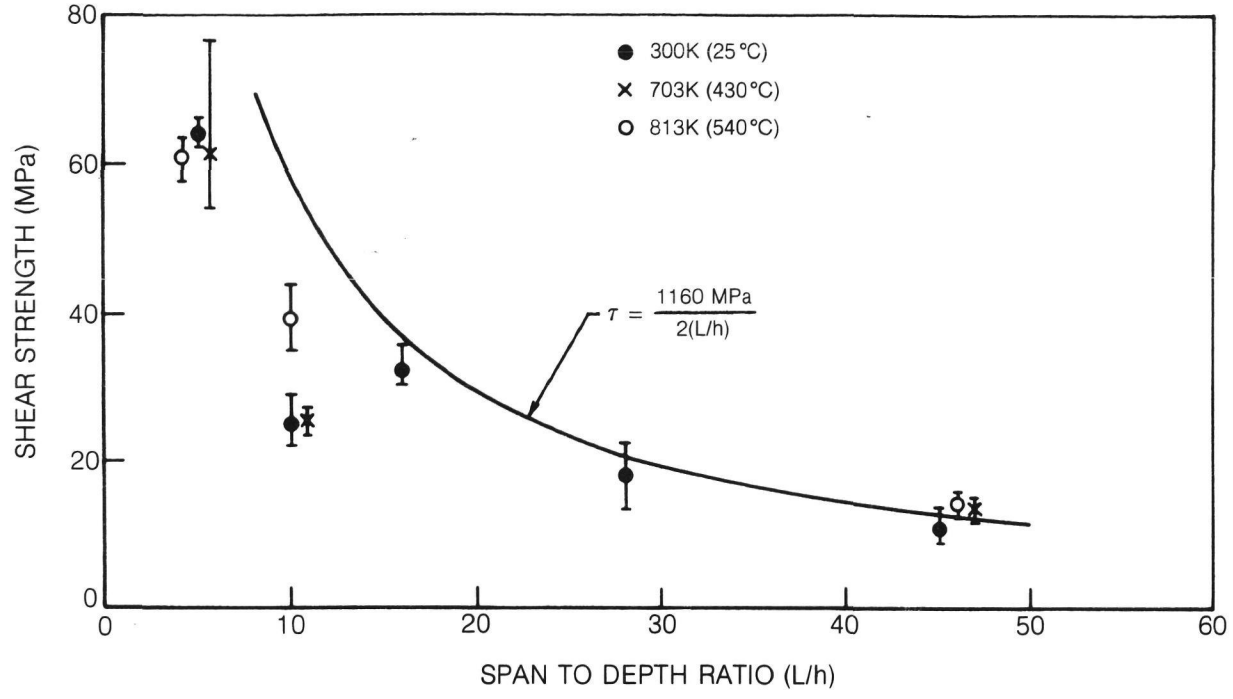

Fig. 39. Observed Shear Strength as a Function of Span to Depth Ratio for 0° HMS/774M (Tested in Air)

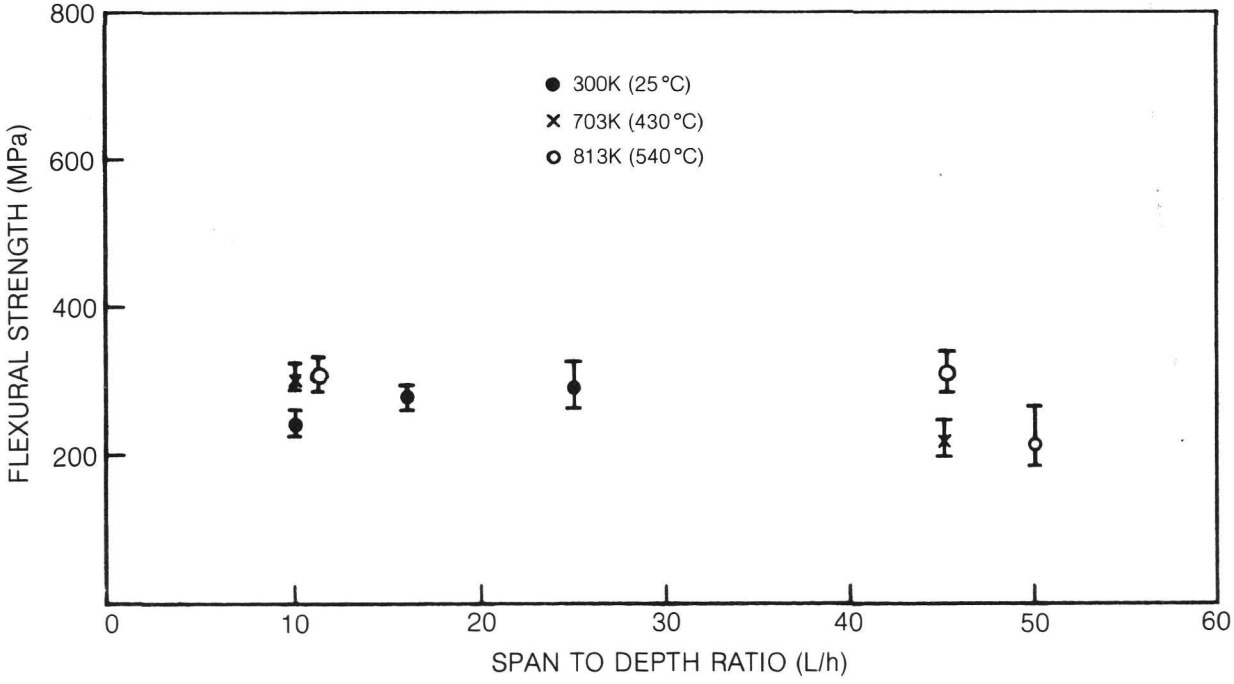

Fig. 40. Observed Flexural Strength as a Function of Span to Depth Ratio for 0/90 GY70/774M (Tested in Air)

80-5-82-5

The data for 0/90 cross ply specimens of both GY70 and HMS fiber reinforced 774M are presented in Figs. 40-43. In these cases both the calculated composite flexural strengths and shear strengths were considerably less than those of the unidirectionally reinforced specimens described above. All of the GY70 fiber reinforced specimens tested in the 0/90 lay-up failed by the formation of visible cracks on their tensile surfaces, while in the case of the HMS fiber reinforced specimens, no evidence of tensile failure could be found at a span-to-depth ratio of 10 indicating the likelihood of shear failure taking place. It is also interesting to note that, for the HMS/774M composites at this lowest L/h value, the calculated shear strength (and thus also calculated flexural strength) decreased with increasing test temperature.

C. Composite Three Point Flexural Creep and Oxidative Exposure

The times to rupture vs the applied maximum flexural stress for unidirectionally reinforced HMS and GY70 fiber reinforced 774M glass are presented in Figs. 44 and 45. The three-point flexural strengths of as-fabricated specimens are also shown at the zero hour position. In both fiber cases it was found that all specimens tested at 813 K failed prior to the 200 hr time used as a "run out" condition. In contrast, at 703 K almost all specimens survived for the full 200 hrs even though some of the applied maximum flexural stresses were within the range of the original composite strength.

To aid in interpretation of the stress rupture data, both figures also include data which indicate the residual composite strength obtained from specimens that were exposed to the test temperatures indicated without any applied stress (Ref. 7). Thus, at 813 K it would appear that the application of stress accelerated composite degradation and that specimen failures occurred at times and stress levels less than anticipated simply on an oxidative basis. At 703 K, however, the stress rupture times extend into the residual strength band indicating that the continuous application of stress was not important in degrading composite strength.

The residual strengths of both the GY70 and HMS fiber reinforced specimens which survived 200 hrs of stressed exposure at 703 K were also measured and found to coincide with, or exceed, the strengths expected for specimens exposed to unstressed oxidation (Ref. 7).

A detailed description of the elevated temperature oxidative degradation of graphite fiber reinforced glass composites can be found in Ref. 7 where it is shown that the primary mechanism of degradation is simply oxidation of the graphite fibers. It was shown that the three point bend test is particularly sensitive to this phenomenon due to the degradation having occurred on the specimen outer surface which is most highly stressed in the flexural test. Also of note was the observation that fiber oxidation occurred in directions both parallel and transverse to the principal fiber axis; the more rapid rate of oxidation occurring in the axial direction.

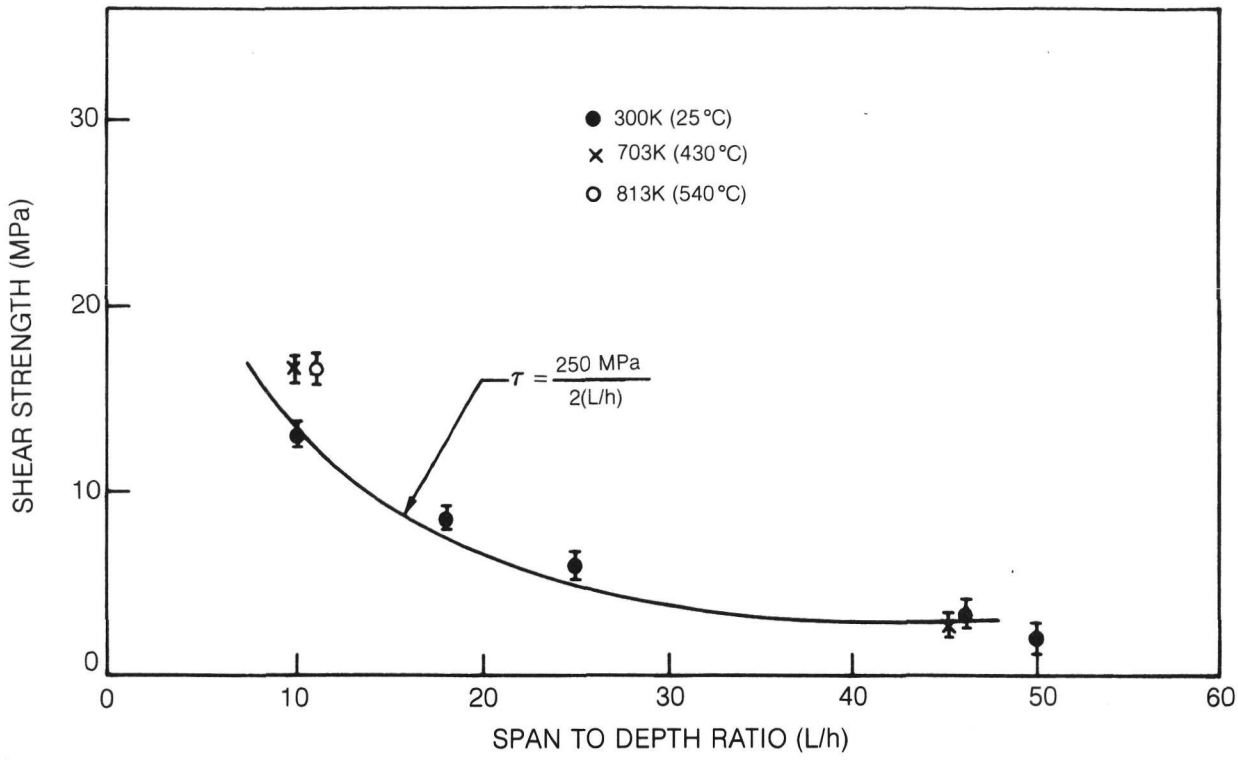

Fig. 41. Observed Shear Strength as a Function of Span to Depth Ratio for 0/90 GY70/774M (Tested in Air)

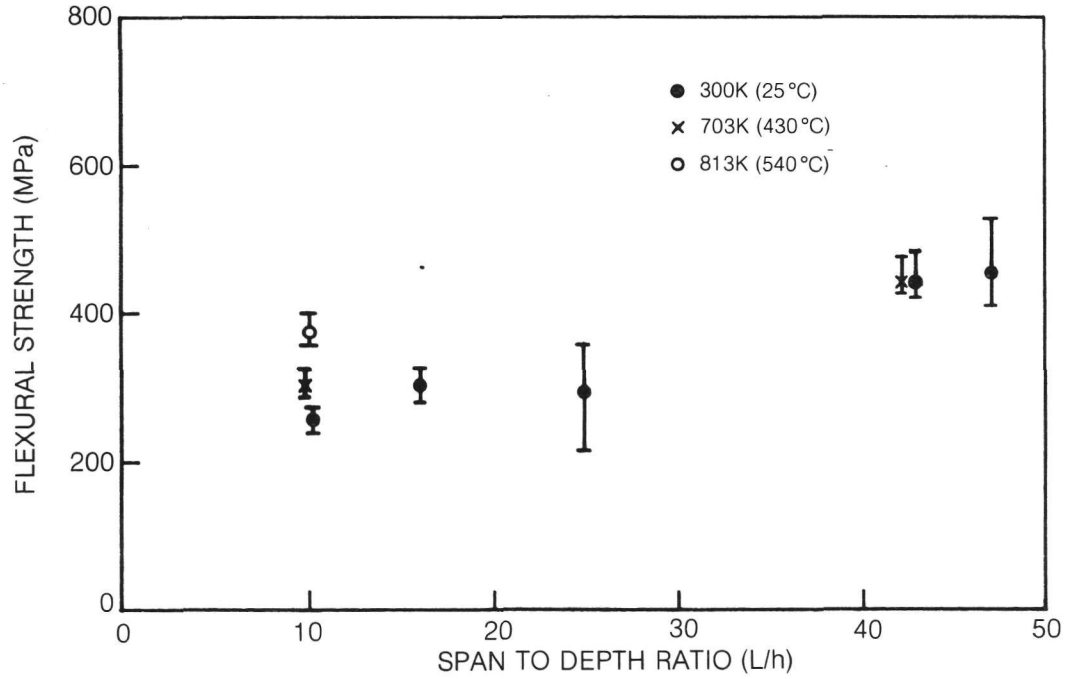

Fig. 42. Observed Flexural Strength as a Function of Span to Depth Ratio for 0/90 HMS/774M (Tested in Air)

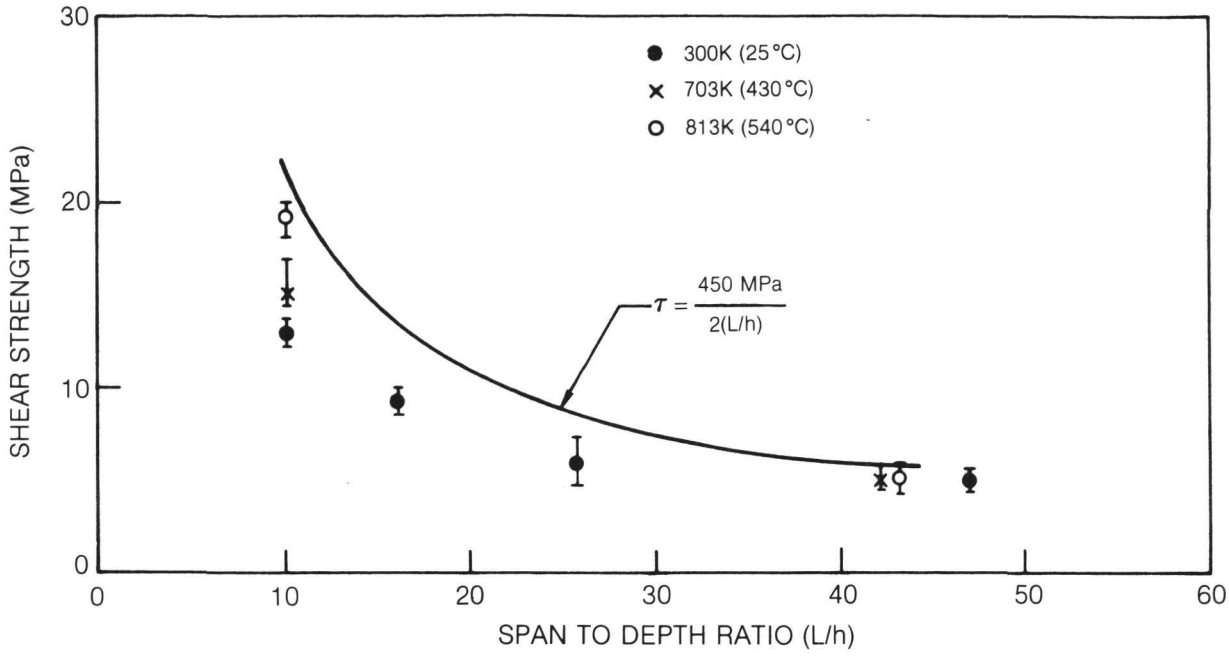

Fig. 43. Observed Shear Strength as a Function of Span to Depth Ratio for 0/90 HMS/774M (Tested in Air)

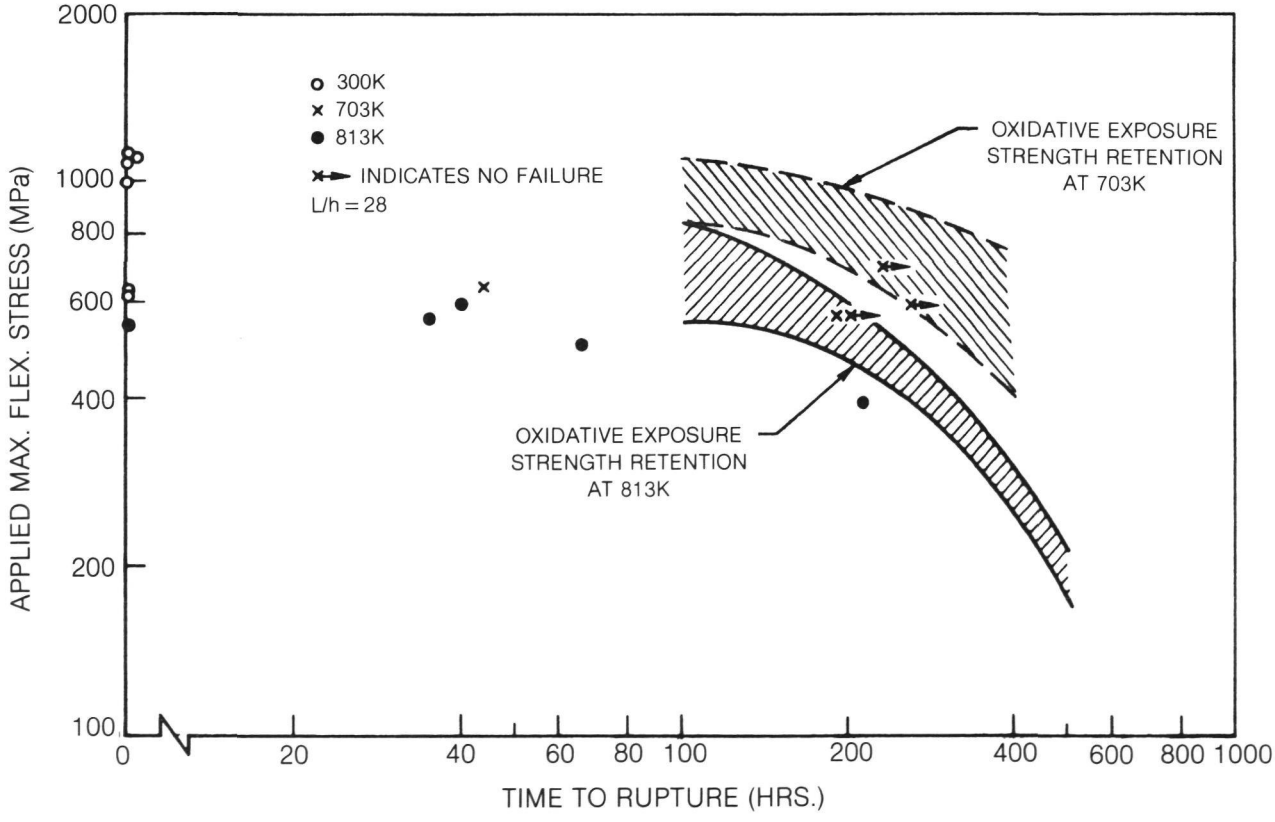

Fig. 44. Applied Maximum Flexural Stress vs. Time to Rupture for 0° — HMS/774M (Tested in Air)

80–5–82–7

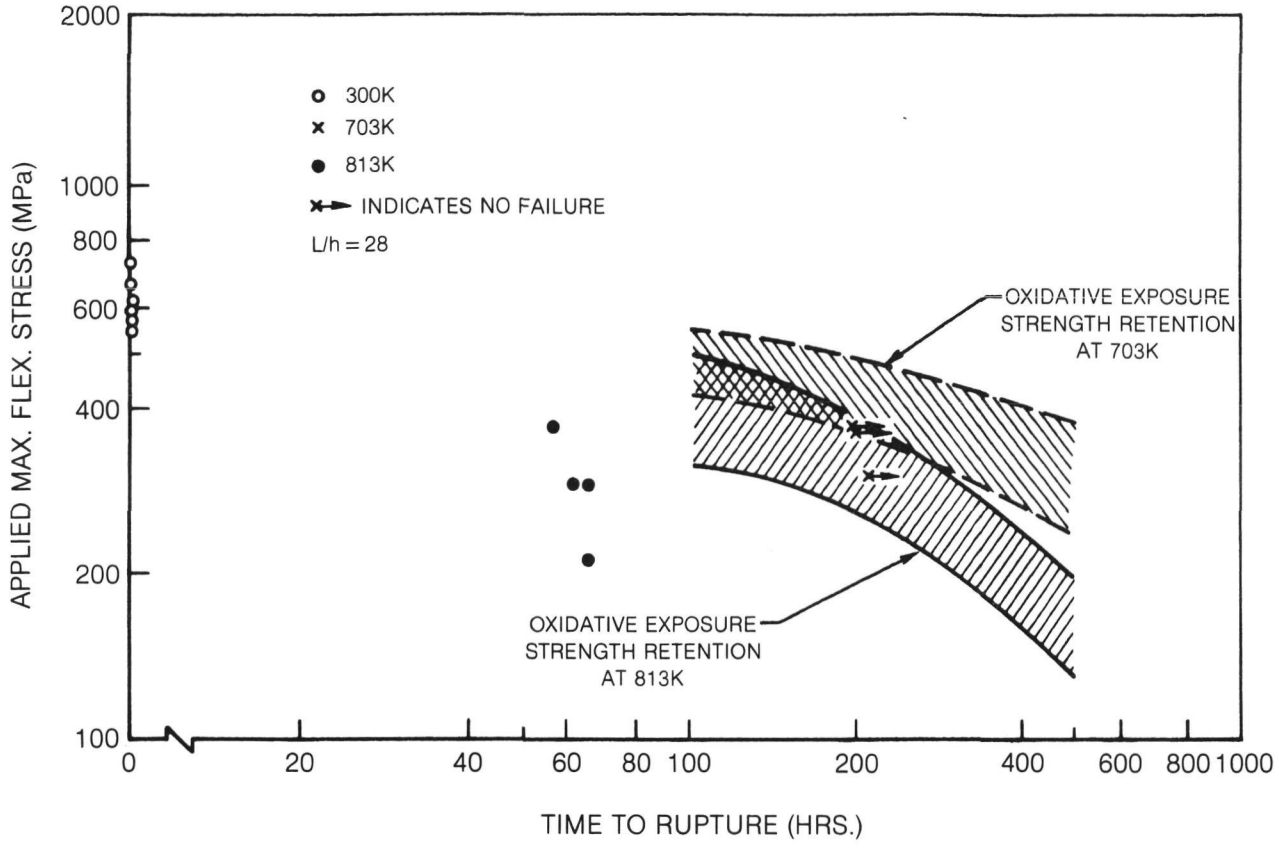

Fig. 45. Applied Maximum Flexural Stress vs. Time to Rupture for 0° — GY70/774M (Tested in Air)

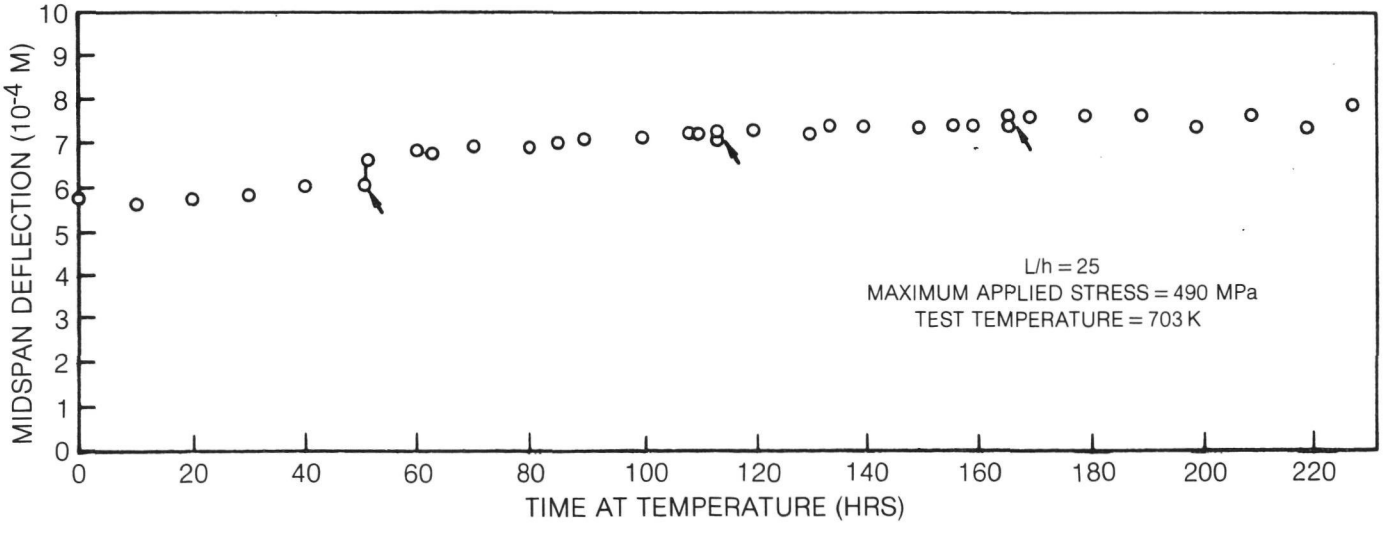

Fig. 46. Flexural Creep of 0° — HMS/774M at 703K

80-5-82-8

Specimen creep deformation, as measured by changes in mid-span deflection, was found to be quite small for the 703 K test condition and very large for 813 K. The data in Fig. 46 are for a specimen loaded at 703 K to 490 MPa, which is approximately 70% of the average room temperature flexural strength of this material. The initial deflection, recorded at the onset of loading, is a purely elastic response of the specimen while the increase in deflection with time implies gradual creep of the material. After 230 hrs the total extent of this additional deflection is equal to approximately 38% of the total initial elastic deflection of the specimen. Although most of this deformation occurred at a nearly constant rate, there are three instances noted on the chart where small discontinuous increases in deflection were recorded. The sum total of these displacement increments can account for approximately 50% of the total creep deflection recorded.

The second creep curve, Fig. 47, was obtained by first loading (at 703 K) a specimen to 500 MPa and then, after 138 hrs, increasing that stress to 640 MPa. The latter stress level is approximately 90% of the average room temperature flexural strength of this material; however, no extensive specimen creep was noted after an additional 60 hr exposure.

At 813 K specimen deformation occurred much more rapidly, Fig. 48, with the rate of deformation increasing with increasing time. This is undoubtedly due to the degradation and progressive fracture of graphite fibers due to oxidation. In addition, the fractured composites did not appear to be bent, indicating the absence of any major matrix deformation controlled mode of failure.

D. Three Point Flexural Fatigue

The fatigue data are presented in Figs. 49-52 where the maximum applied flexural stress is plotted vs the number of cycles to failure. Those specimens which did not fail after 10^6 cycles were then monotonically loaded in three-point bend to determine their residual strength. The 300 K data for 0^o-GY70/7740 composites are presented in Fig. 49 where it can be seen that maximum applied fatigue stresses well into the range of the monotonic composite strength were sustained for 10^6 cycles. Only one specimen failed prior to the run out level and the applied maximum stress on that specimen was well within the unfatigued strength range. In addition, the residual strengths of all of the fatigued specimens were also well into this range indicating that the fatigue process had not degraded overall composite performance. The 703 K data, Fig. 50, also indicated excellent composite fatigue strength; however, in this case more premature failures were noted. The high residual strength of the specimens that survived 10^6 cycles at 703 K also indicates that the oxidative degradation process was not accelerated by fatigue testing. A 10^6 cycle run out required air exposure at temperature for 93 hrs. The unstressed static exposure of

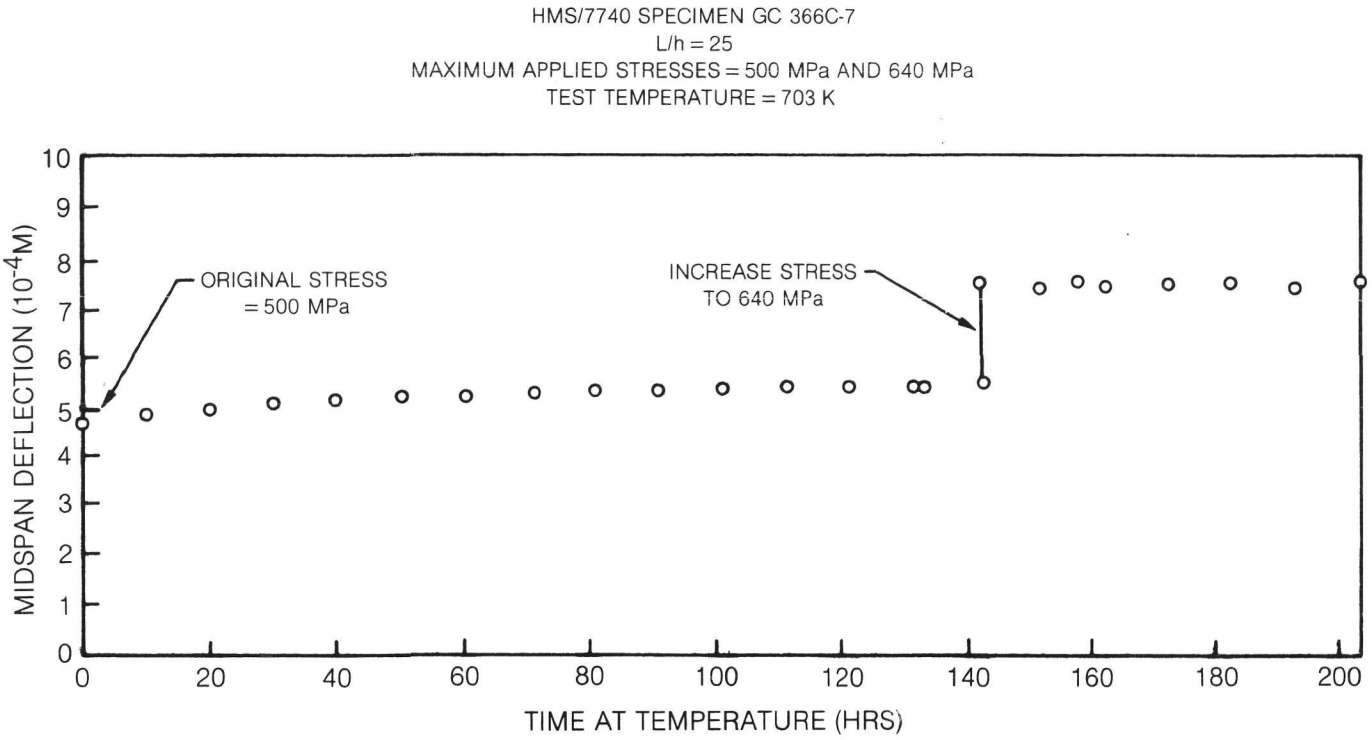

Fig. 47. Flexural Creep of 0° — HMS/774M at 703K

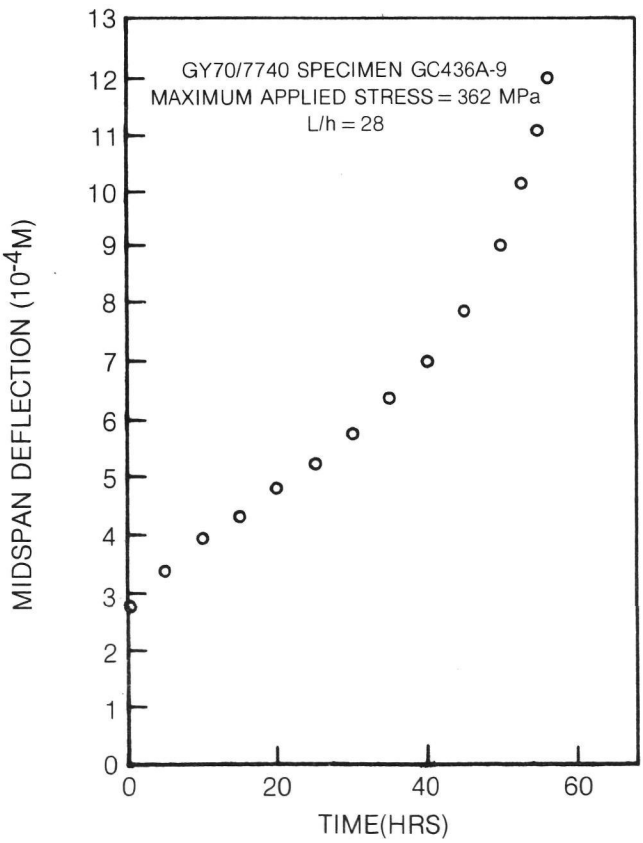

Fig. 48. Flexural Creep of 0° GY70/774M at 813K

80—5—82—9

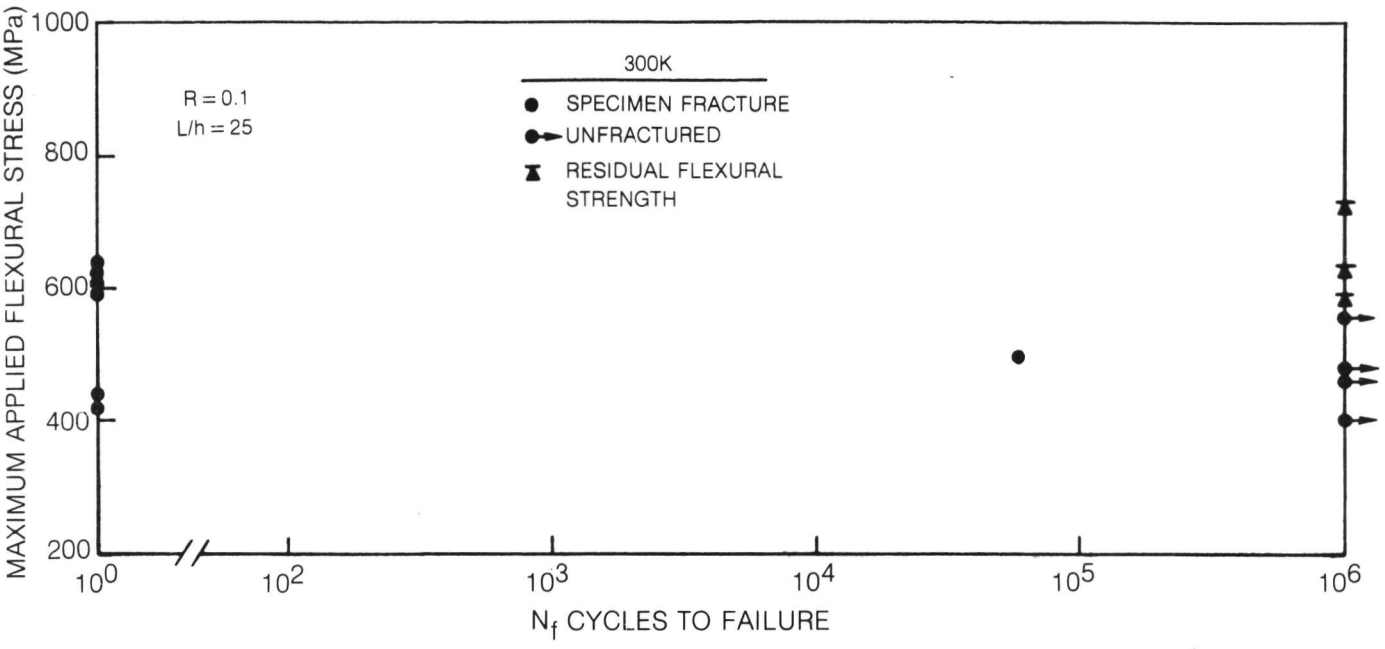

Fig. 49. Three Point Flexural Fatigue of 0° — GY70/774M

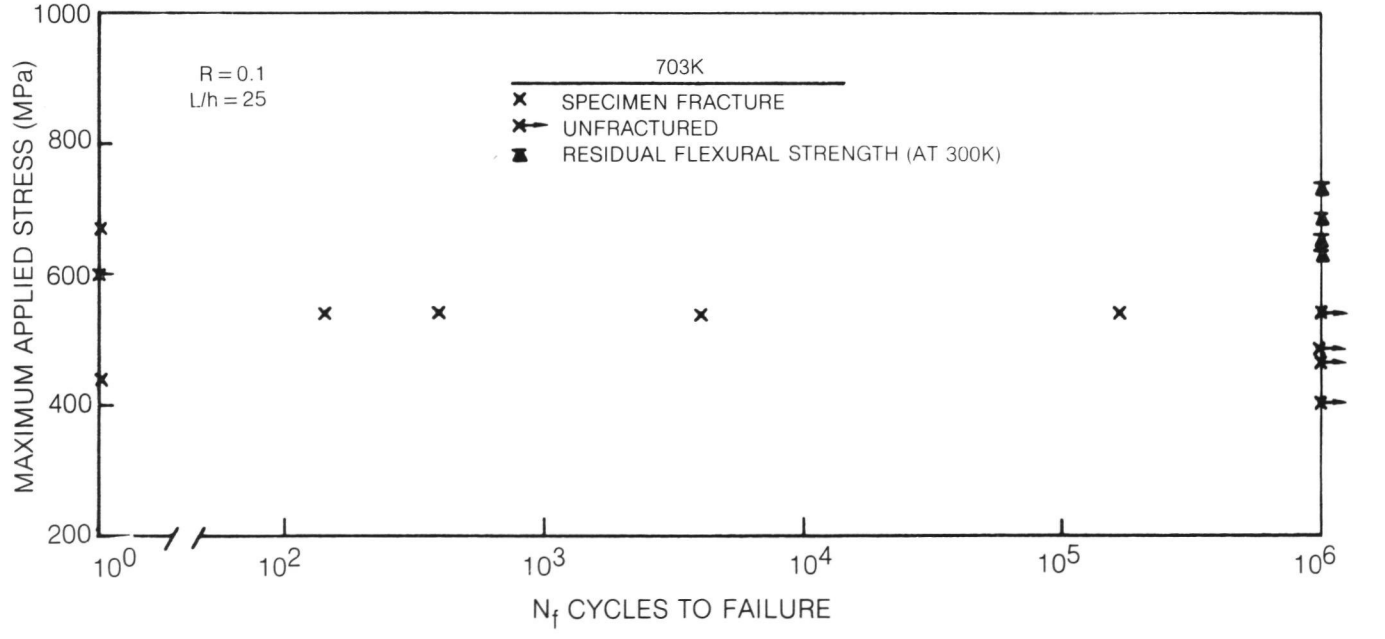

Fig. 50. Three Point Flexural Fatigue of 0° — GY70/774M (Tested in Air)

80–5–82–10

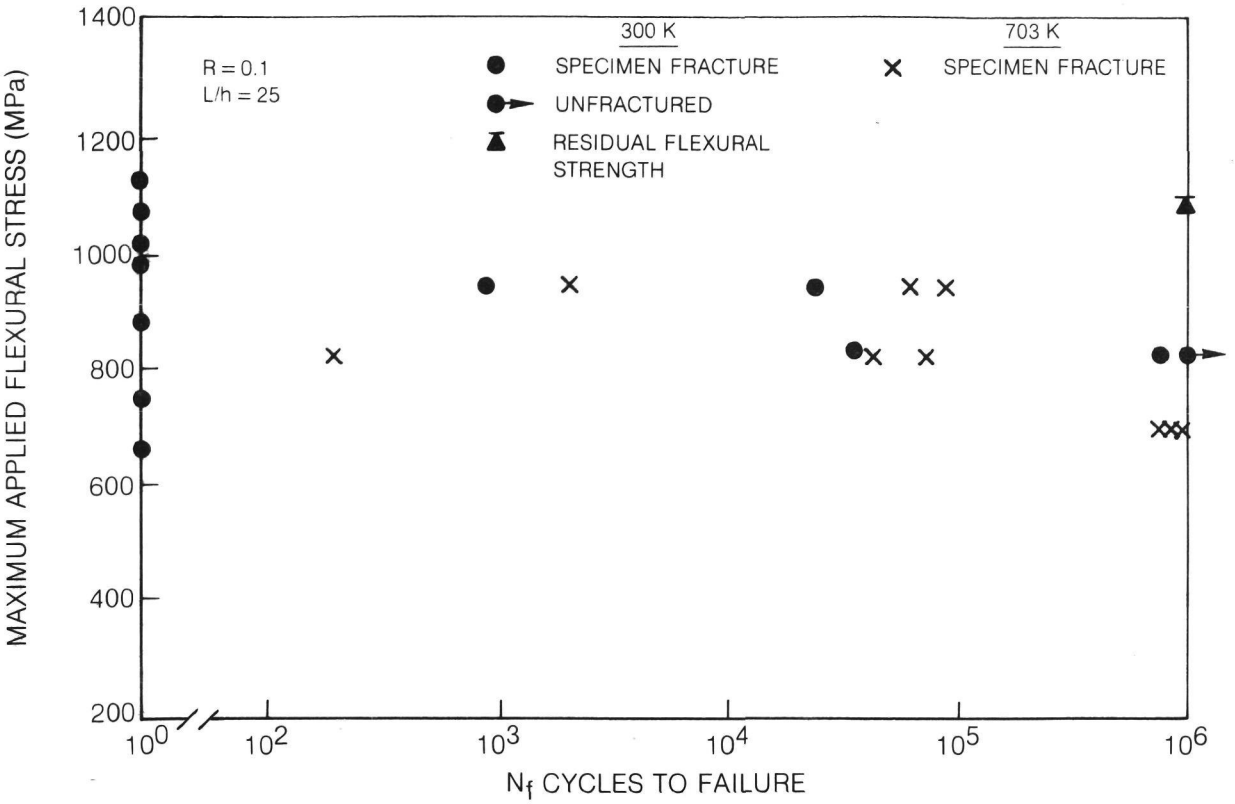

Fig. 51. Three Point Flexural Fatigue of 0° — HMS/774M (Tested in Air)

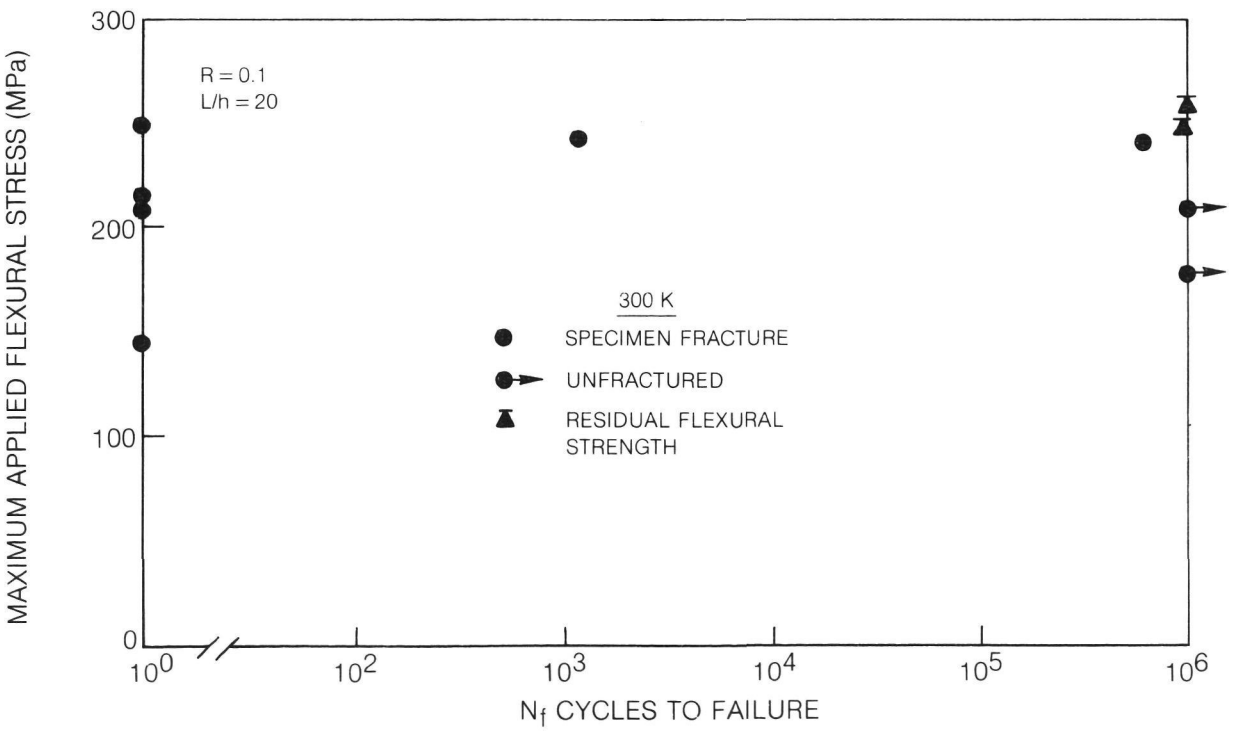

Fig. 52. Three Point Flexural Fatigue of 0/90 — GY70/774M

81–2–100–4

GY70/774M specimens to this condition was shown in Fig. 45 to have only a minor effect on composite properties.

The data for 0°-HMS/774M are presented for both test temperatures in Fig. 51. As in the case of the GY70/774M, fatigue resistance was excellent at 300 K. At 703 K it was not possible to achieve a full 10^6 cycle run out at even the lowest stress level of 689 MPa. However, three specimens tested approached this number of cycles, with one reaching 916,690 cycles prior to fracture.

Several 0/90 GY70/774M cross ply specimens of 0.25 cm thickness were tested in fatigue at 300 K, Fig. 52. The span-to-depth ratio of these test specimens was only 20 because they were not surface ground to the usual specimen thickness prior to testing. Grinding was avoided to prevent damage of the 0° surface plys of the specimens. As in the case of the 0° specimens described above, the cross ply material exhibited excellent fatigue resistance with 10^6 run out occurring at relatively high stress levels and residual strength being equal to or greater than that of the unfatigued material.

E. Composite Thermal Fatigue

Both HMS and GY70 fiber reinforced 774M matrix specimens were thermally cycled in air between room temperature and either 703 K or 813 K. Each total thermal cycle required approximately 12 min to complete and included a hold at the maximum temperature for approximately 4.5 min. The heating and cooling portions of the cycles occurred over approximately 2 min each (Ref. 7). The results of these experiments indicated that specimen flexural strength degradation occurred in a manner similar to that observed for static thermal exposure. Both the HMS and GY70 fiber reinforced composites exhibited gradual mass loss with increasing number of cycles and this mass loss caused a measurable decrease in composite flexural strength, Figs. 53 and 54. In the case of thermal cycling HMS/774M to 813 K, examination of the thermal history which took place during each cycle (Ref. 7), it can be judged that 1000 cycles corresponds to approximately 117 hrs at temperatures above 573 K and nearly 75 hrs at 813 K. The 70 to 85% strength retention after 1000 cycles, Fig. 53, is in good agreement with the level of strength retained after 100 hrs of constant temperature exposure, Fig. 44.

Several thermal cycling experiments were also performed on 0/90 cross plied composite material to ascertain whether the degradation mechanism is accelerated by a complex lay-up pattern. The data (Ref. 7) indicate no degradation after 500 thermal cycles which is, in fact, superior to the data presented for unidirectionally reinforced material.

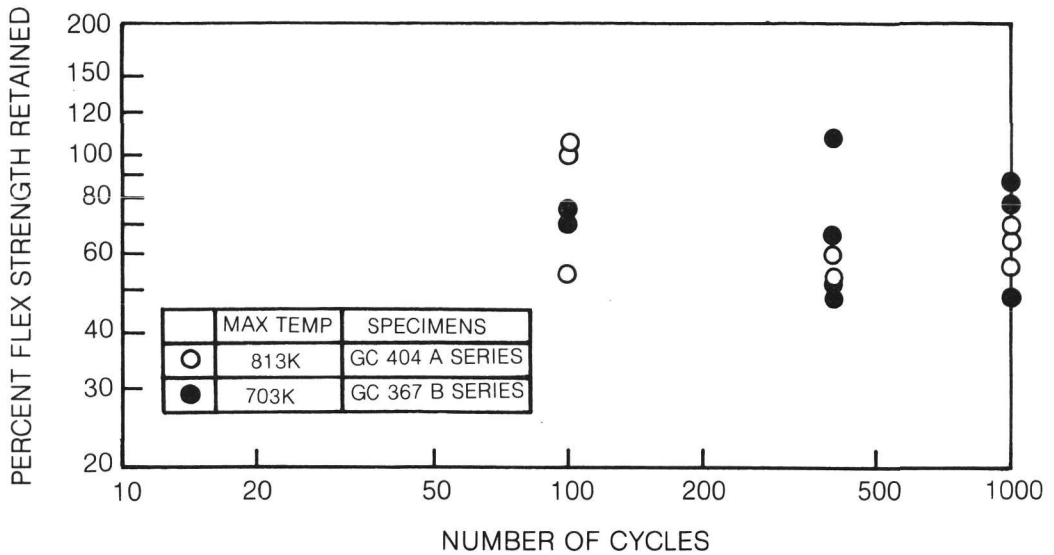

Fig. 53. Change in Flex Strength of HMS Fiber Reinforced 774M Glass as a Function of Number of Thermal Cycles in Air

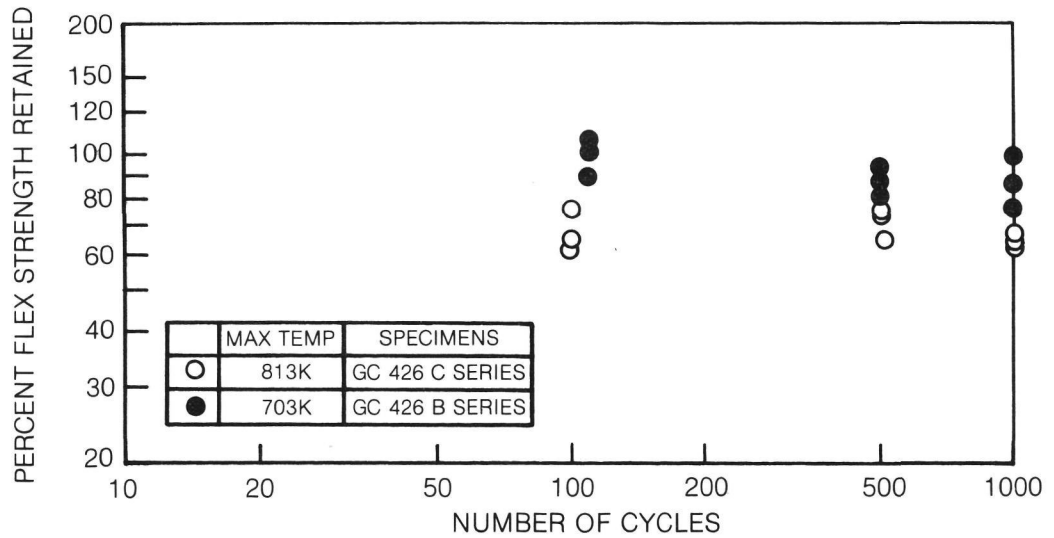

Fig. 54. Change in Flex Strength of GY70 Fiber Reinforced 774M Glass as a Function of Number of Thermal Cycles in Air

F. Composite Crack Growth Resistance

Prenotched HMS fiber reinforced 774M matrix composites were tested under both monotonic loading and in fatigue to ascertain material resistance to crack growth. Stress intensity factors, K, were used in each of the following tests as a measure of material performance with the calculation of K performed using the following formula (Ref. 10).

$$K = \frac{3\ PL\sqrt{c}}{2\ bh^2}\left[A_o + A_1\left(\frac{c}{h}\right) + A_2\left(\frac{c}{h}\right)^2 + A_3\left(\frac{c}{h}\right)^3 + A_4\left(\frac{c}{h}\right)^4\right]$$

where $X = h/b$ $\quad A_o = 1.9 + 0.0075X$
$A_1 = -3.39 + 0.08X$
$A_2 = 15.40 - 0.2175X$
$A_3 = -26.24 + 0.281X$
$A_4 = 26.38 - 0.145X$

P = P_{max} - breaking force or maximum load reached
L = Span - distance between supports
c = notch depth
b = width of specimen
h = thickness of specimen.

The particular specimen dimensions and test procedures used for each of these tests are described in section

1. Temperature and Loading Rate Effects

Prenotched specimens of HMS fiber uniaxially reinforced 774M glass were tested with the direction of crack growth transverse to the fibers. Referring to Fig. 8, the overall dimensions were approximately L = 5.0 cm, B = 1.0 cm, D = 0.8 cm and C = 0.3 cm and all specimens were tested in three point bend using a span of 4.0 cm. The specimens were tested using two different loading rates and three temperatures, Table XII. The maximum load achieved prior to fracture, P_{max}, was taken from load vs time traces obtained through the use of an instrumented impact procedure described in greater detail in Ref. 5.

The fracture toughness data summarized in the table indicate that composite toughness was quite high at room temperature. For comparison, the fracture toughness of uniaxially reinforced graphite epoxy has been measured to be approximately 35 $MN/m^{3/2}$ (Ref. 11) while that of a 6061-T651 aluminum alloy is 30 $MN/m^{3/2}$ (Ref. 12). Unreinforced high strength ceramics, on the other hand, typically exhibit fracture toughness values of 5 $MN/m^{3/2}$ (Ref. 13) or less. The HMS/774M specimens also did not exhibit any dependence of toughness on loading

Table XII

0°-HMS/774M Fracture Toughness.

Test Speed (cm/min)	Test Temp K	Fracture Toughness $MN/m^{3/2}$	Energy Per Unit Area Joules/m^2
20,000	295	21.4	23,500
0.127	295	22.1	
20,000	873	15.8	10,600
20,000	923	19.0	11,800

rate over a factor of 10^5 change. A temperature dependence, however, was noted with a lower number measured at 873 K which, as described earlier, corresponds to the temperature at which composite maximum flexural strength was achieved, Fig. 34. Specimen fracture at this temperature also appeared less fibrous than that at room temperature; however, no mechanism to describe this behavior was discerned.

2. Fatigue Crack Growth

Composite fatigue crack growth resistance was measured by prenotching specimens and then applying cyclic loads in a three point bend test configuration. The material tested consisted of HMS fibers in 774M matrix with the presence of scrim in each layer of the composite. The tensile test data for this material was reported earlier in Table XI. The overall specimen dimensions (referring to Fig. 8) were L = 7.5 cm, B = D = 0.5 cm and all tests were performed with a span of 4.0 cm. In the case of fatigue loading, all specimens were tested with the same starting notch depth, C, of 0.25 cm while specimens with two different notch depths were tested monotonically to failure to determine the starting material fracture toughness. Both 0° unidirectionally reinforced and 0/90 cross ply reinforced specimens were tested with the latter tested in two orientations referred to as "normal" and "edge", Fig. 9, to ascertain the importance of crack growth direction.

The fracture toughness values calculated from the monotonic fracture tests are presented in Fig. 55. The data were obtained for both notch depths and are shown as a function of the ratio of notch depth (C) to total specimen depth (D) and specimen orientation. It is interesting to note that, at the (C/D) ratio of 0.25 the fracture toughness of the 0° and 0/90 "normal" specimens were both lower than the 0/90 "edge" specimen value. This was due to the fact that both specimens exhibited evidence of shear failure. At this notch depth the net specimen section to span ratio is approximately 10 which, in this case, was low enough to cause shear failure. At the larger notch depth the 0° specimen fracture toughness value increased significantly and approached the value reported in the previous section for 0° HMS fiber reinforced specimens that did not contain any scrim. Because of this evidence for a shear contribution to failure, and the following observations of composite failure modes in fatigue, it is questionable as to whether the fracture toughness calculations should be taken as valid measurements of toughness. However, at present there does not appear to be a better method to express the severity of the presence of the notch and hence the values are used as a relative measure of crack growth resistance.

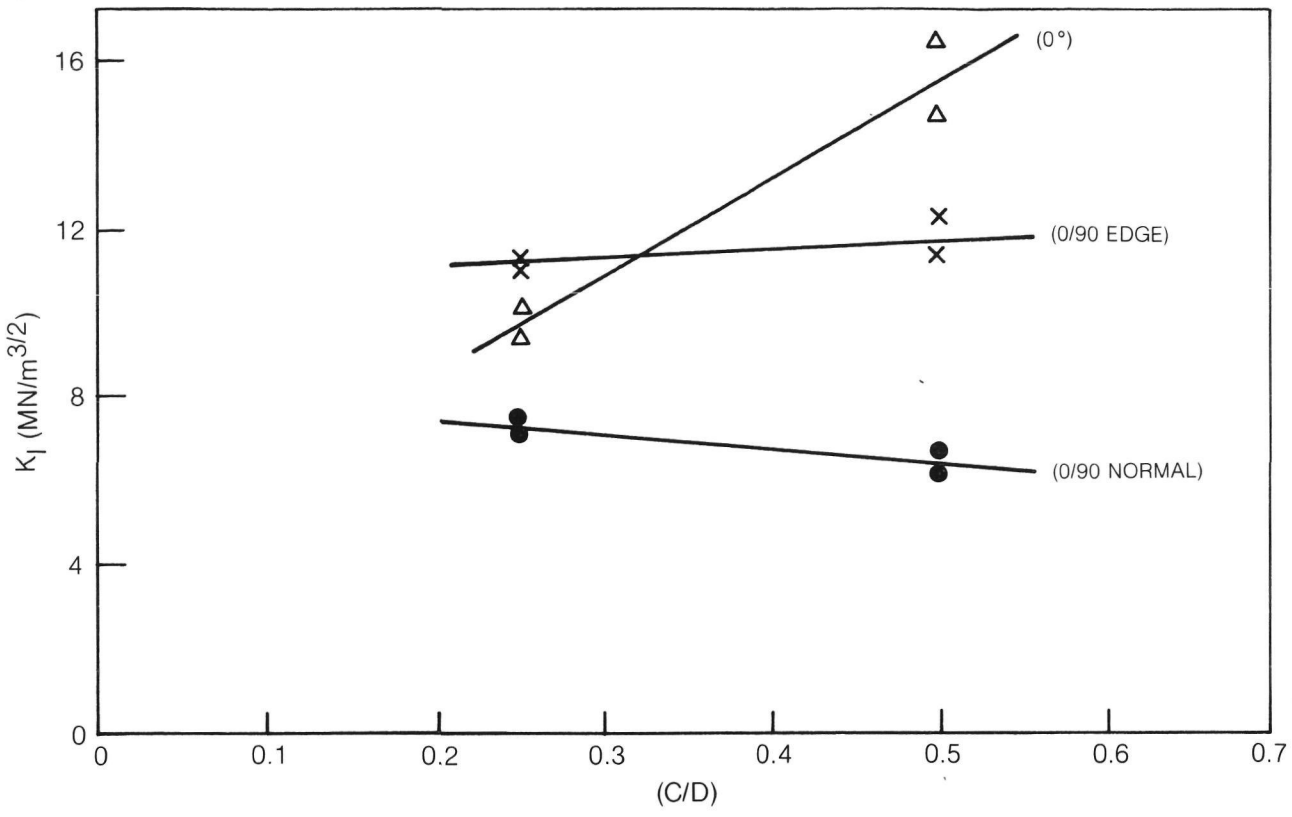

Fig. 55. Prenotched Specimen Fracture Toughness for HMS/774M with Scrim

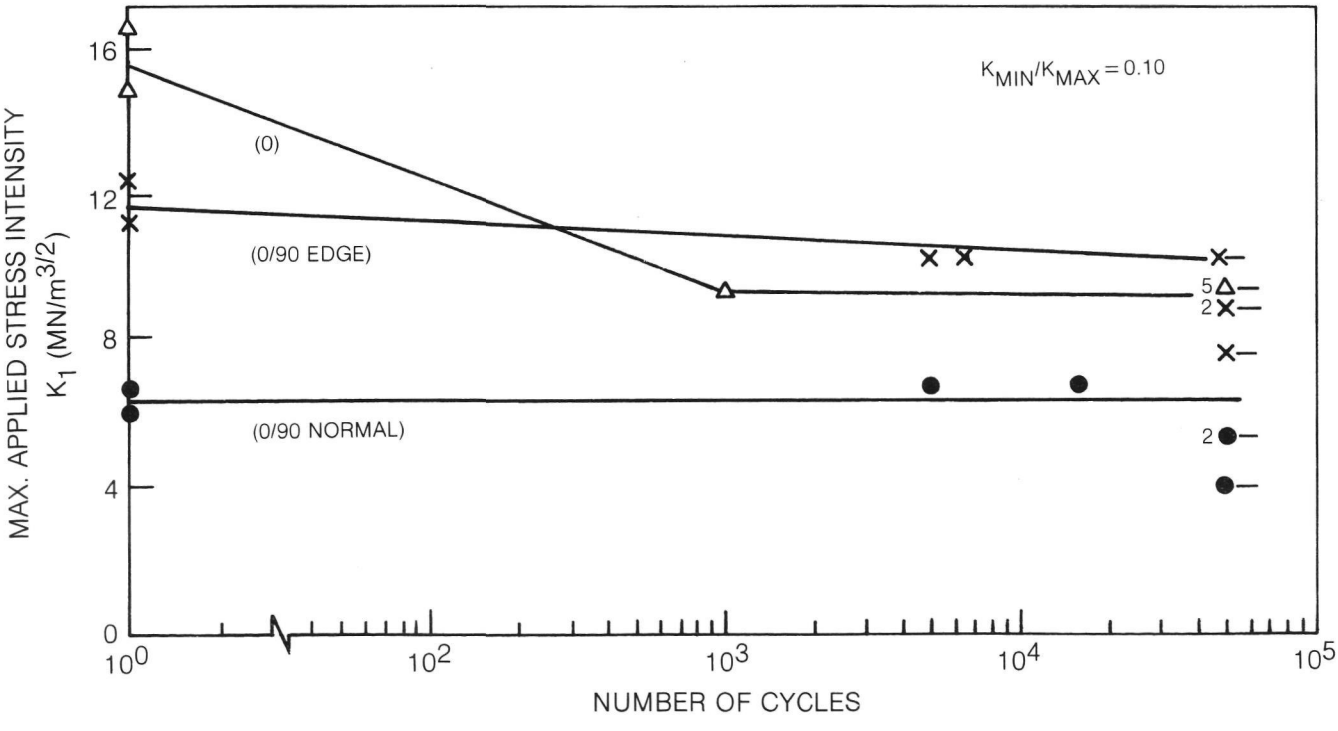

Fig. 56. Fatigue of Prenotched Specimens of HMS/774M with Scrim

81–2–100–8

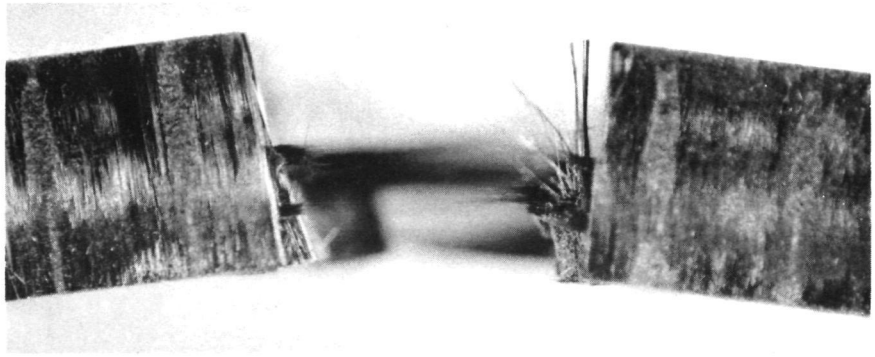

a) "EDGEWISE" ORIENTED SPECIMEN 740-9 FRACTURE AT 6,500 CYCLES

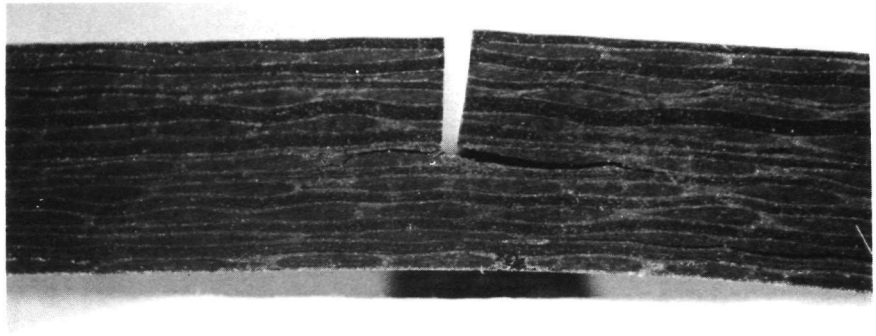

b)'NORMAL' ORIENTED SPECIMEN 739-7 DELAMINATION AFTER 50,000 CYCLES

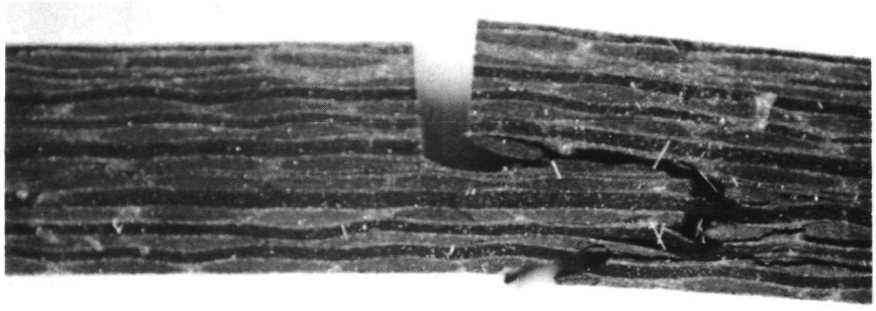

c) 'NORMAL' ORIENTED SPECIMEN 739-9 FRACTURE AT 5,170 CYCLES

Fig. 57. 0/90 Notched Fatigue Specimens

80–07–06–2

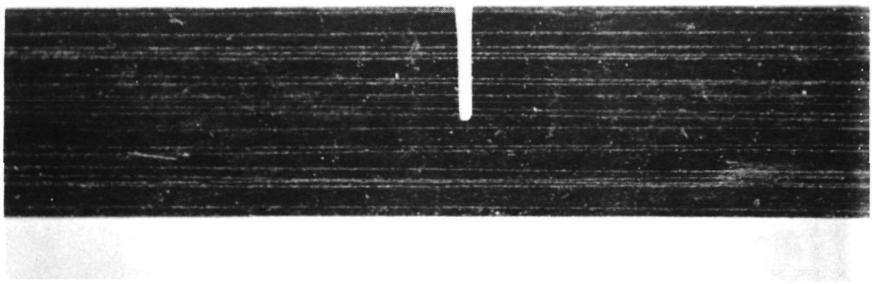

a) SPECIMEN 777-9 AFTER 50,000 CYCLES AT K = 9.2 MN/m$^{3/2}$

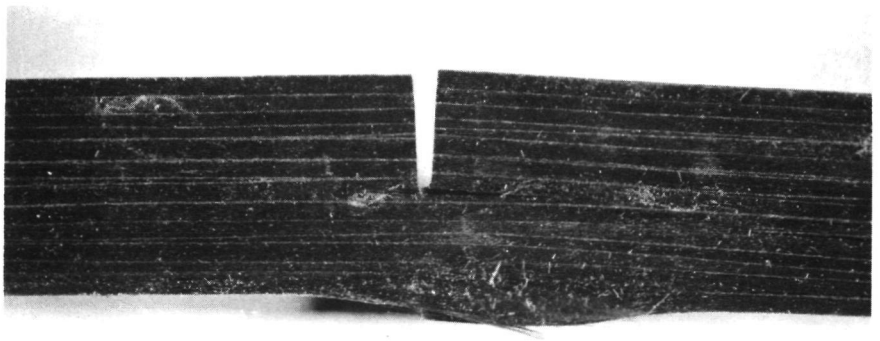

b) SPECIMEN 777-9 AFTER 50,000 CYCLES AT K = 9.2 MN/m$^{3/2}$ AND FRACTURE AT K = 11.9 MN/m$^{3/2}$

Fig. 58. 0° Notched Fatigue Specimens

The fatigue data for the 0° and 0/90 reinforced specimens are shown in Fig. 56 where the maximum stress intensity applied to each specimen is plotted along with the number of cycles to cause fracture. Both of the 0/90 orientations tested, edge and normal, exhibited run out (survival of 50,000 cycles) at high stress intensity levels when compared with their monotonic loading fracture value. In the case of the edgewise oriented specimens, the highest run out condition was 10.3 $MN/m^{3/2}$ which is 87% of the average monotonic fracture toughness value of 11.9 $MN/m^{3/2}$. However, two specimens also fractured prematurely at this stress level after 6500 and 5040 cycles. The major fracture characteristic of these specimens was the very "brushy" nature of the fracture surface, Fig. 57a. The extensive fiber pullout was visible after the specimen was separated into two pieces and was not accompanied by any other fracture modes such as delamination or compression failure as will be described below.

The normal specimens exhibited fatigue fracture after 5170 and 15,970 cycles at a maximum stress intensity value of 6.7 $MN/m^{3/2}$. This level was actually slightly higher than the average monotonic K_I value of 6.45 $MN/m^{3/2}$. These specimens exhibited fractures characterized by extensive evidence of interlaminar cracking occurring at the base of the notch and, as fracture progressed, in regions removed from the notch, Figs. 57b and 57c.

The unidirectionally reinforced composites exhibited both interlaminar and compression failure modes, Figs. 58a and 58b. The latter mode occurred near the location of the central loading nose and appeared as a region of delamination. The fatigue data for the 0° specimens are presented in Fig. 56. In this case, five out of six specimens survived fatigue to 50,000 cycles at a K_{max} value of 9.2 $MN/m^{3/2}$ while one specimen failed after 6020 cycles.

The residual fracture toughness of prefatigued specimens was determined by loading them to failure after fatigue cycling. Because of the difficulty in assessing an effective crack length after prefatigue, the residual toughness values were calculated using the original premachined notch depth. Thus, the calculated residual toughness values are just a measure of residual structural performance rather than material toughness. The resultant data, Table XIII indicate that, for the 0/90 oriented specimens, fatigue cycling did not cause a major degradation of composite performance. Specimen 739-7 (edgewise) which had been shown in Fig. 57b to have a longitudinal crack at the base of the notch, exhibited a residual toughness which was approximately 20% lower than the average of the unfatigued composite. However, this difference may not be significant within the overall population of specimen performance. In the case of the 0° data, one specimen in particular (777-12) definitely indicated that specimen degradation had occurred. This was probably due to the extension of the initial machined notch depth while the fact that the other two specimens still retained the toughness of the unfatigued material relates to the fact that the initial notch had been effectively blunted.

Table XIII

Residual Fracture Toughness of Prefatigued
HMS Fiber Reinforced 774M Composites with Scrim

Composite Specimen	Orientation	Prefatigue K_{max} $MN/m^{3/2}$	Prefatigue # Cycles 10^3	Residual Toughness+ $MN/m^{3/2}$
739-7	0/90 Edge*	4.0	50	5.0
-9		5.3	50	7.1
740-7	0/90 Normal**	7.7	50	10.0
-8		10.3	50	12.1
-10		9.0	50	10.7
-12		9.0	50	11.0
777-8	0°***	9.2	50	15.3
-9		9.2	50	11.9
-12		9.2	50	6.7

+ Residual toughness calculated using the original specimen machined notch depth

* Range of fracture toughness for unfatigued specimens of this orientation was 6.2-6.7 $MN/m^{3/2}$

** Range of fracture toughness for unfatigued specimens of this orientation was 11.4-12.3 $MN/m^{3/2}$

*** Range of fracture toughness for unfatigued specimens for this orientation was 14.7-16.3 $MN/m^{3/2}$

G. Composite Thermal Expansion Behavior

The combination of a low thermal expansion matrix and fiber provides the unique possibility to achieve a composite of exceptional dimensional stability. The following describes the results obtained for a wide variety of fiber and matrix combinations.

1. Continuous Fiber Reinforced Composites

The axial and transverse thermal expansion of unidirectionally reinforced HMS/774M composites is presented in Figs. 59-62. In both cases a series of six thermal cycles was performed with the first three cycles going to a maximum temperature of approximately 725 K and the last three cycles extending the maximum temperature to 860 K. The initial axial thermal expansion curve, Fig. 59, presents several interesting features. First, the initial deformation of the specimen on heating is a contraction. The rate of contraction decreases with increasing temperature until, at about 510 K, the specimen reverses the direction of deformation and begins to expand. Thus, over a limited temperature range, the thermal expansion coefficient is approximately zero due to the reversal of deformation. Also of importance is the observation that the heating and cooling curves do not coincide, but instead there is evidence of a hysteresis effect. By comparison with cycle 2 it is clear that this hysteresis is transient and, for almost all of the second thermal cycle, has disappeared. A residual strain at room temperature remains, however. Because of the very small magnitude of the residual strain it was not clear whether this is an artifact, due to a failure of the system to return completely to the initial starting condition, or whether it is indeed a true residual contraction of the specimen.

By increasing the maximum temperature, Fig. 60, it can be seen that the hysteresis effect once again becomes prominent. Additional thermal cycles also tend to decrease the magnitude of this difference between heating and cooling, although it is still quite evident in the sixth cycle and may require additional cycles to eliminate its presence.

To further examine the nature of this effect, this tested specimen GC 377-1 was allowed to "age" in the ambient laboratory environment for 60 days after which time it was placed once again in the dilatometer and cycled between 300 K and 680 K. No hysteresis effects were noted during this thermal excursion and the shape of the strain versus temperature curve agreed with that shown in Fig. 59. Thus the "precycling" treatment succeeded in substantially stabilizing composite thermal performance.

For the thermal cycles shown in Figs. 59 and 60, cooling produced more negative strain values than heating. Also, the residual strain was always negative. The reason for this probably relates to the fact that the graphite fiber has a

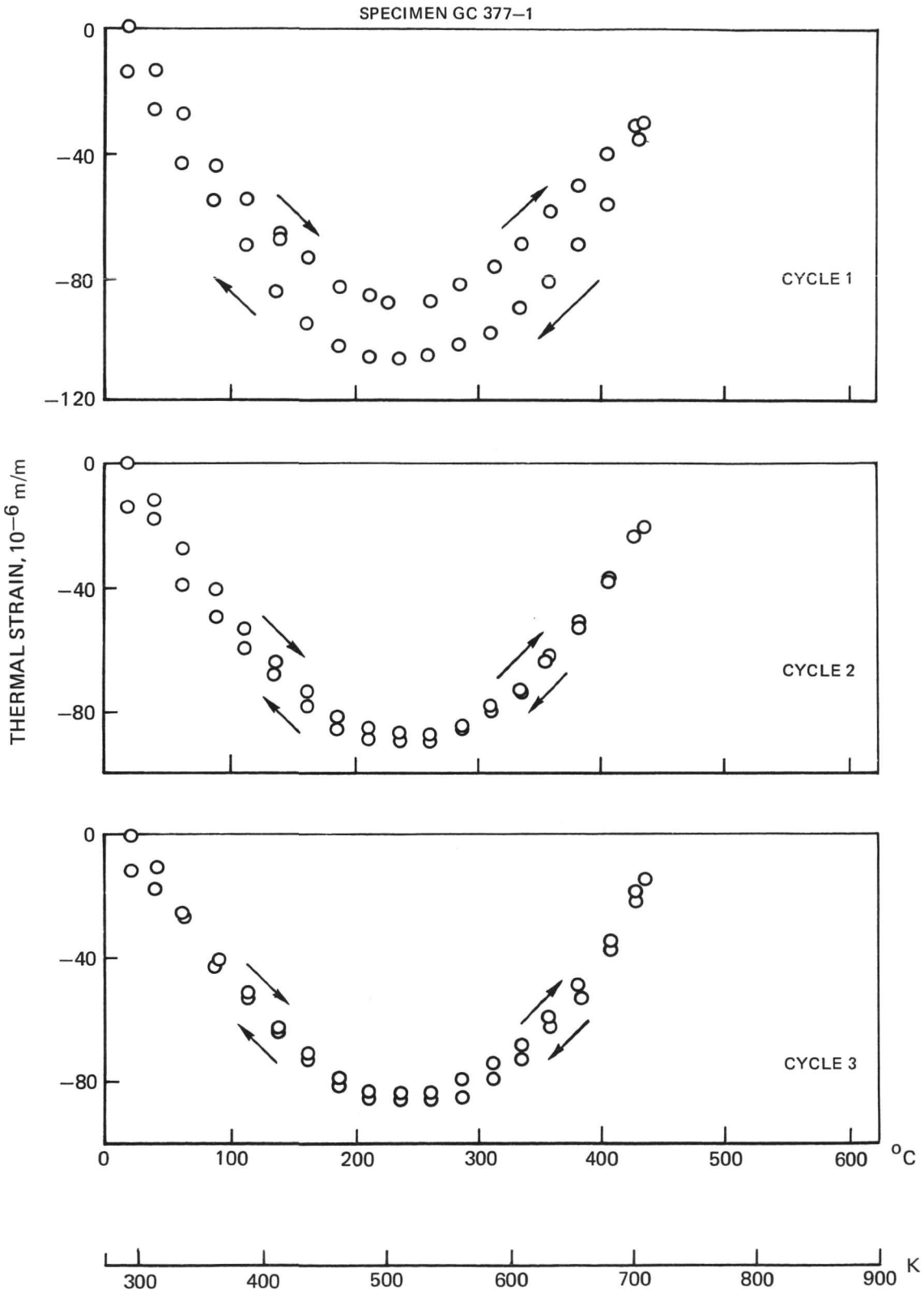

Fig. 59. Axial Thermal Expansion of Unidirectionally Reinforced HMS/774M Cycles 1,2,3

79–04–144–1

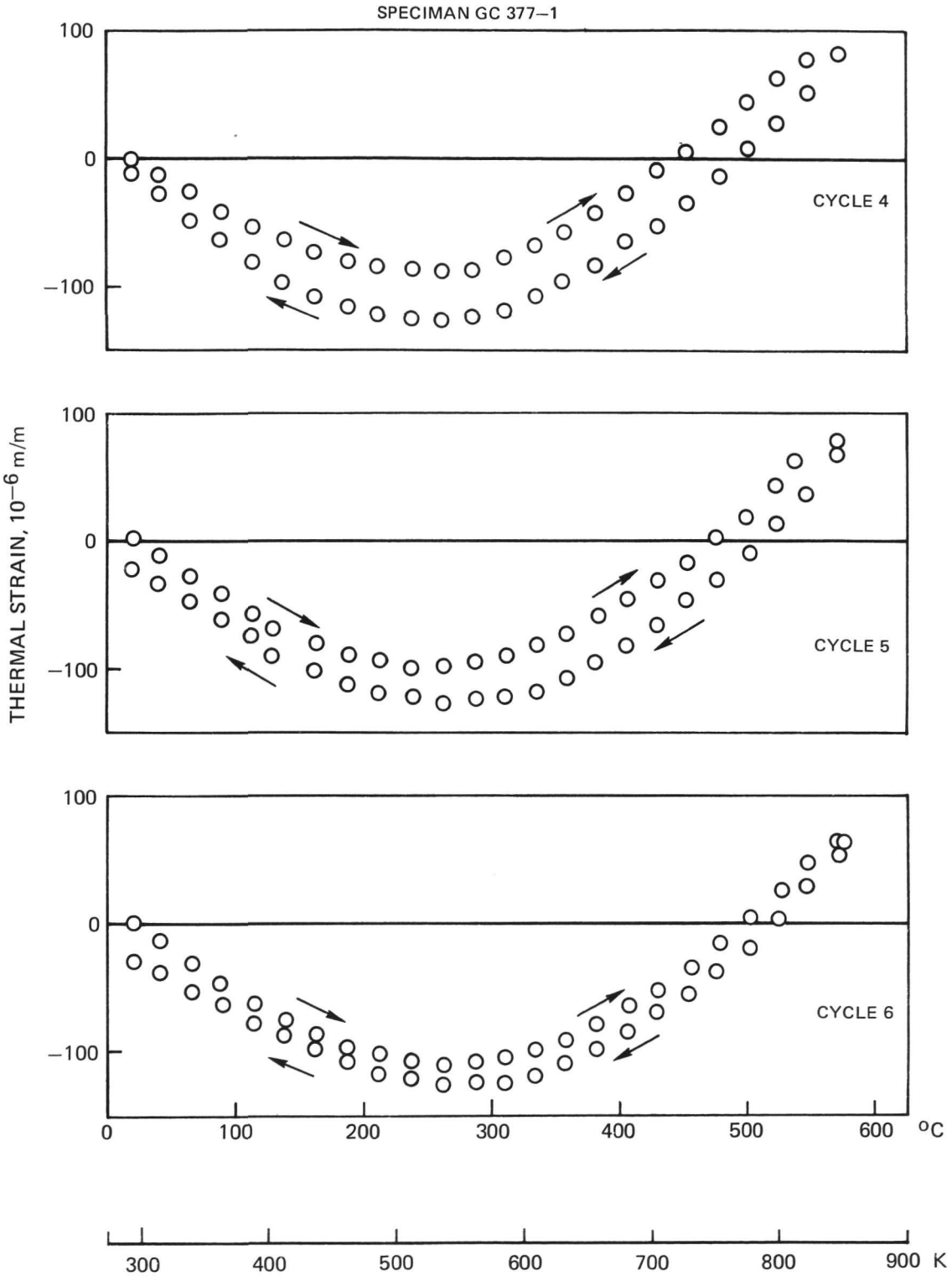

Fig. 60. Axial Thermal Expansion of Unidirectionally Reinforced HMS/774M Cycles 4,5,6

79–04–144–2

highly negative axial thermal expansion coefficient (approximately -1×10^{-6} K^{-1}) while 7740 glass has a positive value of 3.2×10^{-6} K^{-1}. Thus, on heating the composite contracts and the matrix is loaded in compression. It is likely that the fibers may slip slightly along the fiber-matrix interface. On cooling the specimen attempts to return to its initial room temperature dimension; however, because of the above effects which occurred at the elevated temperature, it cannot. Thus cooling produces more negative strain and a residual negative strain remains after test. It should be noted, however, that this material was fabricated at elevated temperature and was subjected to one very large cooling cycle prior to the cycles herein reported. From the above data it would appear that if the composite were subjected to several thermal cycles prior to removal from the fabrication hot press almost all signs of hysteresis would be removed from subsequent tests. It should also be noted that the levels of strain which are being measured are extremely small, i.e. 20×10^{-6} m/m. For a 2.54 cm long specimen this corresponds to 5×10^{-5} cm.

The transversely oriented specimen thermal expansion behavior, Figs. 61-62, differs significantly from that of the axial material. The magnitude of strain measured is much larger and is everywhere positive. The first three cycles, run to a maximum temperature of 725 K, exhibit no evidence of hysteresis using the scales shown. In actual fact, however, there was some hysteresis which is observable on a higher resolution scale. As in the case of the axial specimens, however, it was not possible to demonstrate that the residual strain measured at room temperature is purely due to the composite and not an artifact of the experimental apparatus and procedure. Reheating to the higher temperature of 865 K, Fig. 62 cycle 4, caused a larger hysteresis effect which decreased with additional cycles. The reasons for this transverse hysteresis are less clear since the fiber transverse thermal expansion (α_f^t) is not well known. Values of α_f^t larger than that of the 774M matrix, however, have been quoted in the literature and the overall composite transverse thermal expansion coefficient would agree with this.

Similar axial and transverse thermal strain vs temperature curves for unidirectional GY70 (Figs. 63,64), Thornel Pitch (Figs. 65,66), and Thornel 300 (Figs. 67,68) fiber reinforced composites are also presented for temperatures of up to 625 K. The general features of these materials' behavior agree with those of the above described HMS/774M. Two major differences, however, are the values of thermal expansion coefficient and location of the axial specimen inflection point ($\alpha = 0$). It appears that this point occurs at a higher temperature for the higher modulus Thornel pitch fiber than for either of the other materials. The thermal expansion coefficients for all of the fiber reinforced glass composites are listed in Table XIV. These values, taken from the figures at 300 K in both the axial and transverse directions, indicate the tendency for a more negative axial coefficient with increasing fiber elastic modulus. The following expression, which has been used successfully to calculate composite axial thermal expansion, illustrates how this can happen:

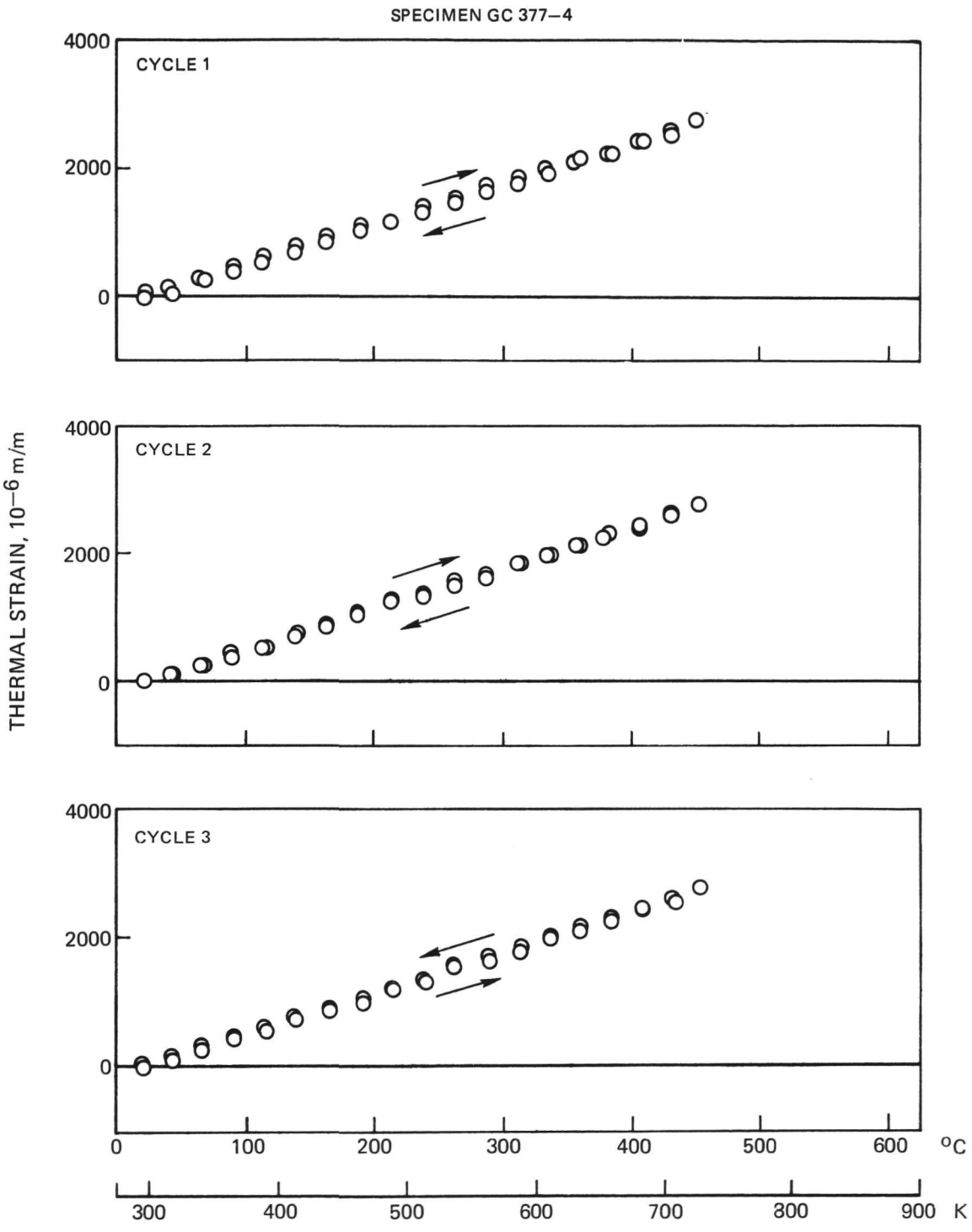

Fig. 61. Transverse Thermal Expansion of Unidirectionally Reinforced HMS/774M Cycles 1,2,3

79–04–144–3

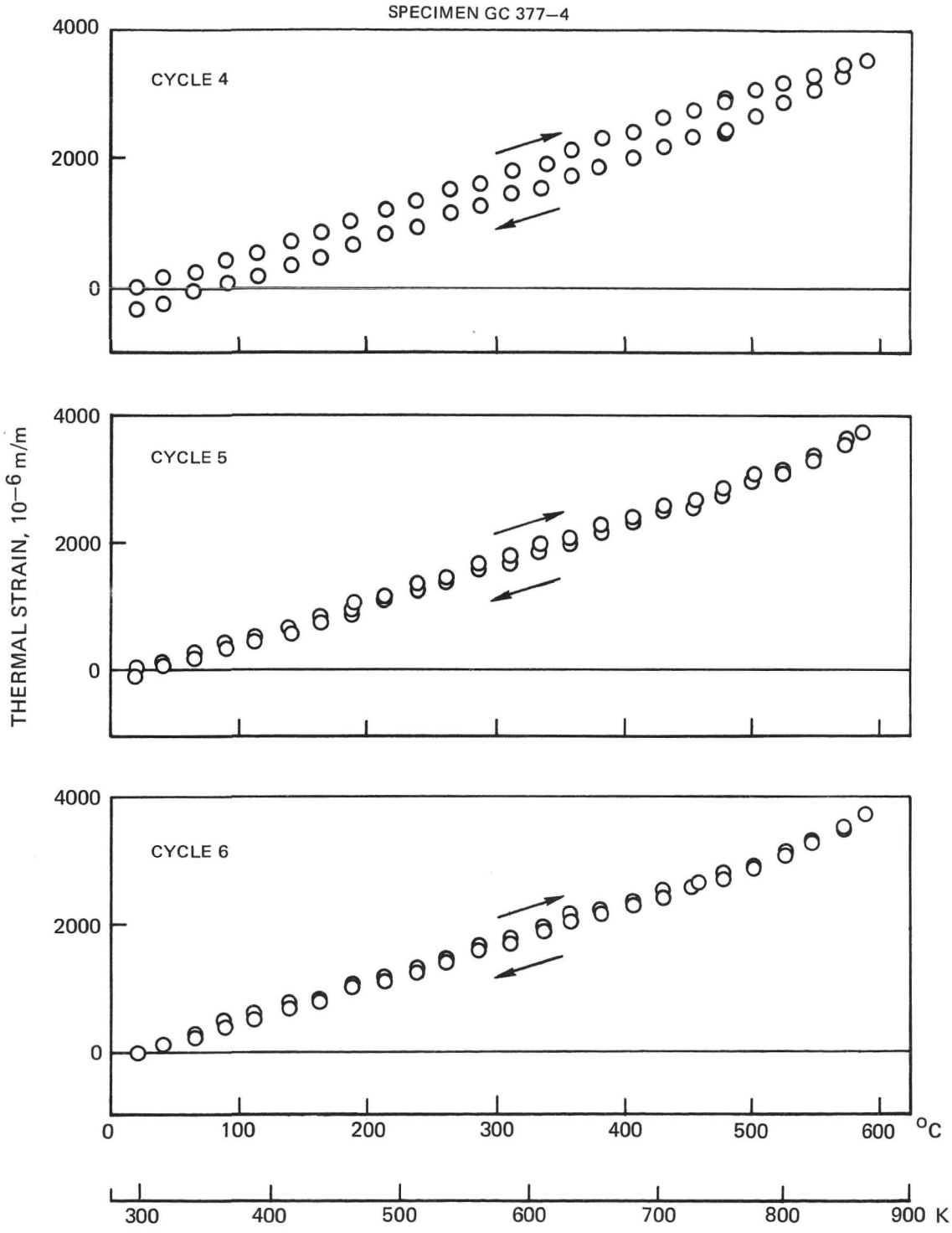

Fig. 62. Transverse Thermal Expansion of Unidirectionally Reinforced HMS/774M Cycle 4,5,6

79–04–144–4

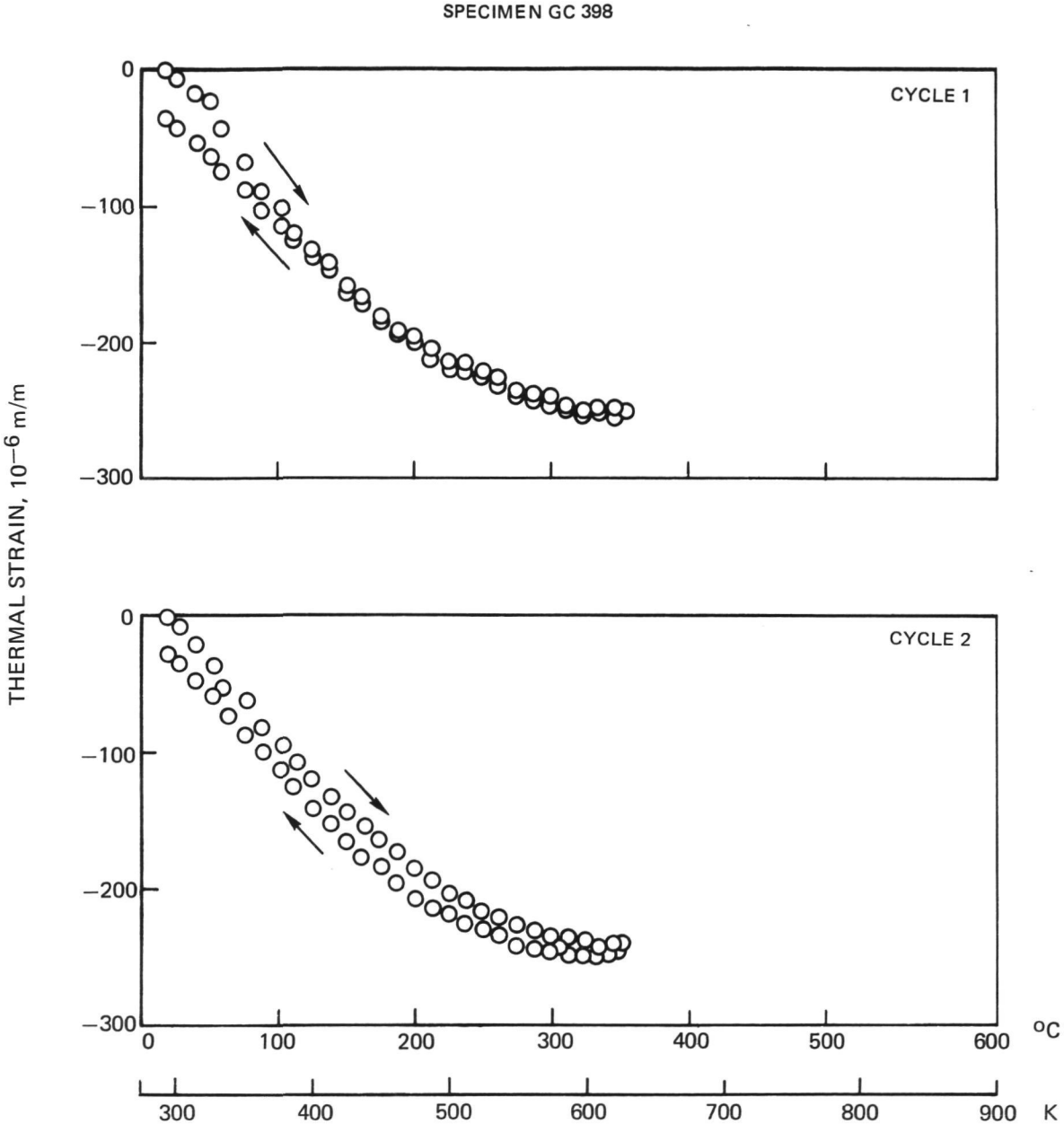

Fig. 63. Axial Thermal Expansion of Unidirectionally Reinforced GY70/774M Cycles 1,2

79-04-144-5

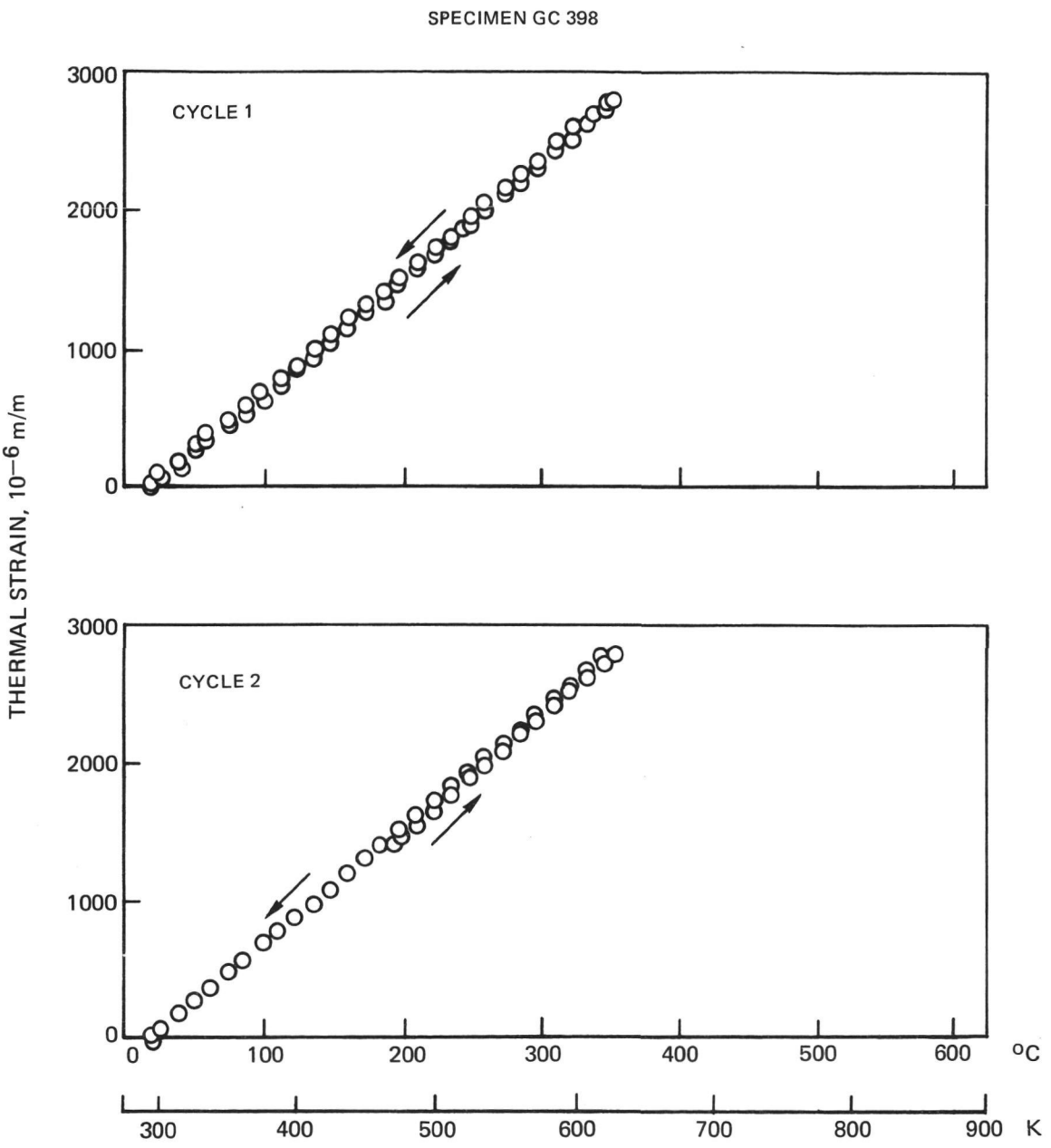

Fig. 64. Transverse Thermal Expansion of Unidirectionally Reinforced GY 70/774M Cycles 1,2

79-04-144-6

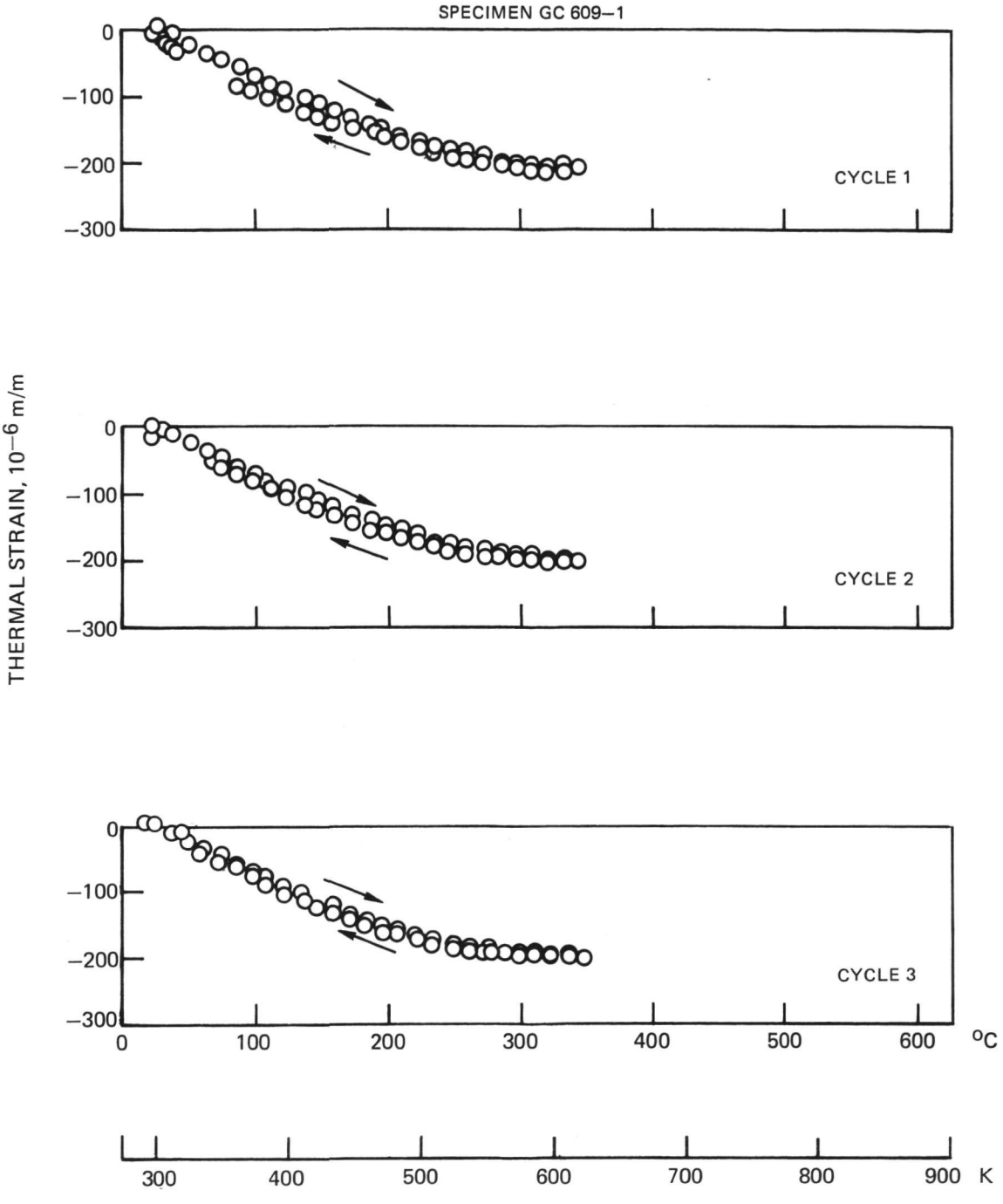

Fig. 65. Axial Thermal Expansion of Unidirectionally Reinforced Thornel Pitch (VS0054-0)774M, Cycles 1, 2, 3

79–06–70–3

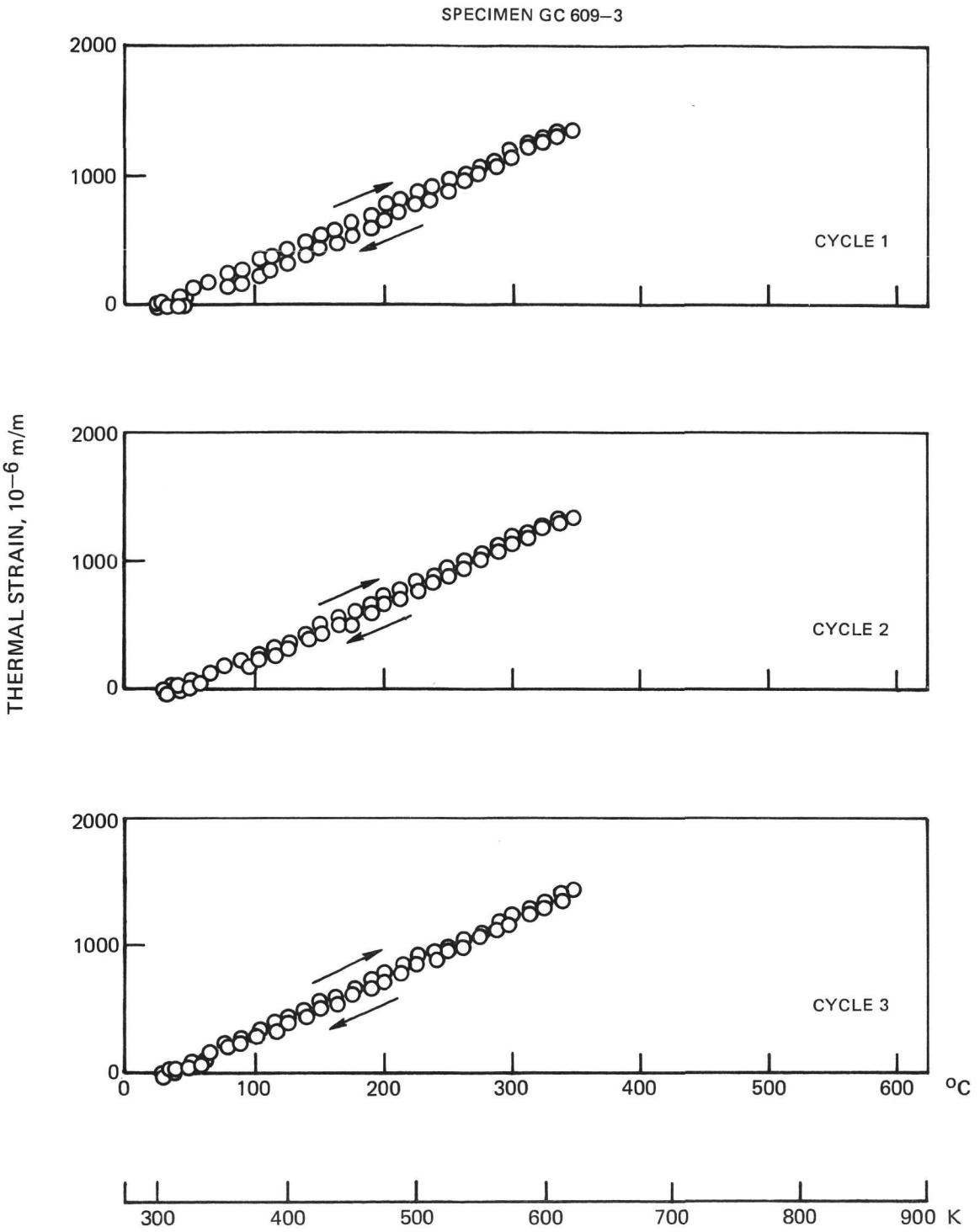

Fig. 66. Transverse Thermal Expansion of Unidirectionally Reinforced Thornel Pitch (VS0054-0) 774M, Cycles 1, 2, 3

79–06–70–2

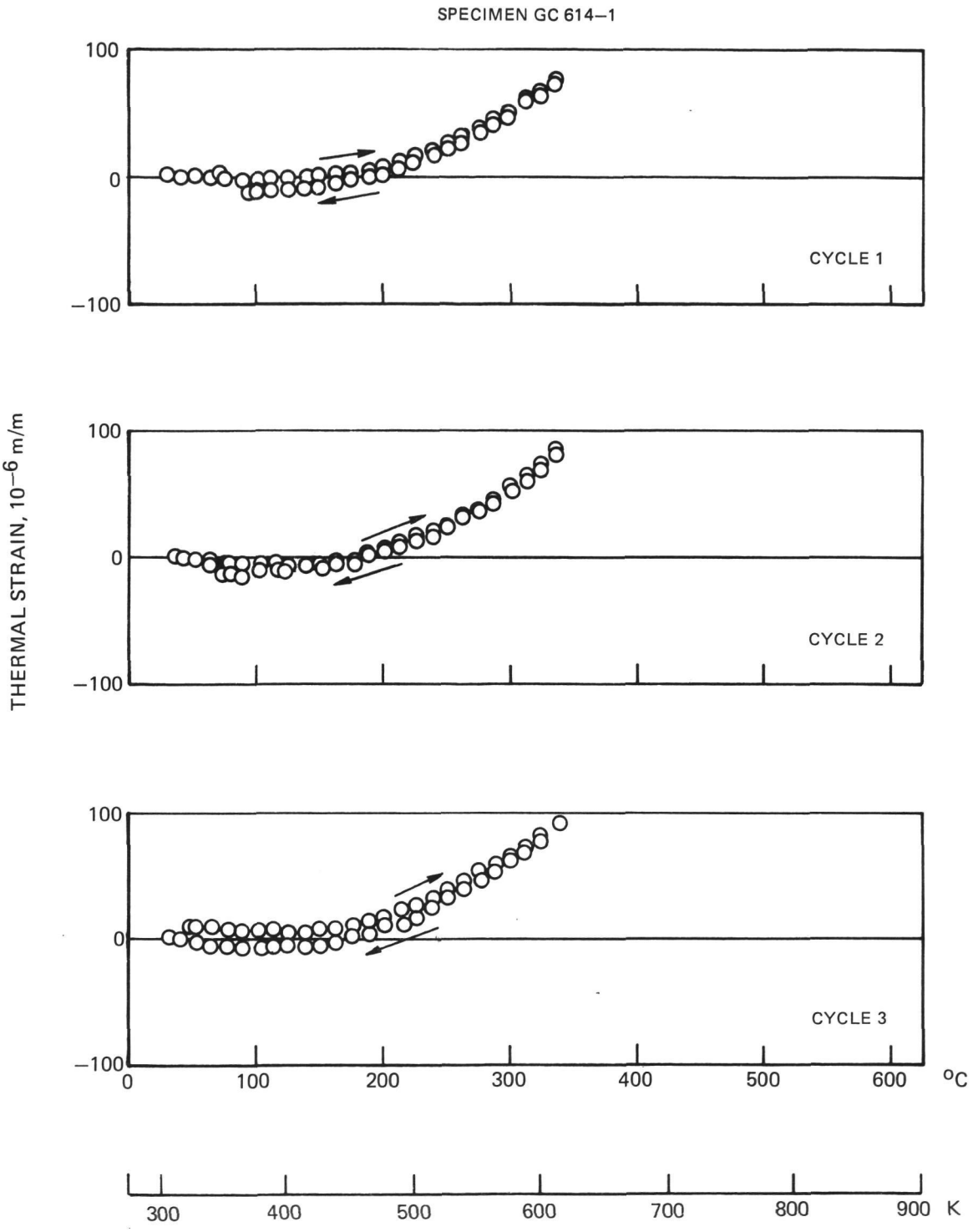

Fig. 67. Axial Thermal Expansion of Unidirectionally Reinforced Thornel 300/774M, Cycles 1,2,3

79–06–70–4

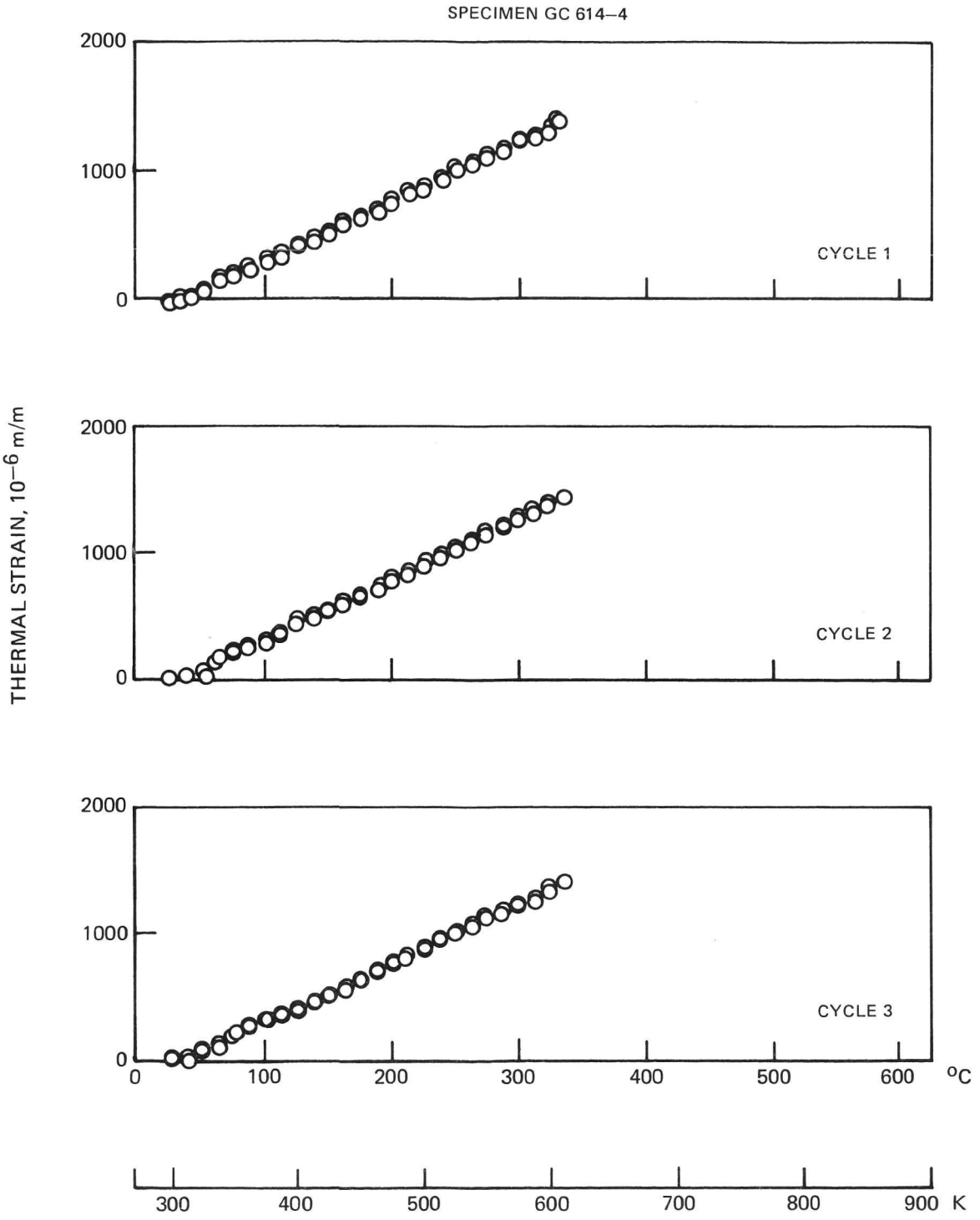

Fig. 68. Transverse Thermal Expansion of Unidirectionally Reinforced Thornel 300/774M, Cycles 1, 2, 3

79–06–70–5

Table XIV

Thermal Expansion at 300 K of Graphite Fiber
Unidirectionally Reinforced 774M

Composite	Fiber Type	Fiber Elastic Modulus (GPa)	v/o Fiber	Thermal Expansion Coefficient (10^{-6} m m^{-1} K^{-1})	
				0^{o}	90^{o}
377	HMS	350	70	-0.50	+6.5
398	GY70	537	75	-1.0	+8.1
609	Pitch (VS0054-0)	654	50	-1.0	+4.4
614	Thornel 300	234	54	-0.10	+4.6

Table XV

GY 70 Fiber Reinforced 774M Composite
Thermal Expansion Coefficients

Composite Lay-Up	$\alpha_{300\ K}$ (10^{-6} m m^{-1} K^{-1})	$\alpha_{300-550\ K}$ (10^{-6} m m^{-1} K^{-1})
Unidirectional @ 0^{o}	-1.0	-0.95
@ 90^{o}	+8.1	+8.1
0/90 Cross Ply	-0.8	-0.6

$$\alpha_{11}{}^{c} = \frac{E_m \alpha_m V_m + E_f \alpha_f^a V_f}{E_m V_m + E_f V_f}$$

E, V and α are the elastic modulus, volume percent and thermal expansion of fiber and matrix, and the α_f^a term refers to the axial component of fiber thermal expansion. Thus, even without altering the already negative value of α_f, an increase in fiber elastic modulus will result in a more negative value of composite axial thermal expansion, $\alpha_{11}{}^{c}$.

A recent tabulation of GY 70 fiber data (Ref. 14) permits an examination of the validity of the above expression. The fiber properties are E_f = 537 GPa, $\alpha_f^a = -1.08 \times 10^{-6}$ K^{-1} while 7740 matrix properties are E_m = 62.7 GPa and $\alpha_m = 3.25 \times 10^{-6}$ K^{-1}. Using these values and a fiber volume fraction of 75% obtained experimentally, a resultant value for $\alpha_{11}{}^{c}$ was calculated to be -0.92×10^{-6} K^{-1}. This is in excellent agreement with the value of -1.0×10^{-6} K^{-1} obtained experimentally.

The composite transverse thermal expansion coefficient $\alpha_{22}{}^{c}$ did not indicate a consistent trend with fiber elastic modulus. At present an accurate formulation for the calculation of $\alpha_{22}{}^{c}$ based on fiber and matrix properties is not available because of the extreme complexity introduced by the orthotropic nature of the fiber.

The thermal expansion of a 0/90 cross ply GY70 fiber reinforced 774M composite is presented in Fig. 69. These curves bear a close resemblance to those obtained for the axial thermal expansion of unidirectionally reinforced GY70/774M, Fig. 63. However, there are some differences. First, the slope of the curve is slightly less than that for the unidirectional case at 300 K and the overall specimen contraction up to 500-600 K is significantly less. The data are compared in Table XV in terms of thermal expansion coefficients. Second, the apparent extent of hysteresis is less for the 0/90 composite. Within the resolvable limits of the experimental system, it does not appear that, after the first cycle, there is any residual specimen strain after thermal cycling. As can be seen in Fig. 69, the final specimen dimensions are equivalent to the starting dimensions.

2. Continuous Fiber Reinforced Composites with Scrim

Thermal expansion measurements were also made for continuous fiber reinforced composites which contained discontinuous fiber scrim in each layer. Thornel 300, HMS and Thornel high modulus pitch based fibers were all tested in unidirectional and 0/90 cross ply configurations. The general shapes of the thermal strain vs temperature curves were very similar to those described in the previous section for composites fabricated with these fibers and no scrim present. Data obtained for each of these composites are presented in Table XVI. As in the case of the previous continuous fiber reinforced specimens, the 0° and

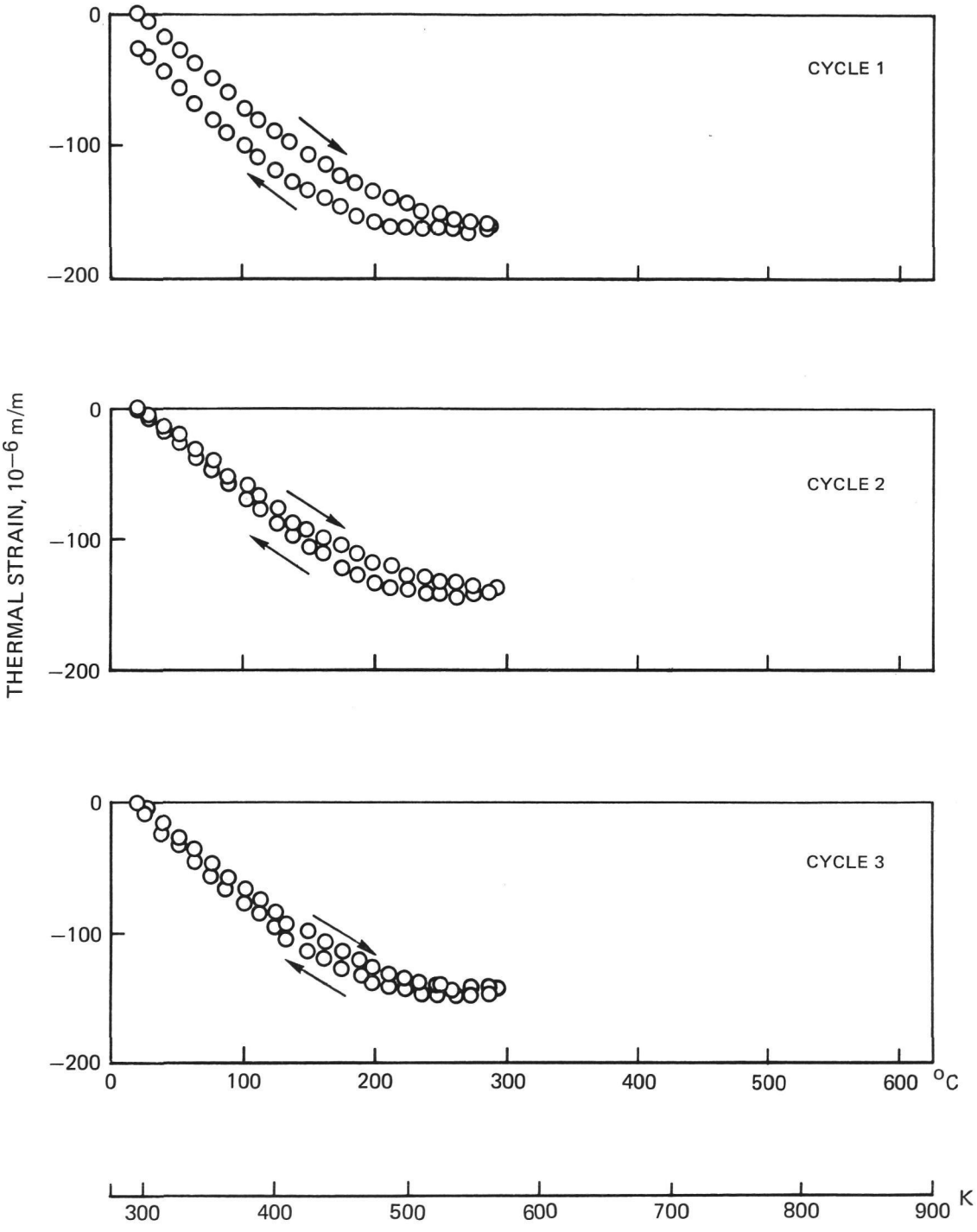

Fig. 69. 0° Thermal Expansion of 0/90 Reinforced GY70/774M Cycles 1, 2, 3

79−04−144−9

0/90 composite thermal expansion curves are not linear and hence the table includes a listing of the temperature ranges over which the coefficient of thermal expansion is zero.

The 0° values of thermal expansion coefficient agree well with those of the corresponding all continuous fiber composites, Table XIV. This would be expected since the addition of a small amount of scrim would not be expected to affect the dominance of the 0° fibers. In the transverse (90°) direction, however, this equality of performance does not appear to hold and instead the thermal expansion coefficients of the composites containing scrim are significantly lower than those of the composites without scrim. In the case of the Thornel 300 fiber reinforced composites the use of scrim reduced the 90° α value from 4.6 to 2.8 x 10^{-6} K^{-1}. In the case of HMS fiber reinforcement the reduction is from 6.5 to 4.1 x 10^{-6} K^{-1} while for the Thornel pitch based fiber it is from 4.4 to 2.7 x 10^{-6} K^{-1}. It is apparent that the presence of the scrim has had a marked beneficial affect on the 90° thermal expansion behavior as it did on the transverse strength.

3. Discontinuous Fiber Reinforced Composites

The thermal expansion behavior of discontinuous Celion 6000 fiber reinforced glass was measured previously at UTRC under an internally funded program and was found to be linear over the temperature range measured, 300 to 573 K. The average value of thermal expansion coefficient over that temperature range was found to be 1.7 x 10^{-6} K^{-1}.

Composite reinforcement using a fiber of higher elastic modulus was considered as a possible way of decreasing composite thermal expansion and still retaining the advantages of discontinuous fiber reinforcement. For this reason 774M matrix composites were fabricated using the Fortafil 5 fiber, Table I. This fiber has an elastic modulus of 330 GPa as compared to 234 GPa for the Celion 6000 fiber. The thermal expansion behavior of a composite containing 36 v/o of the Fortafil 5 discontinuous fiber is shown in Fig. 70 and the α data obtained are presented in Table XVI where it can be seen that a decrease in α was indeed achieved at 300 K. A comparison of composite mechanical properties, Table XVII, also indicates that the higher elastic modulus fiber causes an increase in composite elastic modulus, however, accompanied by a significant decrease in composite flexural strength.

Table XVI

Thermal Expansion of Graphite Fiber Reinforced 774M Composites Containing Scrim

Composite	Matrix	Fiber	Orientation	v/o Fiber	v/o Glass	v/o Porosity	Thermal Expansion Coefficient @ 300 K 10^{-6}/K	Temp. for $\alpha = 0$ K
818-1	7740	Th 300 with scrim	0	60	40	0	0.06	300-400
-2							-0.16	350-400
-7	"	"	90				2.8	-
817-1	"	"	0/90	60	40	0	0.13	300-400
813-1	7740	HMS with scrim	0	67	32	1	-0.47	440-475
-2	"	"	0				-0.48	475-495
-7	"	"	90				4.1	-
814-1	"	"	0/90	60	39	1	-0.44	400-440
816-1	7740	Th Pitch with scrim	0	65	34	1	-1.4	620-700
-7	"		90				2.7	-
815-1	"	"	0/90	54	46	0	-0.79	535-575
819-1	7740	Fort. 5 chopped fiber	0	36	64	0	1.0	-
-2	"						0.81	-

Table XVII

Discontinuous Fiber Reinforced 774M Matrix
Composite Properties

Fiber	v/o F	v/o G	v/o P	Avg. Flex Str. MPa	Avg. Elas Mod. GPa
Celion 6000	22	78	0	335	48.0
Fortafil 5	22	78	0	222	65.0

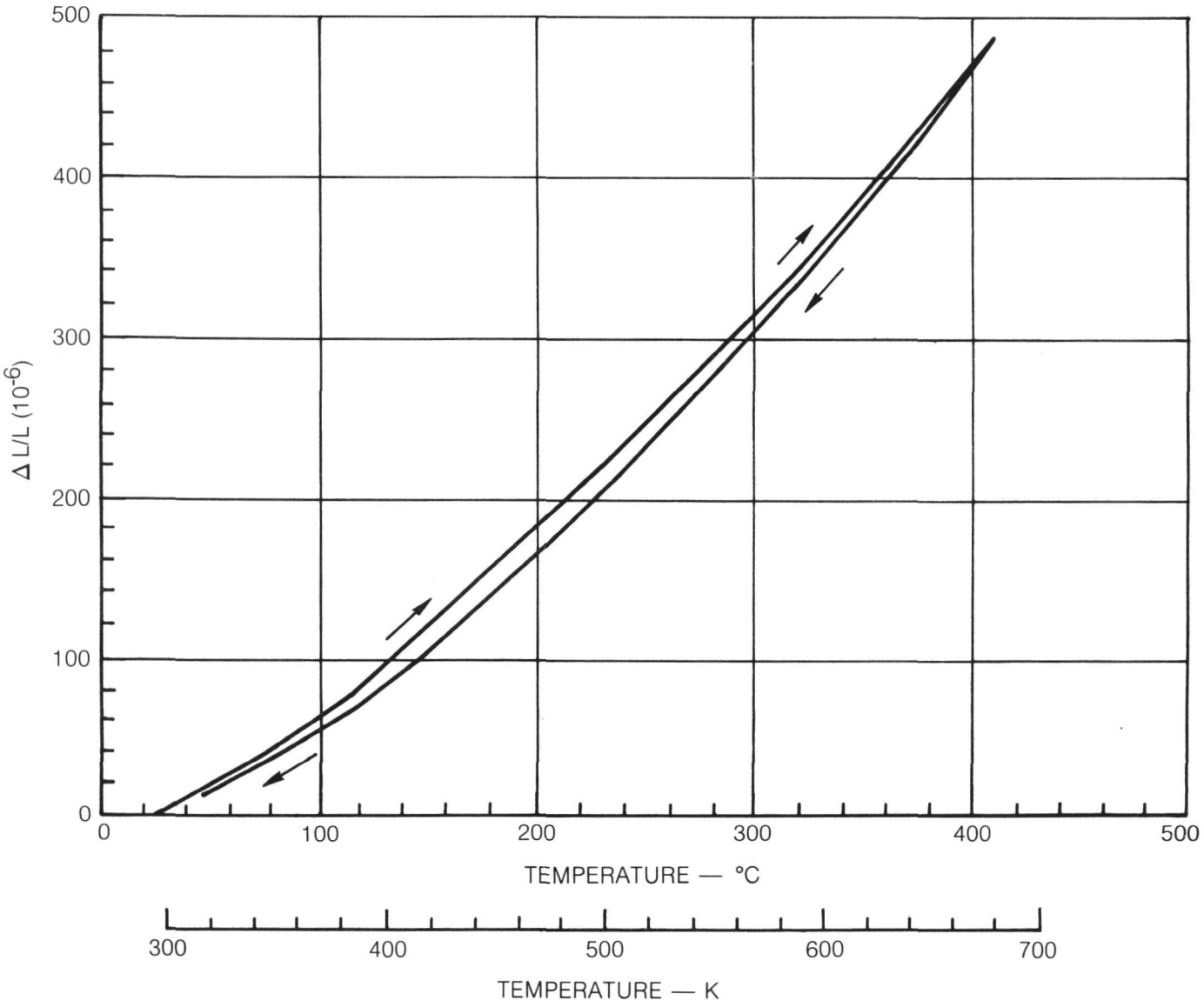

Fig. 70. Thermal Expansion of Chopped Fortafil 5 Fiber Reinforced 774M (GC819-2)

80-9-148-5

IV. RESULTS AND DISCUSSION
HIGH TEMPERATURE MATRIX COMPOSITES

The portion of this program which is directed at the development of higher temperature composite systems is being performed on this NASA-Langley sponsored program through funding provided by the Materials Laboratory of the Air Force Wright Aeronautical Laboratories. The purpose of this work is to increase the high temperature thermal stability of graphite fiber reinforced glass matrix composites. In the previously described graphite reinforced borosilicate glass system the maximum use temperature of the composite is limited by two factors. First, in an oxidizing environment the graphite fibers are rapidly degraded at temperatures in excess of 703 K (800°F). Second, in an inert environment the maximum use temperature is defined by the temperature at which the glass matrix begins to soften excessively. Data developed under this program have indicated that, for 7740 borosilicate glass matrix composites, this occurs at temperatures just above the glass annealing point of 833 K (1040°F). Through the use of more refractory glasses it should be possible to raise this inert environment use temperature.

A. Discussion of Composite Material Choices

As has been shown in the earlier phases of this program, several different graphite fibers have been successfully used to reinforce borosilicate glass. Fibers with elastic moduli in the range of 234 GPa (34 Msi) to 654 GPa (95 Msi) have all been successfully used to achieve composites which are both high strength and dimensionally stable. There are, however, differences in composite performance significant enough to permit choices, based on properties, to be made. The data in Table XVIII illustrate this point for several fiber reinforced composites.

It can be seen, for instance, that the smallest value of composite coefficient of thermal expansion, CTE, is achieved through the use of a low elastic modulus fiber. This is in direct contrast to metal matrix composites and is due to the fact that in the case of a glass matrix, the matrix CTE is already very low. The negative fiber CTE and relatively high fiber elastic modulus are thus able to produce a negative composite 0° CTE which becomes highly negative when the highest elastic modulus fibers are used. Thus, solely on the basis of achieving a low CTE material one would choose the Thornel 300 fiber as a reinforcement.

Referring again to the table, both composite 0° elastic modulus and composite through thickness and transverse thermal conductivity are maximum when the highest elastic modulus fibers are used. These properties can also be extremely important in applications considered by this program; however, as discussed above, the absolute value of 0°-CTE is increased tenfold over that for composites reinforced with low elastic modulus graphite fibers.

Table XVIII

Unidirectionally Reinforced Borosilicate
(774M) Matrix Composites

Fiber Type	Fiber Elastic Modulus		Composite Properties 0° El. Modulus		0° CTE*		90° Thermal Conductivity	
	GPa	(Msi)	GPa	(Msi)	$10^{-6}K^{-1}$	($10^{-6}°F^{-1}$)	Watts M^{-1} K^{-1}	(***)
Thornel 300	234	(34.0)	125	(18.1)	-0.10	(-.055)	-	-
HMS	350	(50.8)	190	(27.6)	-0.50	(-.28)	2.2	(15.5)
GY-70	516	(74.9)	285	(41.4)	-1.0	(-.56)	4.5	(31.0)
Pitch Based	654	(95.0)	335	(48.6)	-1.0	(-.56)	6.5	(45.0)

*Coefficient of thermal expansion at 297 K (75°F)

**Thermal conductivity normal to the principal axis (K values determined as part of UTRC's Corporate funded activity)

***BTU·in·hr^{-1}·ft^{-2}·$°F^{-1}$

The current effort emphasizes the use of glass matrices with higher temperature capability than the current borosilicate. There are several approaches which can be taken to achieve this end. The data in Table XIX represent some of the glass matrix choices available and all can be compared with the borosilicate glass listed in the first column. The two high silica glasses (96% and 100%) present major increases in glass annealing point and thus probably will increase composite use temperature significantly. They also, however, introduce two additional complexities. Their very high thermal stability is accompanied by the need for much higher fabrication temperatures thus enhancing the probability of fiber damage. In addition, their CTE values are much lower than that of the borosilicate. This will probably lead to more negative values of composite 0° CTE than are typical of the borosilicate glass matrix composites.

A second approach is to utilize two intermediate temperature glass systems. The aluminosilicate and calcia aluminosilicate glasses listed both offer significant increases in annealing point over the borosilicate without the accompanying decrease in CTE posed by the high silica glasses. These more complex glasses also provide greater ease of fabrication.

Finally, the glass ceramics listed provide a very different option. They can be processed in the glassy state to form a dense fiber reinforced composite and then crystallized (ceramed) to develop a crystalline ceramic structure that is stable to over 1273 K (1832°F). The lithia aluminosilicate (LAS) glass has been used successfully as a matrix for SiC fibers (Ref. 15) and this composite has been demonstrated to maintain useful strength to temperatures of up to 1273 K (1832°F). The magnesia aluminosilicate (MAS) glass has presented greater fabrication difficulties; however, a previous effort at UTRC successfully achieved discontinuous graphite fiber reinforced MAS composites that attained a three point flexural strength of 252 MPa (36.6 ksi) and elastic modulus of 48.9 GPa (7.1 Msi). The discontinuous fiber reinforcement approach, because it achieves lower fractions of fiber reinforcement, provides fewer difficulties in achieving a dense mircostructure.

The following sections describe the progress made in achieving dimensionally stable composites in each of these matrix categories. A comprehensive tabulation of the composites fabricated for this purpose is presented in Table XX.

B. Aluminosilicate Glass and Calcia Aluminosilicate Glass Matrix Composites

1. Discontinuous Fiber Reinforcement

Discontinuous Celion 6000 fiber reinforced composites were fabricated using both the modified borosilicate (774M) and aluminosilicate (1723 glass) matrices to permit a comparison of composite elevated temperature performance. The resultant composite data are presented in Figs. 71 and 72. Composite three point flexural

Table XIX

Glass Matrix Comparison

	Borosilicate (CGW 7740)	96% Silica (CGW 7900)	100% Silica (CGW 7940)	Aluminosilicate (CGW 1723)	Calcia Aluminosilicate	Glass Ceramics MAS	Glass Ceramics LAS
Density-kg/m^3	2230	2180	2200	2640	2380	2600	2500
Elastic Modulus GPa	63	67	72	88	-	118	86
(10^6psi)	(9.1)	(9.7)	(10.9)	(12.8)		(17)	(1255)
CTE $10^{-7}K^{-1}$	32.5	8.0	5.5	46	21	57	4-20
($10^{-7}°F^{-1}$)	(18.0)	(4.4)	(3.0)	(25.6)	(11.7)	(31.7)	(2.2-20)
Anneal Point K	833	1183	1357	983	1143	-	-
(°F)	(1040)	(1670)	(1983)	(1310)	(1598)		
Working Point K	1525	1723	1853	1181	-	-	-
(°F)	(2285)	(2642)	(3367)	(2158)	-	-	-

Table XX

High Temperature Graphite Fiber Reinforced Composites

Composite	Fiber	Matrix	Pressing Conditions			Composite Properties						
			Temp		Time	v/o Fiber	v/o Glass	v/o Porosity	Avg. Flex. Strength		Avg. Flex. Elastic Modulus	
			K	°F	min				MPa	Ksi	GPa	Msi
666	T-300 (scrim)	96% SiO_2	1973	3090	60	58	40	2	475	69	110	16
778	Disc. Cel 6000	774M	1573	2372	30	22	78	0	335	49	48	7.0
780	Disc. Fort. 5	1723	1573	2372	30	32	67	1	324	47	45	6.6
857	HMS	1723	1573	2370	30	68	30	2	189	27	145	21
858	HMS	774M	1723	2640	60	68	32	0	1090	158	200	29
859	HMS	96% SiO_2	1873	2910	60	49	50	1	430	62	158	23
863	HMS	1723	1673	2550	30	-	-	-	-	-	-	-
864	HMS	96% SiO_2	1973	3090	30	58	41	1	55	8	69	10
869	Disc. Cel 6000	96% SiO_2	1873	2910	60	24	76	0	56	8	72	10
879	T-300	96% SiO_2	1873	2910	30	47	48	5	365	53	128	19
880	T-300	96% SiO_2	1873	2910	30	52	46	2	268	39	143	21
881	Disc. Fort. 5	96% SiO_2	1873	2910	30	22	78	0	69	10	56	8
882	Disc. Fort. 5	96% SiO_2	1773	2730	30	25	75	0	69	10	56	8
883	Disc.	96% SiO_2	1873	2910	30	21	67	12	286	42	45	6.5
889	HMS	96% SiO_2	1773	2730	60	57	42	1	241	35	127	18
894	Th Pitch	774M	1723	2640	30	60	40	0	575	84	388	56.4
903	T-300	CASG	1873	2910	30	51	46	3	276	40	118	17
904	T-300	CASG	1773	2730	30	56	33	11	244	36	116	17
905	T-300	CASG	1923	3000	30	54	41	5	279	40	135	20
925	Th Pitch	774M	1723	2640	30	53	47	0	707	103	335	49
936	Th Pitch	96% SiO_2	1873	2910	60	58	42	0	213	31	-	-
937	HMS	96% SiO_2	1873	2910	60	54	46	0	-	-	-	-
938	HMS	MAS 2969	1823	2822	30	72	26	2	450	65	188	27
939	HMS	MAS 266	1823	2822	30	75	21	4	494	72	216	31

Table XX (Cont'd)

Composite	Fiber	Matrix	Pressing Conditions: Temp K	Temp °F	Time min	v/o Fiber	v/o Glass	v/o Porosity	Composite Properties: Avg. Flex. Strength MPa	Avg. Flex. Strength Ksi	Avg. Flex. Elastic Modulus GPa	Avg. Flex. Elastic Modulus Msi
943	Th Pitch	96% SiO_2	1873	2910	30	50	49	1	213	31	200	29
944	Th Pitch	96% SiO_2	1773	2730	30	50	49	1	169	25	127	18
947	HMS	MAS 266	1773	2730	30	Poorly Bonded			-	-	-	-
948	HMS	MAS 266	1773	2730	30	74	23	3	389	57	192	28
949	HMS	774M	1473	2192	-	52	47	1	707	103	157	23
952	0/90 HMS	96% SiO_2	1873	2910	30	-	-	-	For thermal expansion			-
953	0/90 HMS	96% SiO_2	1873	2910	30	50	47	3	245	36	89	13
954	T-300 (Scrim)	96% SiO_2	1873	2910	30	58	28	14	387	56	153	22
955	Th Pitch	MAS 266	1823	2822	Excessive flash - too thin				-	-	-	-
956	T-300	MAS 266	1823	2822	-	69	28	3	179	26	117	17
957	HMS	MAS 266	1723 (twice)	2640	30	71	28	1	329	48	205	30
958A	HMS	MAS 266	1723	2640	30	69	25	6	455	66	225	33
958B	HMS	MAS 266	1673	2552	30	73	26	1	343	50	215	31
959	HMS	MAS 266	1723	2192	30	66	32	2				
961	0/90 T-300	96% SiO_2	1973	3090	60	64	34	2	150	22	74	11
962	Th Pitch	MAS 266	1723	2192	30							
965	0/90 T-300	96% SiO_2	1973	3090	60							
966	"	"	"	"	"							
967	"	"	"	"	"							
968	"	"	"	"	"	For delivery						
969	"	"	"	"	"							
970	"	"	"	"	"							
971	0/90 HMS	774M	1573	2370	30	For delivery						
972	Disc. Cel 6000	96% SiO_2	1873	2910	30	For thermal expansion						
973	0/90 HMS	774M	1573	2370	30	For delivery						
974	0/90 T-300	96% SiO_2	1973	3090	60				144	21	103	15

strengths, Fig. 71, indicate that the aluminosilicate matrix does indeed provide an increase in elevated temperature stability. The borosilicate matrix composite strength begins to drop off rapidly at between 775 K (935°F) and 875 K (1115°F) while the aluminosilicate matrix composites retain their strength to 875-975 K (1115-1295°F) before exhibiting a significant strength loss. Composite flexural elastic modulus retention, Fig. 72, is also improved by a 100-200 K (180-360°F) increment, although in this case a gradual decrease in stiffness occurs with increasing temperature over the entire test regime.

2. Continuous Fiber Reinforcement

HMS fiber reinforced glass matrix composites were fabricated utilizing 774M (borosilicate) and 1723 (aluminosilicate) glasses, composites 857, 858, 863, Table XX. The 774M system is used as a reference standard while the 1723 glass matrix composite was chosen to achieve high volume fractions of fiber reinforcement; however, only the borosilicate glass (858) resulted in a high strength composite, Fig. 73. The 1723 matrix composite specimens (857, 863) failed extensively in shear and compression at very low stress levels while the 7740 matrix specimens failed primarily in tension at temperatures below 873 K (1112°F). This propensity for matrix controlled failure in the 1723 matrix composites probably relates to the higher value of CTE of this matrix, Table XIX. The matrix is probably cracked extensively as a result of the larger fiber - matrix CTE mismatch which, for the present case, applies tensile stresses to the matrix on cool down from the fabrication temperature.

A series of composites were fabricated using Thornel 300 fibers to reinforce calcia aluminosilicate glass (CASG). Composites 903, 904 and 905 (Table XX) were hot pressed over a range of temperatures and it was found that densification required temperatures of 1873 K (2912°F) and above. Resultant composite flexural strength was in excess of 250 MPa, which as will be shown in the next section, is approximately equivalent to what is achievable using the 96% SiO_2 glass.

C. 96% SiO_2 Matrix Composites

1. Discontinuous Fiber Reinforcement

High silica glass matrix composites reinforced with discontinuous Fortafil V and Celion 6000 fiber were hot pressed under various conditions, Table XX, composites 869, 881, 882, 883. The room temperature three point bend strengths of these composites were all rather low except for composite 883 which exhibited excellent strength despite the existence of some matrix porosity. Additional elevated temperature three point flexural tests were performed in argon on specimens from this composite. The results are shown in Fig. 74 where it can

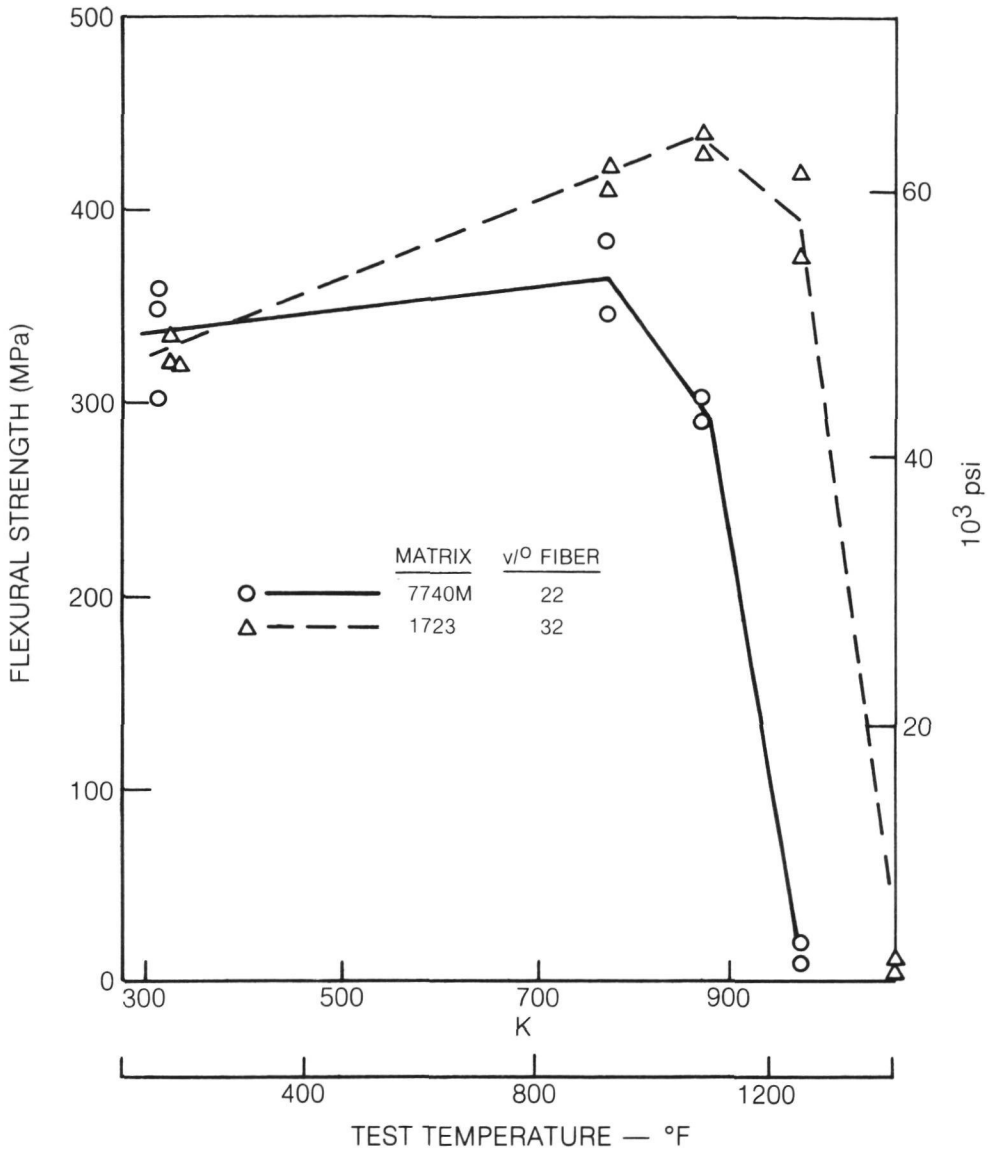

Fig. 71. Three Point Flexural Strength of Discontinuous Celion Fiber Reinforced Glass as a Function of Test Temperature (Tested in Argon)

80-9-39-1

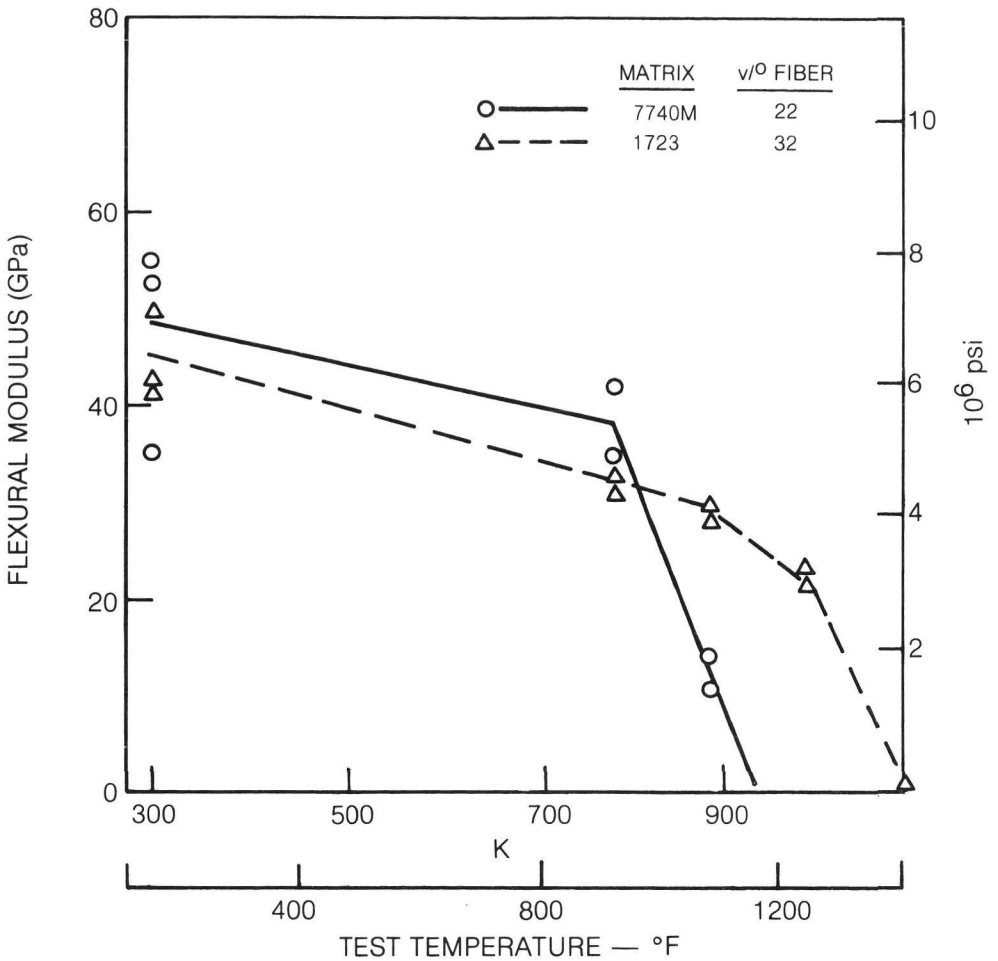

Fig. 72. Three Point Flexural Modulus of Discontinuous Celion Fiber Reinforced Glass as a Function of Test Temperature (Tested in Argon)

80-9-39-2

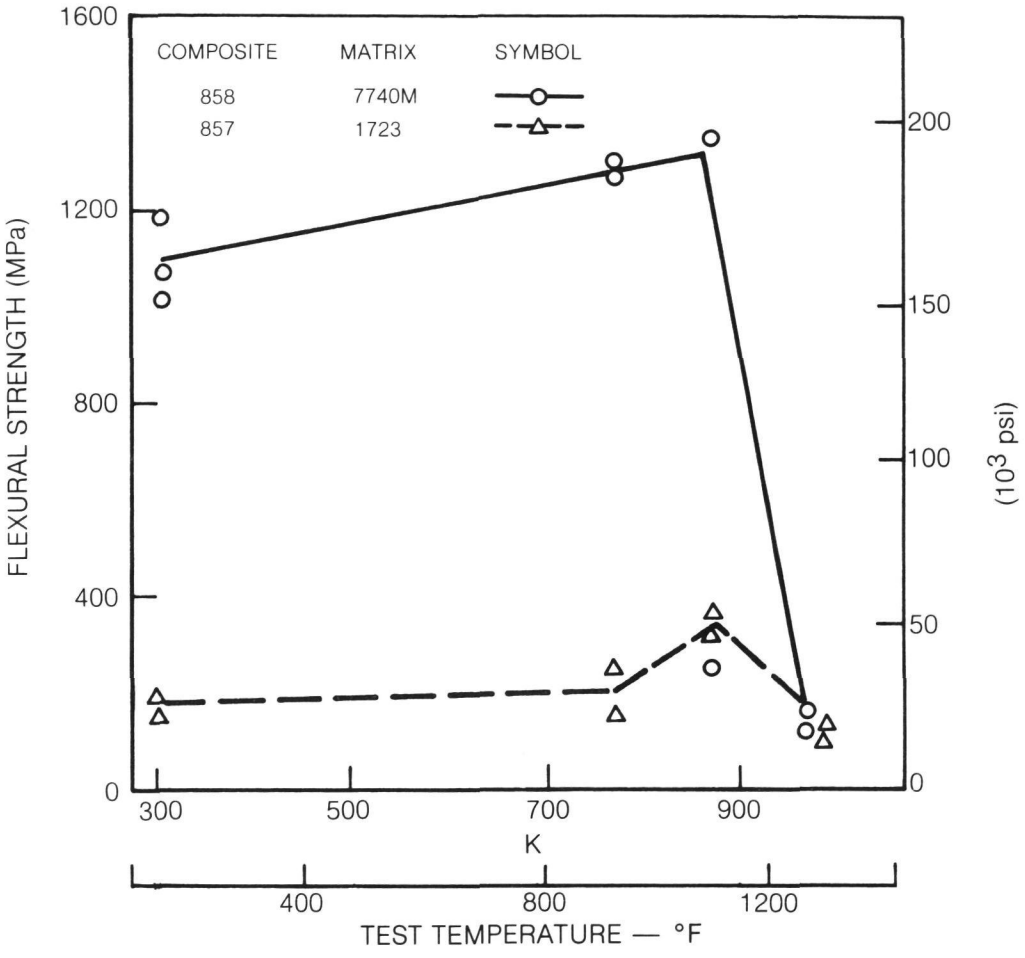

Fig. 73. Three Point Flexural Strength of 0° HMS Fiber Reinforced 774M and 1723 Glass as a Function of Test Temperature (Tested in Argon)

80–9–163–1

be seen that strength was retained to nearly 1300 K (1880°F). The per ply thickness for this composite was only 63 microns (2.5 mils) so that it would appear to be an excellent candidate for thin walled structural elements if the lower value of elastic modulus (45 GPa, 6.5 Msi) can be tolerated. It is interesting to note that average room temperature composite strength of 287 MPa (41.6 ksi) is approximately equivalent to the values for a 774M matrix composite with the same fiber content and no porosity.

Thermal expansion curves were also determined for the discontinuous Celion 6000 reinforced 96% SiO_2 glass matrix composite, Fig. 75. The curve of thermal strain vs temperature is not linear so that the coefficient of thermal expansion (CTE) is increasing with increasing temperature. For the temperature range of 300-400 K (80-260°F) the value of CTE is 5×10^{-7} K^{-1} (2.8×10^{-7} $°F^{-1}$) which is considerably lower than the CTE for similar fiber reinforcement of 774M borosilicate glass (1.7×10^{-6} K^{-1}) (9.4×10^{-7} $°F^{-1}$). This value, in fact, is somewhat less than CTE of the parent matrix, 8×10^{-7} K^{-1} (4.4×10^{-7} $°F^{-1}$).

2. Continuous Fiber Reinforcement

Three continuous graphite fibers, Thornel 300, HMS and Thornel Pitch based fiber, were all used to reinforce the 96% SiO_2 glass matrix.

a. Thornel 300 Fiber Reinforced Composites

The use of T-300 graphite (with and without scrim) to reinforce 96% silica glass matrix composites was demonstrated under UTRC funding prior to the initiation of this portion of the program. Unfortunately, the composite fabricated (666, Table XX) contained only a low percentage of fiber reinforcement (35% by volume). Additional hot pressings were thus performed (Table XX - Composites 879, 880, and 954) to achieve higher fiber contents. Although this was achieved and up to 48% fiber reinforcement resulted, composite strength was not increased. The microstructure of composite 954 is shown in Fig. 76. This composite consists of Thornel 300 fiber reinforced 96% silica glass hot pressed at 1873 K (2910°F). The composite was fabricated using a thin scrim of discontinuous Celion 6000 fiber in the tape. This is evident in the microstructure of the composite where it can be seen that each layer contains a glass rich scrim containing region. It is interesting, and unexpected, to note that rather large pores can be found in some areas of these scrim containing regions, Fig. 76 - bottom, although most of the composite structure, Fig. 76 - top, was typified by some porosity finely distributed within the fiber tows. The overall composite composition, Table XX, reflected the presence of this porosity while composite strength was equivalent or better than that of composites 879 and 880, Table XX, which were fabricated without the use of scrim.

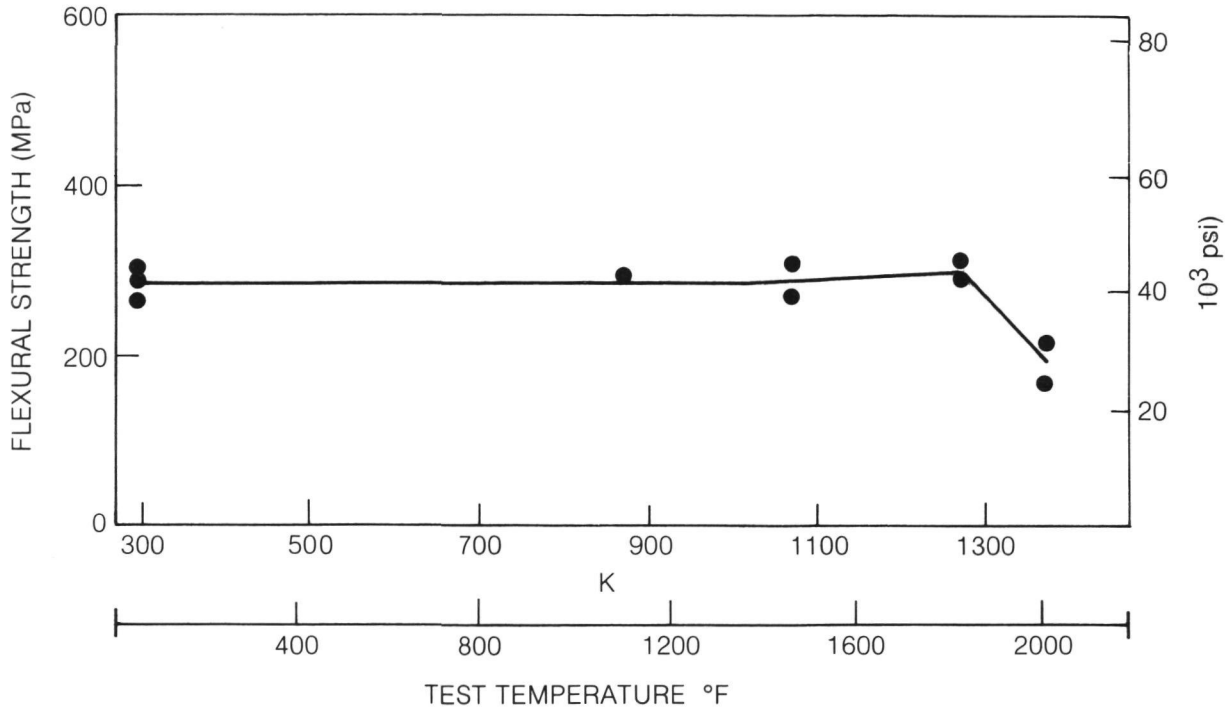

Fig. 74. Three Point Flexural Strength of Discontinuous Celion 6000 Fiber Reinforced 96% Silica Glass as a Function of Test Temperature (Composite 883) (Tested in Argon)

80–11–65–2

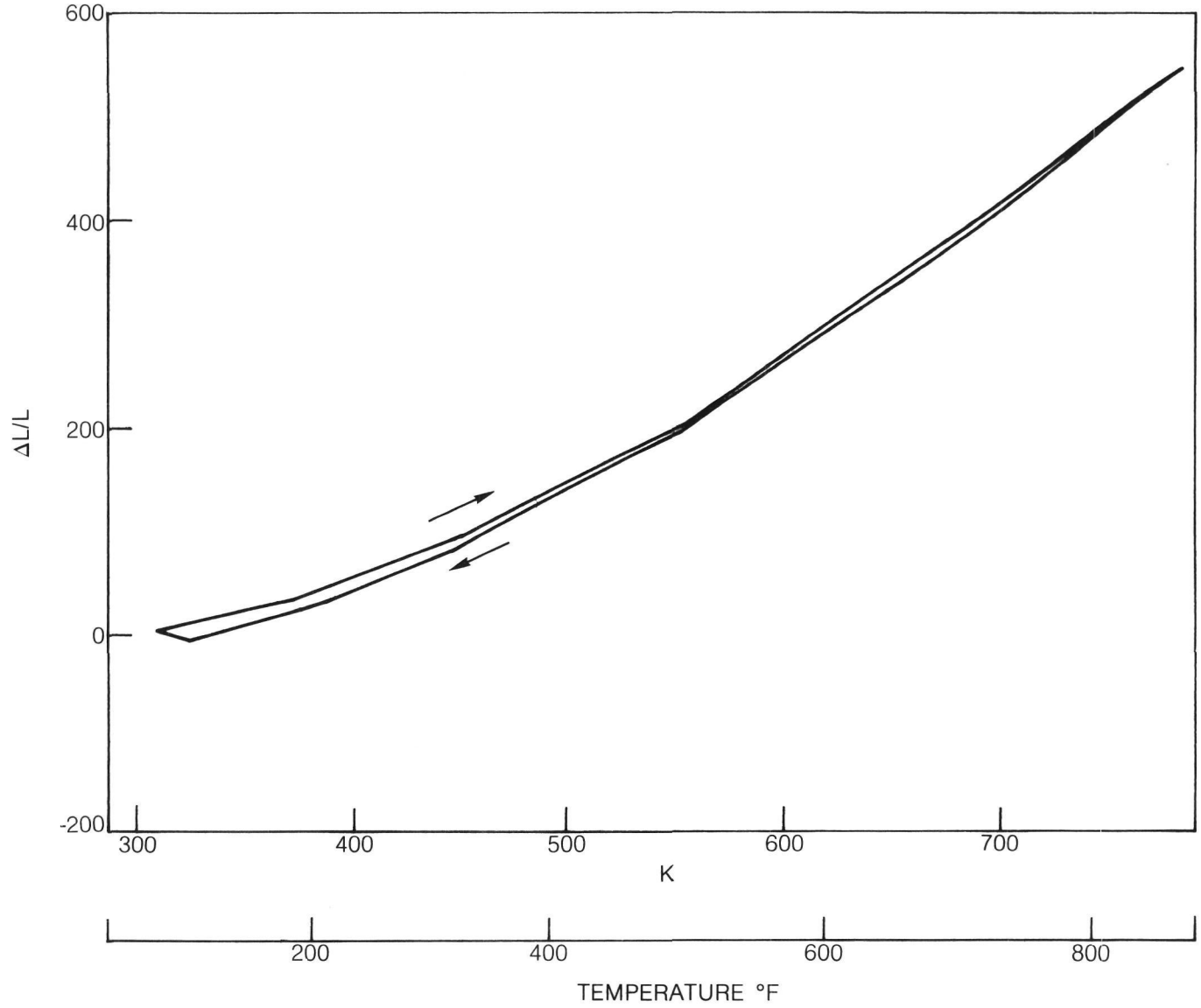

Fig. 75. Thermal Expansion of Discontinuous Celion 6000 Reinforced 96% SiO_2 (Composite 972)

81-2-100-13

Composite flexural strength as a function of test temperature (for 35% fiber reinforcement) is presented in Fig. 77 where it can be seen that excellent retention of strength can be achieved up to over 1300 K (1880°F). The elastic modulus of this unidirectionally reinforced composite was 110 GPa (16 Msi) at 300 K (75°F).

Another important characteristic of the T-300 fiber reinforced 96% SiO_2 high silica glass system is its dimensional stability. The thermal strain vs temperature curves for the 35% fiber content material in the axial and transverse directions are given in Figs. 78 and 79. In the case of the axial test, hysteresis during the first thermal cycle is absent during subsequent cycles, Fig. 78. This is simply due to the need to relieve internal stresses in the composite. The axial coefficient of thermal expansion (CTE) for this composite at near room temperature is measured to be approximately 1.4×10^{-7} K^{-1} (0.78×10^{-7}). In the case of the transverse thermal expansion, Fig. 79, the strain vs temperature curves are relatively linear and the CTE is approximately 1.3×10^{-6} K^{-1} (0.72×10^{-6} $°F^{-1}$) over the entire temperature regime.

Several composites of Thornel 300 reinforced 96% SiO_2 (with scrim) were also fabricated in the 0/90 cross ply orientations. Composites 961 and 974 were tested in three point bend to determine composite strength and elastic modulus while composite 961 was also used to determine thermal expansion behavior. For composites 961 and 974 the average flexural strengths were 150 and 144 MPa (22-21 ksi) respectively and the elastic moduli were 74 and 103 GPa (11 and 15 Msi). Composite thermal expansion curves, Fig. 80, were similar in shape to those developed for the 0°-Thornel 300 reinforced glass. Again a prominent hysteresis effect was noticeable on the first thermal cycle; however, after the fourth thermal cycle it was no longer present. The thermal expansion behavior of this material would indicate a nearly zero coefficient of thermal expansion over the RT-500 K (RT-446°F) temperature range.

b. HMS Fiber Reinforced Composites

The microstructure of HMS fiber reinforced 96% SiO_2 glass matrix composites fabricated under two different conditions are shown in Figs. 81 and 82. The first microstructure, Fig 81, is for a specimen that contains 58% fiber by volume and, according to its flexural strength, was severely weakened by the use of a 1973 K (3092°F) fabrication temperature. The overall microstructure was well consolidated with evidence of only a few regions of microstructural cracking and no observable large regions of voids or porosity. Areas of lower fiber packing density showed good evidence of the ability to densify this high silica matrix and fill in the regions between closely spaced fibers. These areas typically occurred at the periphery of the individual fiber tows, while the inner regions of these tows contained extremely high fiber contents. Hot press consolidation at a 100 K (180°F) lower temperature resulted in a composite that exhibited several regions of extended porosity within individual fiber tows, Fig. 82. This porosity, although easily noticed, constituted only a small portion of the overall composite

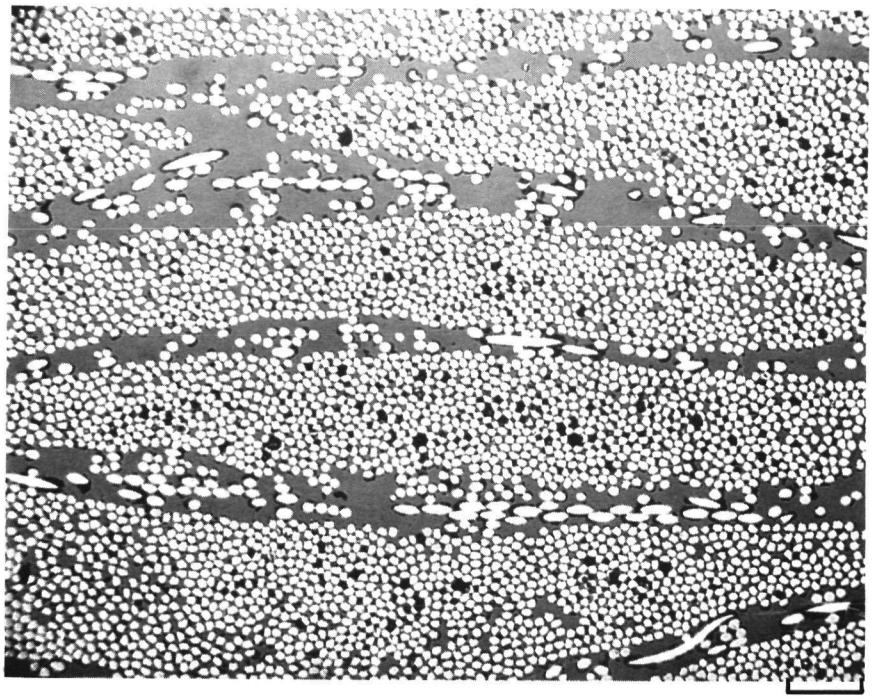

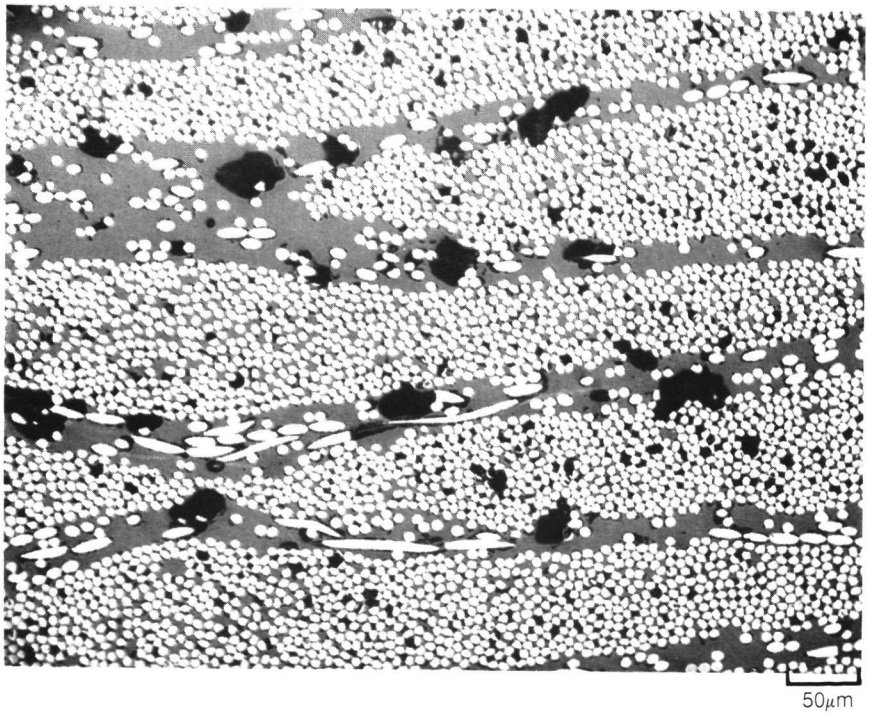

Fig. 76. Thornel 300 Fiber (with Scrim) Reinforced 96% SiO_2 Consolidated at 1873K (2910°F) (GC954)

81-1-53-2

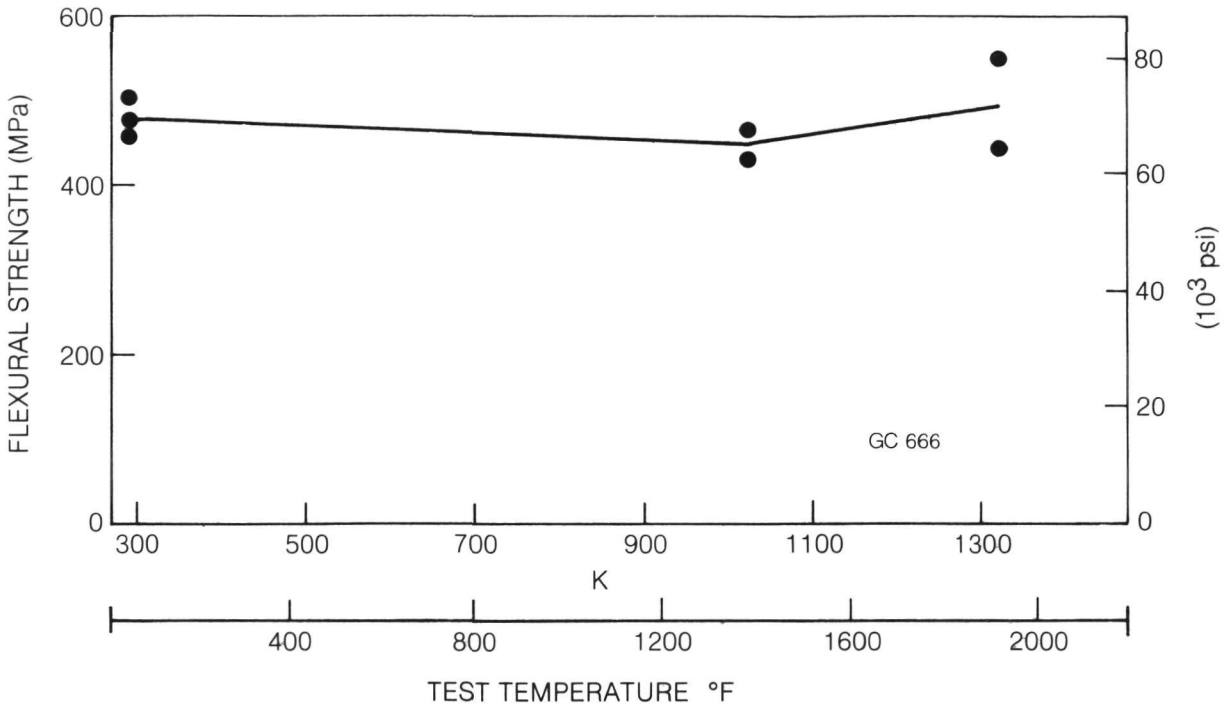

Fig. 77. Three Point Flexural Strength of Th300 Reinforced 96% SiO_2 Glass as a Function of Test Temperature (Tested in Argon)

80–11–65–1

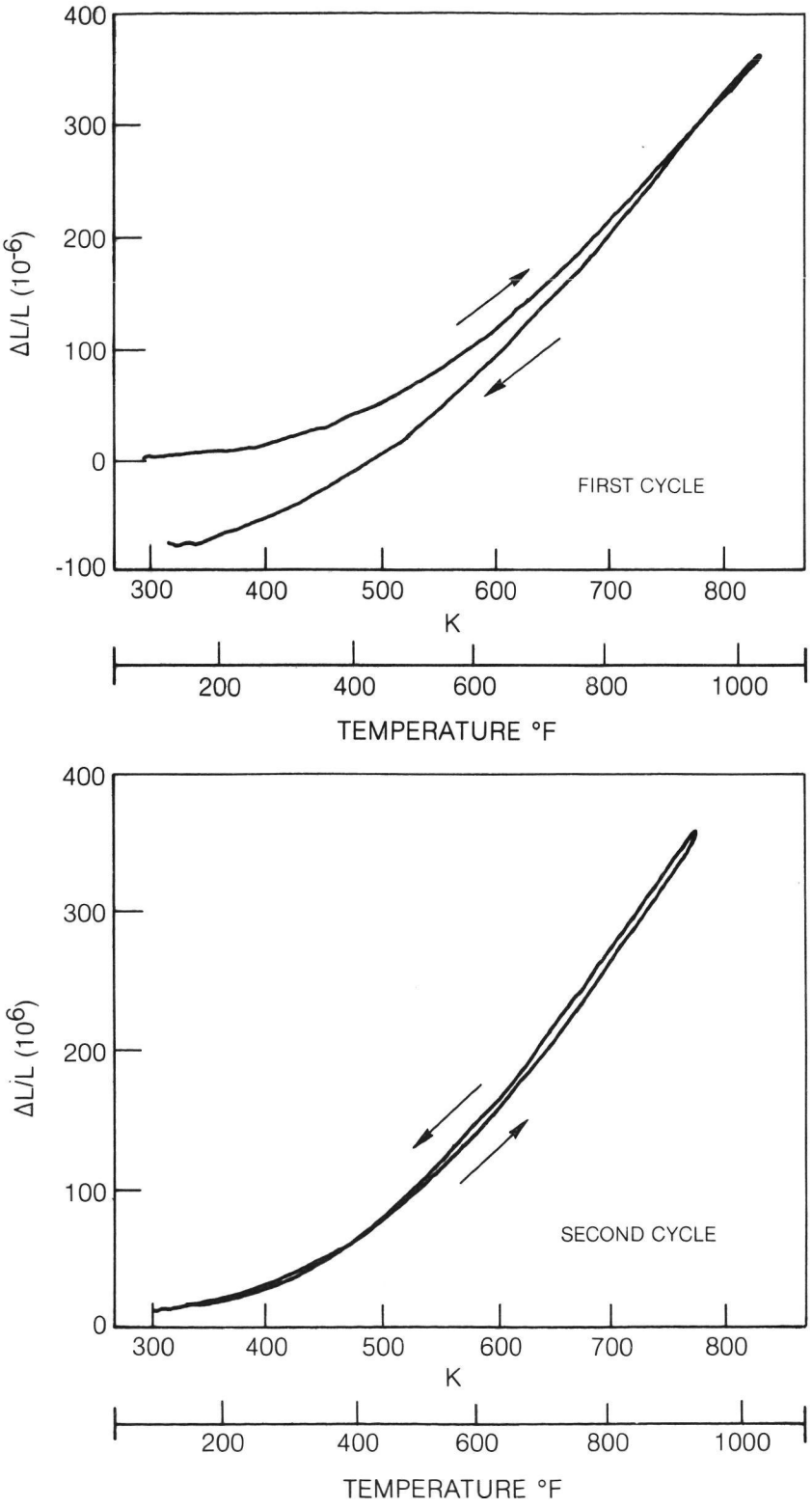

Fig. 78. Axial Thermal Expansion of Unidirectionally Reinforced Thornel 300/96% SiO_2 (with Scrim) (GC 668)

80–11–65–3

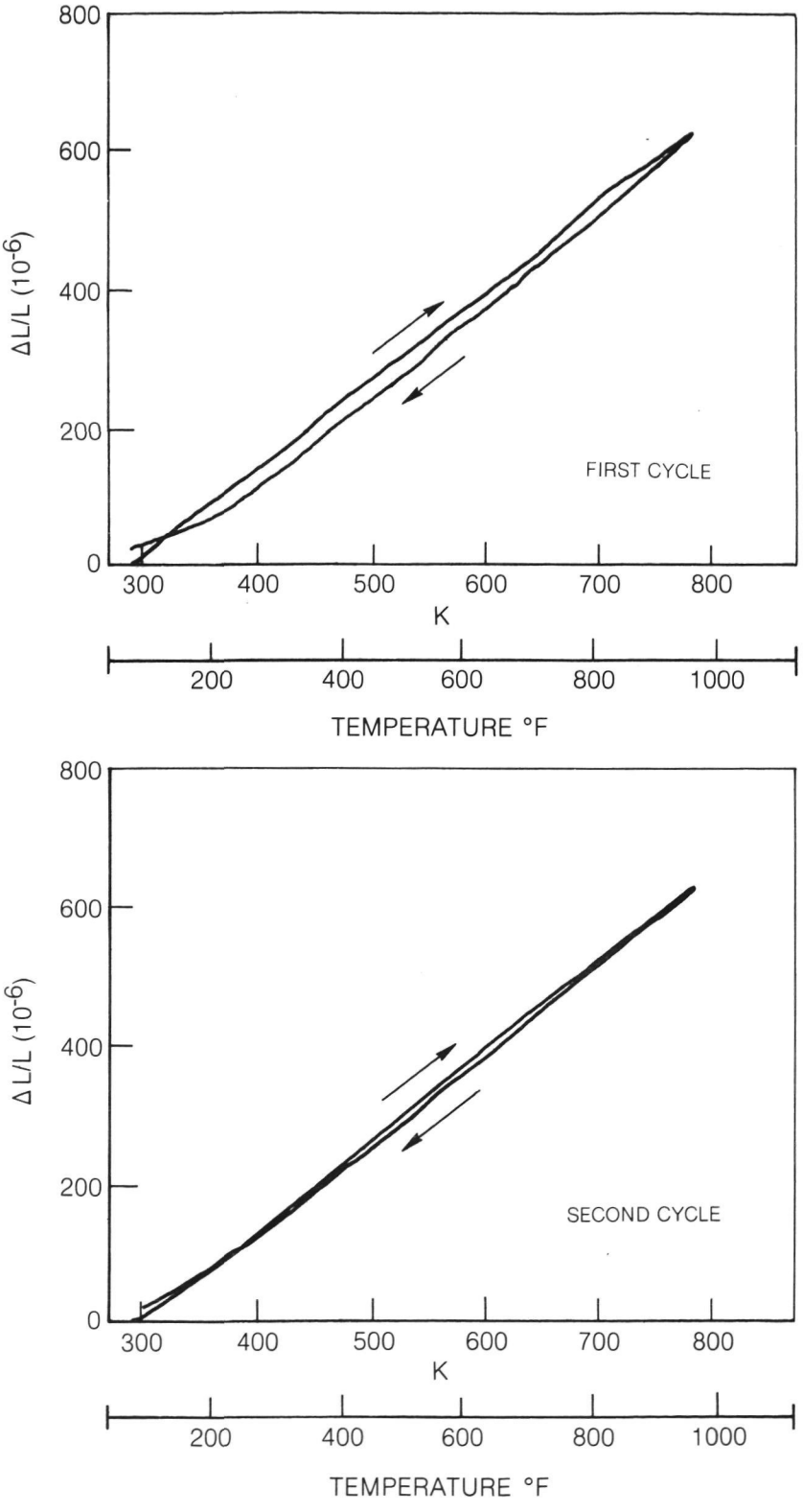

Fig. 79. Transverse Thermal Expansion of Unidirectionally Reinforced Thornel 300/96% SiO_2 (with Scrim) (GC 668)

80–11–65–4

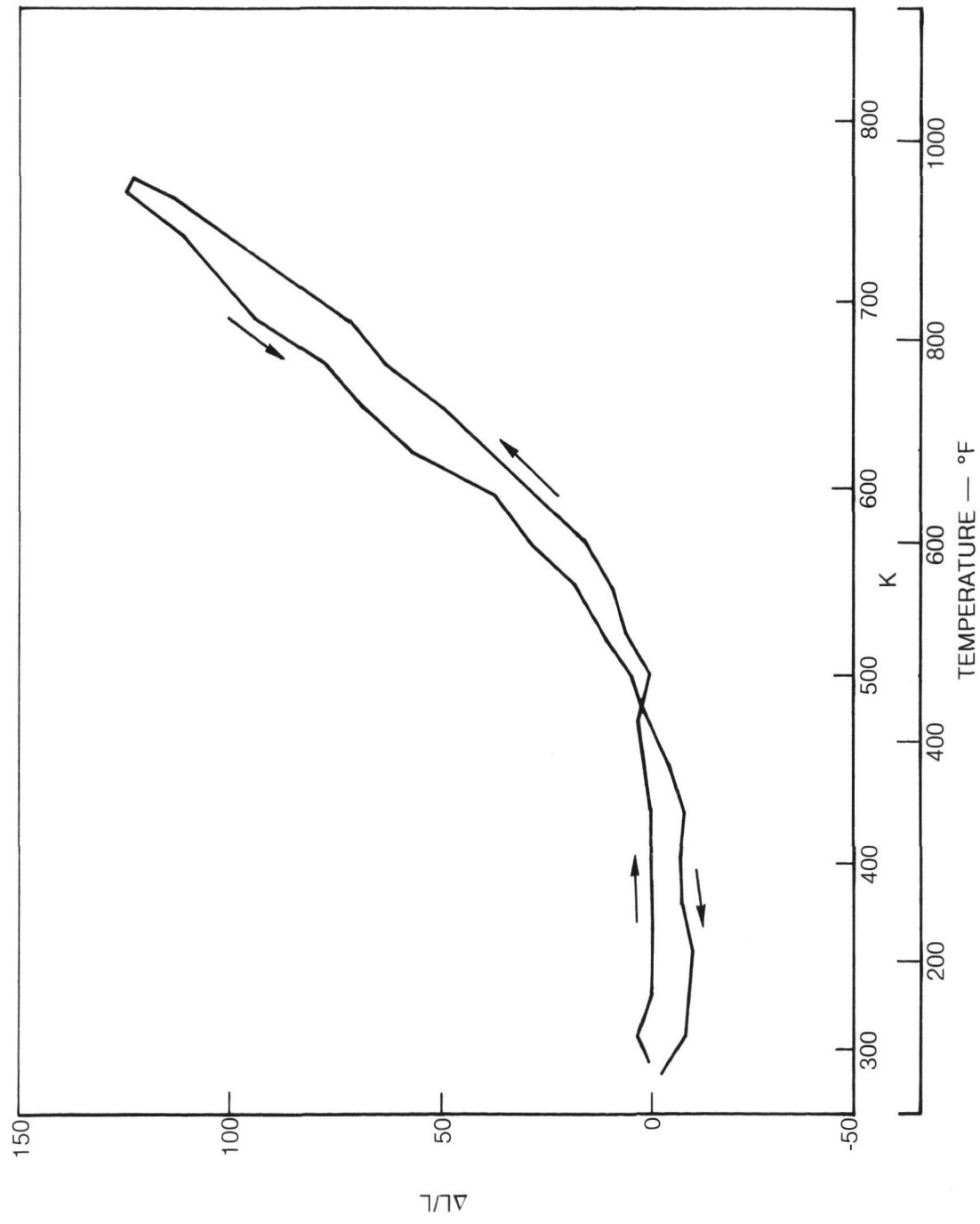

Fig. 80. Axial Thermal Expansion of 0/90 Cross Ply Th300 Reinforced 96% SiO_2 (with Scrim) (GC961) (Thermal Cycle #4)

81–2–100–14

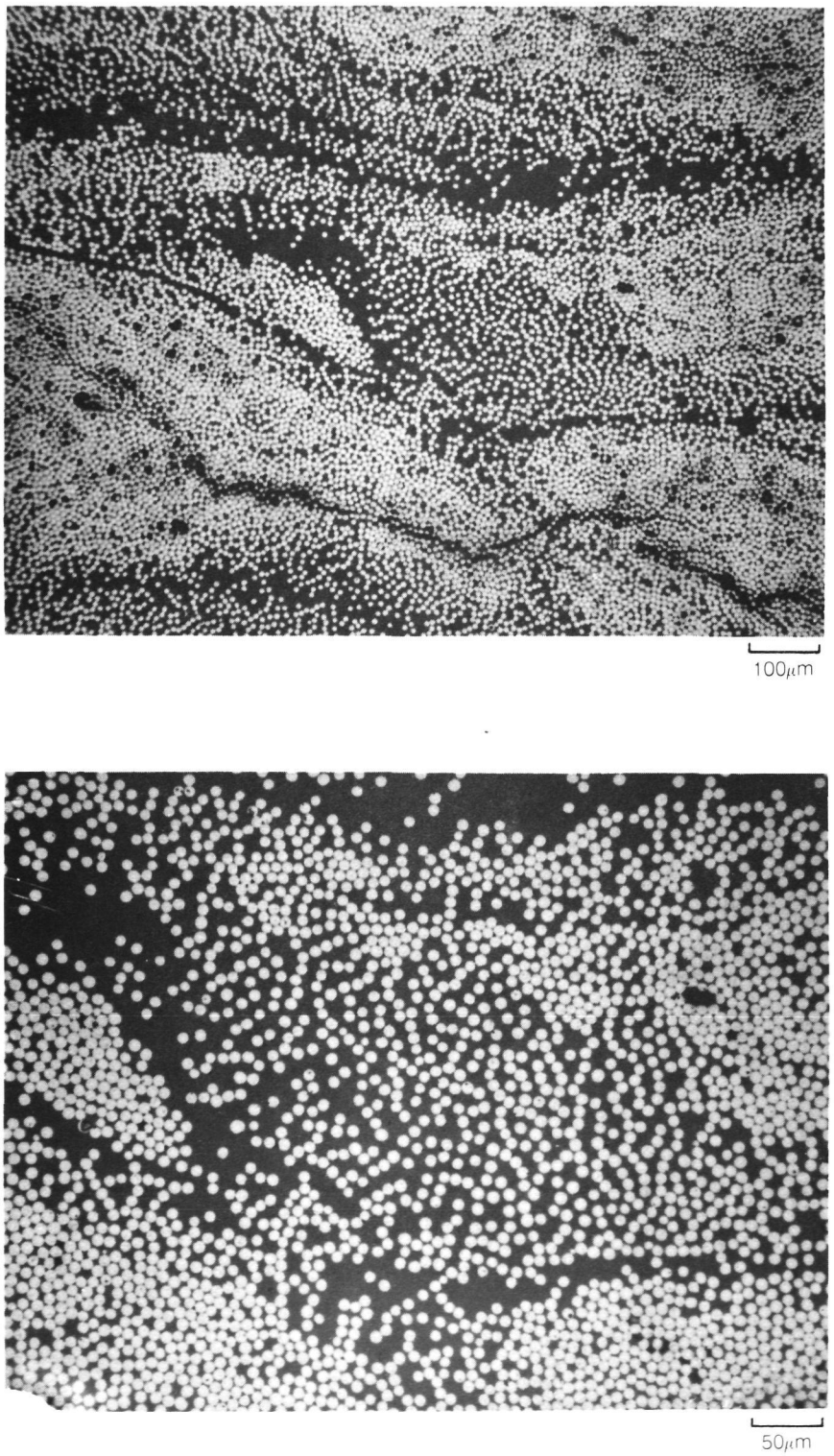

Fig. 81. HMS Fiber Reinforced 96% SiO_2 Consolidated at 1973K (3092°F) GC864)

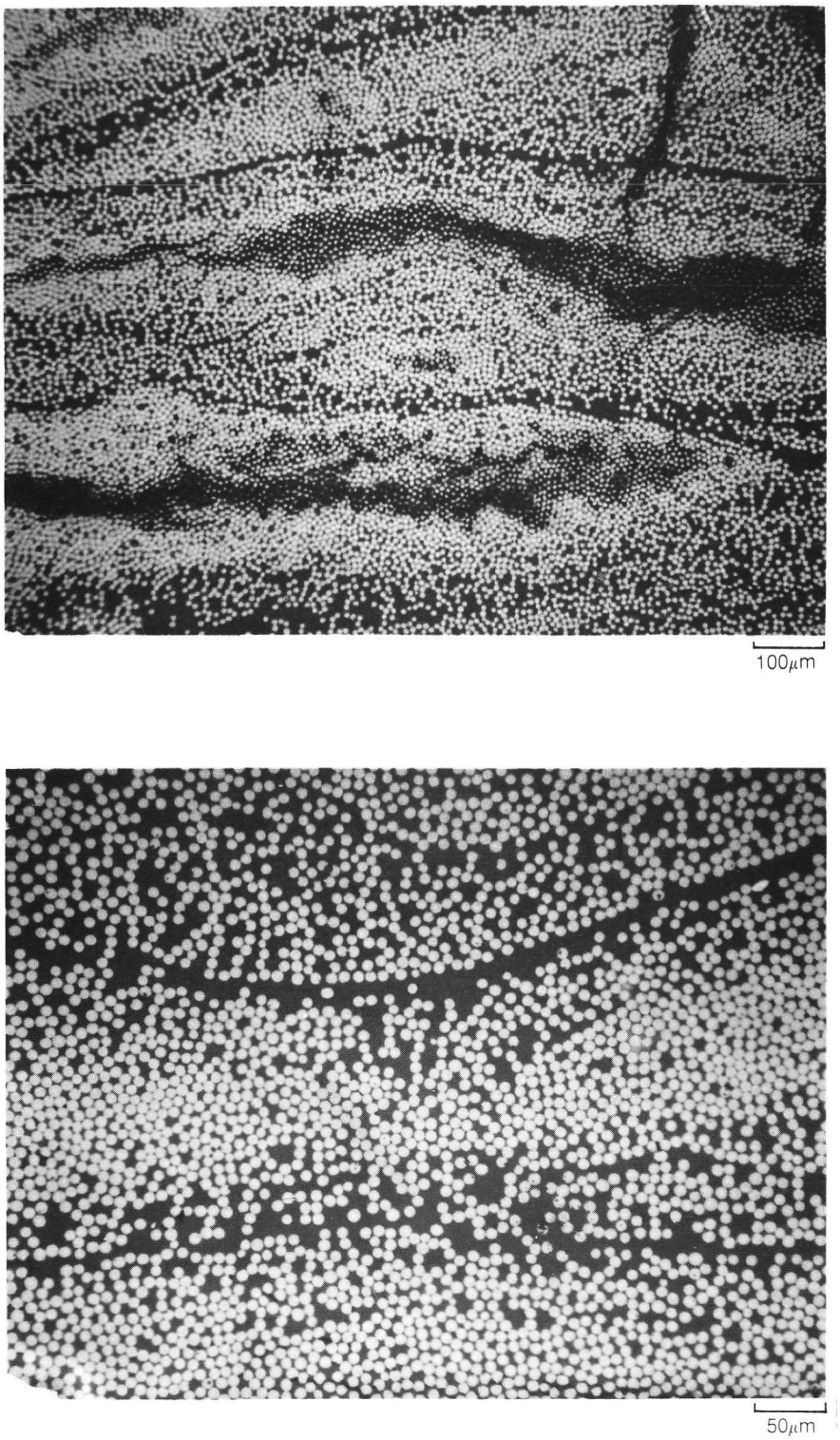

Fig. 82. HMS Fiber Reinforced 96% SiO_2 Consolidated at 1873K (2912°F) (GC859)

structure since overall porosity was only 1% by volume. Regions of composite at the periphery of the tows again showed excellent microstructural consolidation. From this, it would appear that excellent composite microstructures can be achieved at the lower temperature if matrix infiltration within the tows can be accomplished. This is most probably controlled by the original penetration of the tows by glass powder during the tape making process. The lower bonding temperature also provided a much stronger composite, Table XX.

Both of these composites were tested in three point bend over the temperature range of RT to 1423 K (1150°C) in argon. Composite flexural strength is presented in Fig. 83 as a function of test temperature. At RT, average composite strengths were 430 MPa (62.4 ksi) and 486 MPa (70.5 ksi) for composites 859 and 864 respectively. These strengths are substantially less than those obtained for HMS fiber reinforced 774M borosilicate glass (see Fig. 73); however, the flexural strength increases with increasing test temperature to maximum values of nearly 630 MPa (91 ksi). The composite fabricated at 1873 K (2910°F), composite 859, reached this maximum at a test temperature of 1123 K (1560°F) and exhibited a rapid decrease in strength above 1273 K (1832°F). Composite 864, fabricated at the higher temperature of 1973 K (1700°C) exhibited a peak in strength at 1273 K (1832°F) and retained over 50% of its room temperature strength at even 1423 K (2102°F).

Examination of the composite flexural specimens after test indicated that only those which had been tested above the temperatures for peak strength exhibited any permanent deformation. In the case of composite 859 deformation is noted for specimens tested at above 1273 K (1832°F), while composite 864 specimens exhibited deformation only at 1423 K (2102°F). Composite elastic modulus data illustrated the same dependence on test temperature, Fig. 84.

The axial and transverse thermal expansion behavior of HMS reinforced 96% SiO_2 was also measured. Composite 937 was reinforced with 54% by volume HMS unidirectional fibers. The axial thermal expansion curve, Fig. 85, is similar in shape to that measured previously for HMS fiber reinforced 774M matrix composites. The data in Table XXI compare these data and indicate that the axial coefficient of thermal expansion (0°-CTE) is only slightly smaller for the 96% SiO_2 matrix composite even though there is a major difference in unreinforced matrix CTE's. This is most probably due to the fact that the 774M matrix composite contained a higher percentage of graphite fibers and that these fibers are the major controlling factor in the determination of 0° CTE due to their high elastic modulus. One major difference between these two composites is that the 96% SiO_2 matrix composite exhibited some residual positive strain after

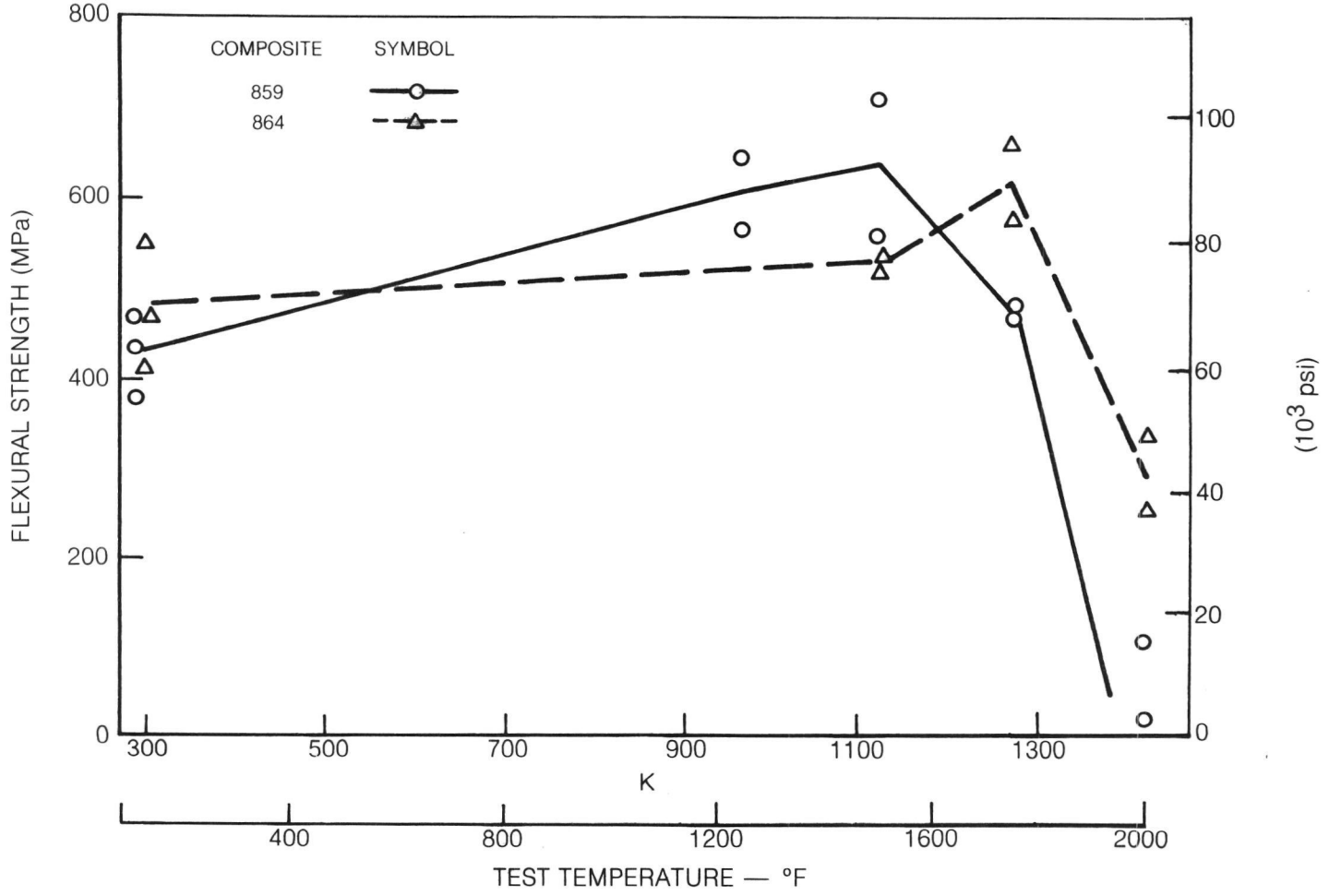

Fig. 83. Three Point Flexural Strength of 0° HMS Fiber Reinforced 96% SiO_2 Glass as a Function of Test Temperature (Tested in Argon)

80-9-163-2

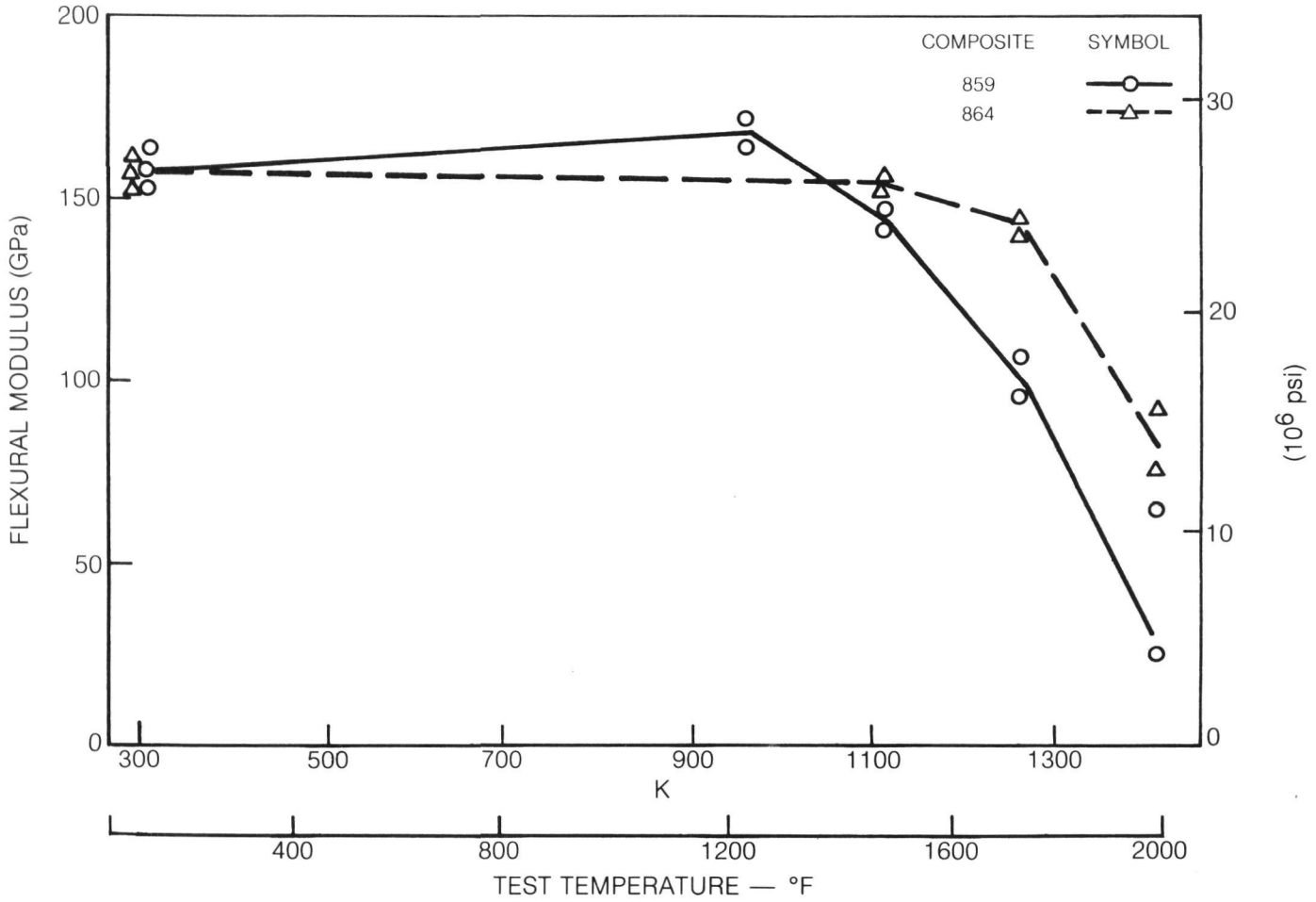

Fig. 84. Three Point Flexural Modulus of 0° HMS Fiber Reinforced 96% SiO_2 Glass as a Function of Test Temperature (Tested in Argon)

80-9-163-3

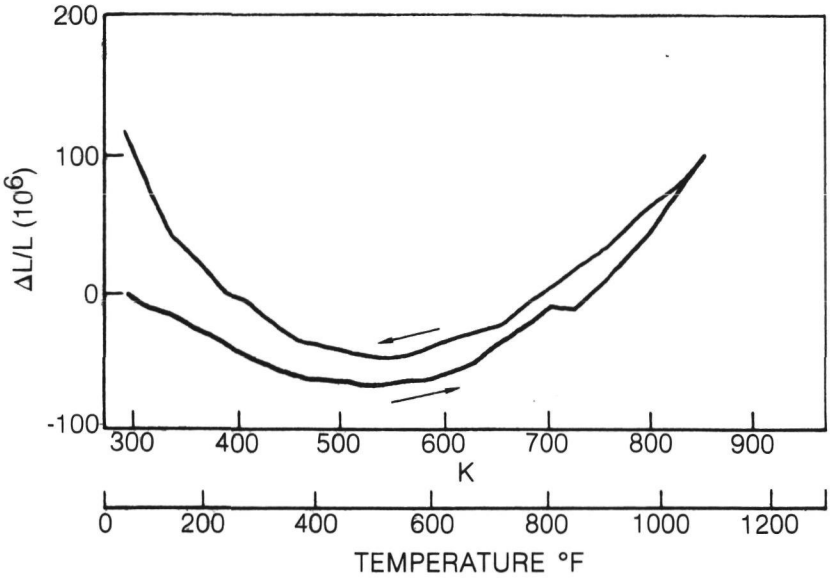

Fig. 85. Axial Thermal Expansion of Unidirectionally Reinforced HMS/96% SiO_2 (GC937)

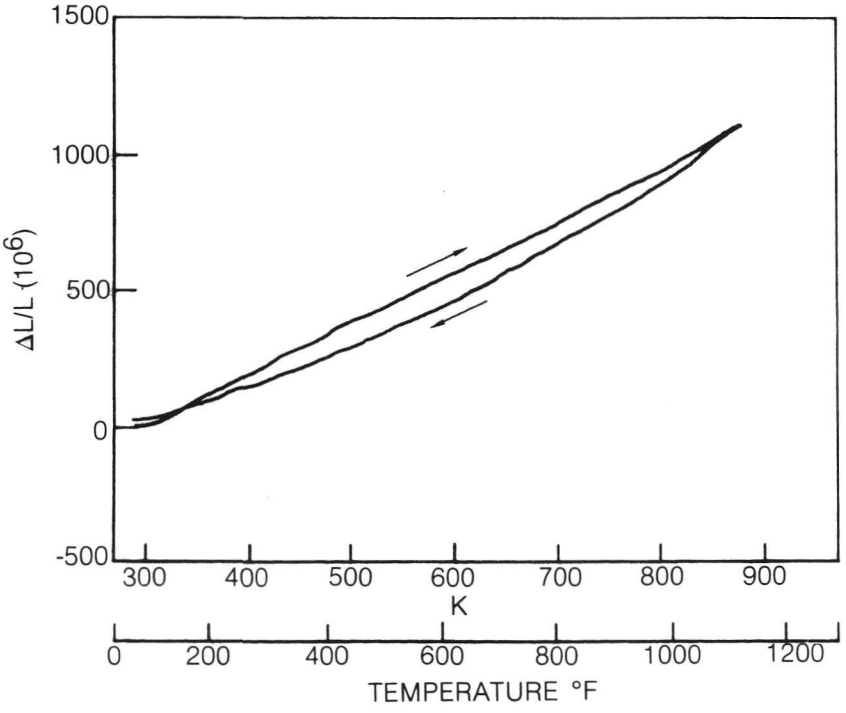

Fig. 86. Transverse Thermal Expansion of Unidirectionally Reinforced HMS/96% SiO_2 (GC937)

81-2-100-10

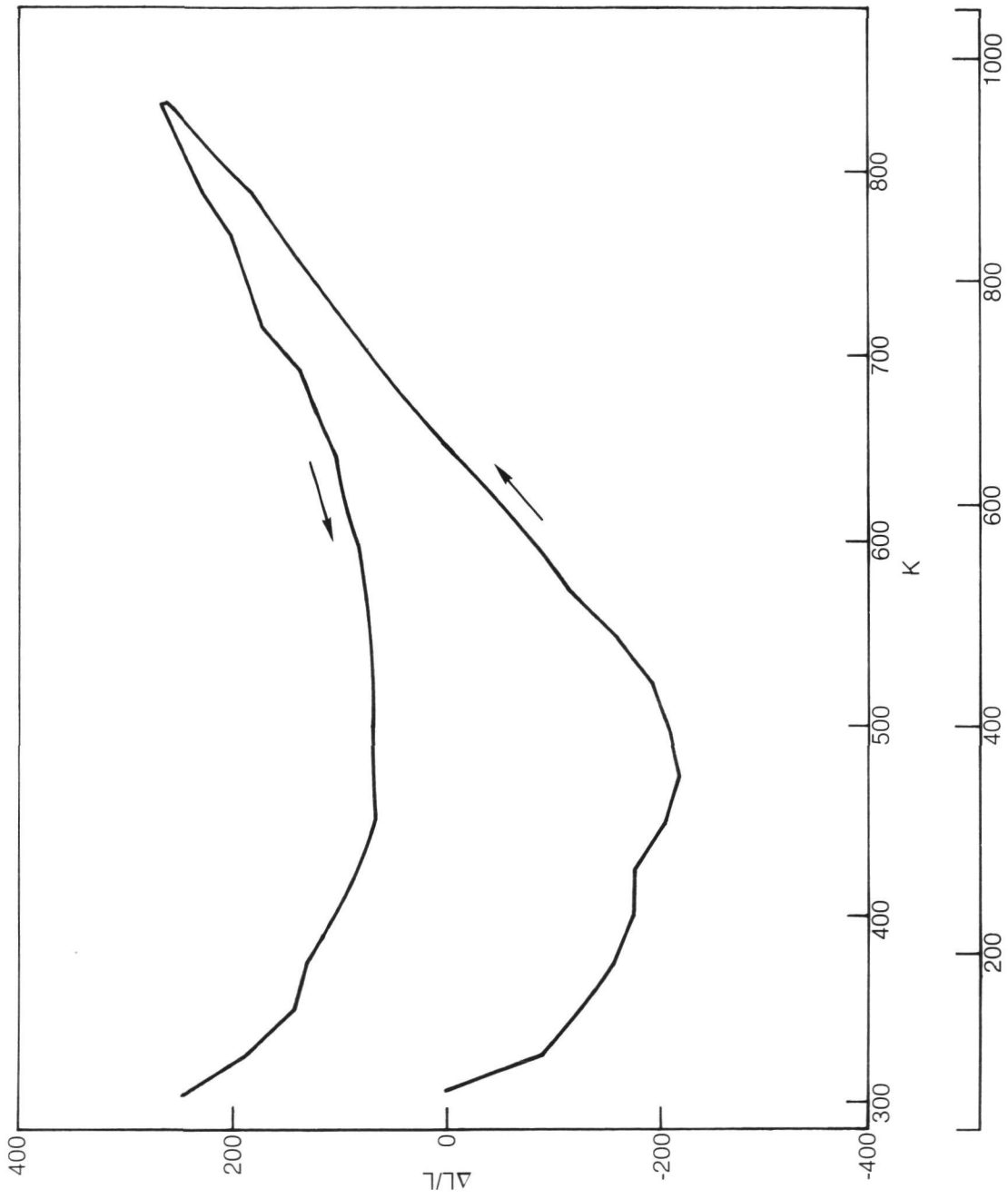

Fig. 87. Thermal Expansion of 0/90 Reinforced HMS/96% SiO_2 (GC952)

81–2–100–11

Table XXI

Comparison of Thermal Expansion Behavior of Graphite Fiber Reinforced Glass Matrix Composites

Composite	Matrix	Ply Lay-Up	Fiber	v/o Fiber	RT Thermal Expansion Coefficient 10^{-6} K^{-1} (10^{-6}°F^{-1})	
					0°	90°
377	774M	0°	HMS	70	-0.50(-0.28)	+6.5(3.6)
937	96% SiO_2	0°	HMS	54	-0.36(-0.2)	+1.9(1.0)
668	96% SiO_2	0°	T-300	35	+0.14(0.08)	+1.3(0.7)
959	MAS (Ht. Treated)	0°	HMS	66	-0.55(-0.3)	10.6(5.9)

each of two thermal cycles to a maximum temperature of 853 K (1076°F). The 7740 matrix composites were found to exhibit much lower levels of residual strain and they also appeared to stabilize their behavior after several thermal cycles.

There was a much larger difference in composite 90°-CTE due to the change in matrix, Table XXI. This would be expected due to the greater importance of matrix CTE in determination of this property. The overall thermal expansion curve, Fig. 86, is nearly linear with some evidence for hysteresis but no significant residual strain.

The existence of a hysteresis effect after thermal cycling to 800 K (980°F) was magnified for a 0/90 cross ply HMS fiber reinforced 96% SiO_2 composite, Fig. 87. This curve which represents the second cycle of testing indicates a significant net increase in specimen length after cycling. Additional cycles were not performed to determine whether this effect can be removed by additional thermal cycles; however, this is likely based on the experience with the T-300 reinforced composite, Fig. 80.

c. Thornel Pitch Based Fiber Reinforced Composites

High modulus Thornel pitch based graphite fiber was used to fabricate several 96% SiO_2 matrix composites using a variety of conditions, Table XX - composites 936, 943, and 944. In every case it was found possible to achieve a nearly full density composite indicating, as in the case of the HMS fiber reinforced composites described above, the matrix flows sufficiently well under these hot pressing conditions to make a sound composite. The composite strength, however, is quite low when compared with 774M matrix composites (894 and 925, Table XX). The failure mode of the 96% SiO_2 matrix composites was found to not be tensile failure of the fibers, but rather an interlaminar shear failure mode indicating that, although dense, the composites are not well bonded. The 774M matrix composites also failed by an interlaminar mechanism (also some evidence of compression failure under the loading nose), however, at a much higher applied stress. The handleability and appearance of the 774M matrix composites would also indicate that they are much better bonded.

D. Magnesia Aluminosilicate (MAS) Glass Matrix Composites

Two different forms of MAS powder were obtained. Designated 266 and 2969, they were both characterized by a -325 mesh powder size. The advantage of this matrix system is that composites can be fabricated when the matrix is in a low viscosity glass state and then a subsequent heat treatment can crystallize the matrix into a cordierite structure, which has high thermal stability and low CTE. Composites 938, 939, and 947 (Table XX) were fabricated using HMS fiber as reinforcement. Successful composite consolidation was achieved by hot pressing

at 1823 K (2822°F), composites 938 and 939. In both cases the matrix flowed extensively into die cavities during fabrication indicating that at this temperature the matrix viscosity is quite low. This is very different from the 96% SiO_2 matrix composites discussed above where no evidence of matrix flow into die cavities could be detected. Composite flexural strength for both of these specimens was as high as that achieved in the past for HMS reinforced 96% SiO_2 matrix specimens. In the case of the MAS matrix specimens, composite failure occurred by an interlaminar mode, rather than fiber tensile fracture.

The microstructure of one of these, composite 939, is shown in Fig. 88 where it can be seen that excellent matrix flow has resulted in matrix densification and fiber encapsulation. A few matrix cracks were evident in the composite, Fig. 88 - bottom; however, overall the composite had few matrix cracks. Composite 939 had been hot pressed at 1823 K (2822°F) which is above the melting point of the cordierite ceramic so that the excellent densification described above could be achieved. Unfortunately, however, the matrix was too fluid at this temperature and excessive matrix flash out of the die occurred. In addition, a bond release agent had to be used on the molybdenum die cover foils to prevent excessive bonding to the composite. It was hoped that hot pressing at a lower temperature would alleviate these problems; however, a drop of only 50 K (90°F) in bonding temperature, composite 947 - Table XX, resulted in incomplete composite densification to the extent that the composite could not be handled. This was due to the fact that the crystalline material was present in sufficient quantity to prevent densification. Some matrix crystallization took place during composite heating. Two additional composites fabricated at the higher temperature of 1823 K (2822°F) were also relatively unsuccessful. Composite 955, consisting of Thornel Pitch fibers in 266, was too thin to evaluate due to excessive flash of the matrix out of the die. A Thornel 300 reinforced 266, composite 956, also produced a great deal of flash and the resultant composite strength was very low, Table XX. Thus, hot pressing at too low a temperature precluded achievement of full density composites while hot pressing at temperatures high enough to insure a fully glassy matrix caused excessive matrix flow.

To overcome these problems, it was decided to preheat the composite to assure sufficient melting of any ceramic present, and then hot press at a lower temperature. Composites 948, 957, 958A and 958B were all hot pressed using this procedure, Table XX. One point to note is that composite 957 was hot pressed twice due to an error in the hot pressing operation, thus its flexural strength is somewhat lower than that of the other composites. The strengths of the other three composites, 948, 958A and 958B were somewhat less than the strength of the composite (939) pressed at the highest temperature of 1823 K; however, the removal of the molybdenum surface foil was facilitated by this lower temperature procedure. The microstructure obtained for composite 948 is shown in Fig. 89. Excellent matrix densification was achieved. One very

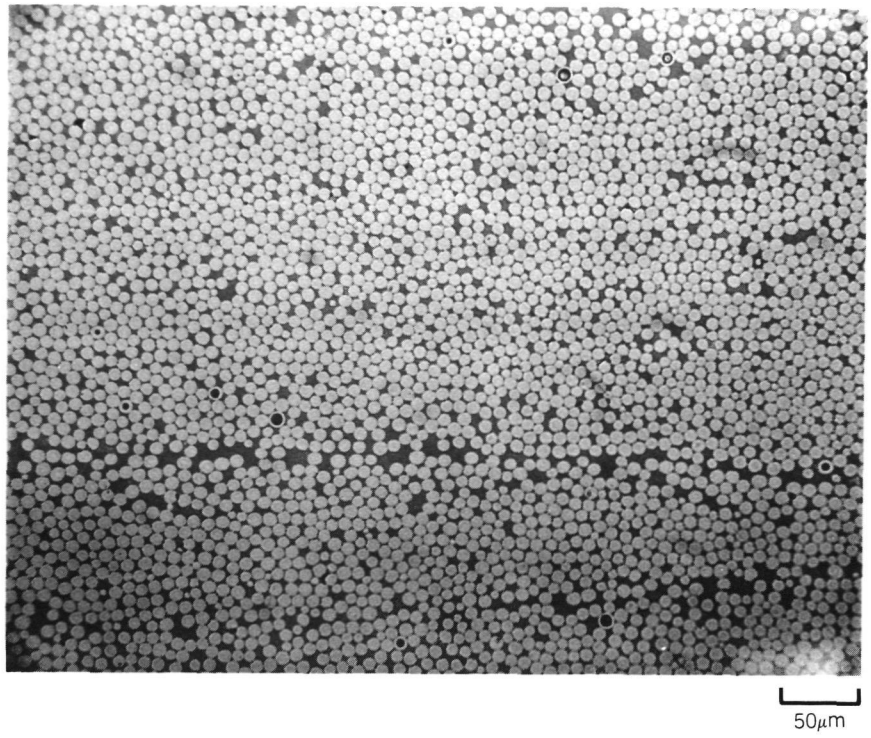

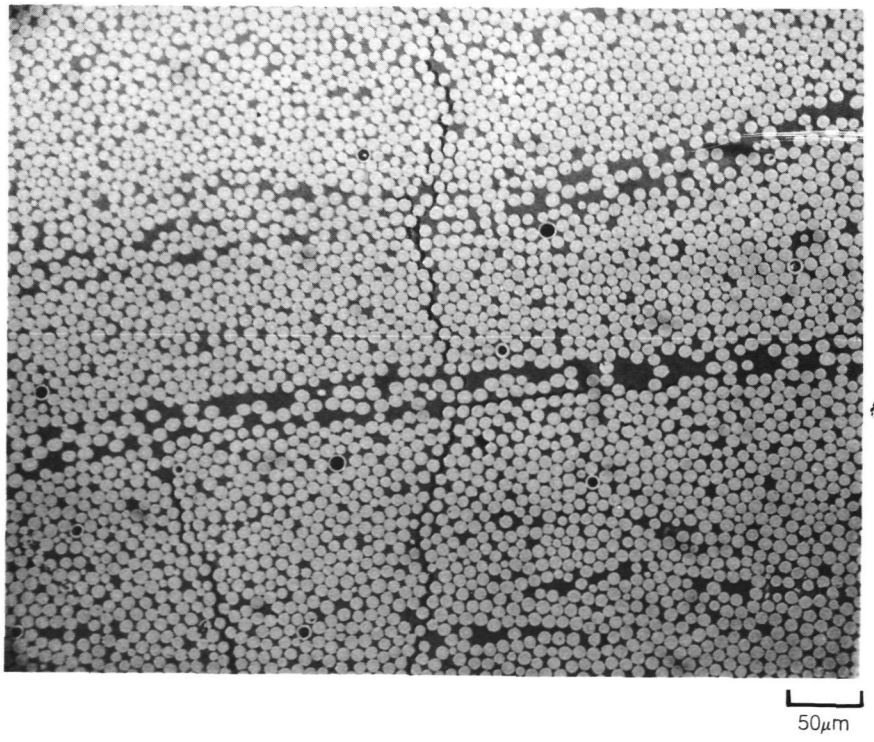

Fig. 88. HMS Fiber Reinforced MAS Consolidated at 1823K (2822°F) (GC939)

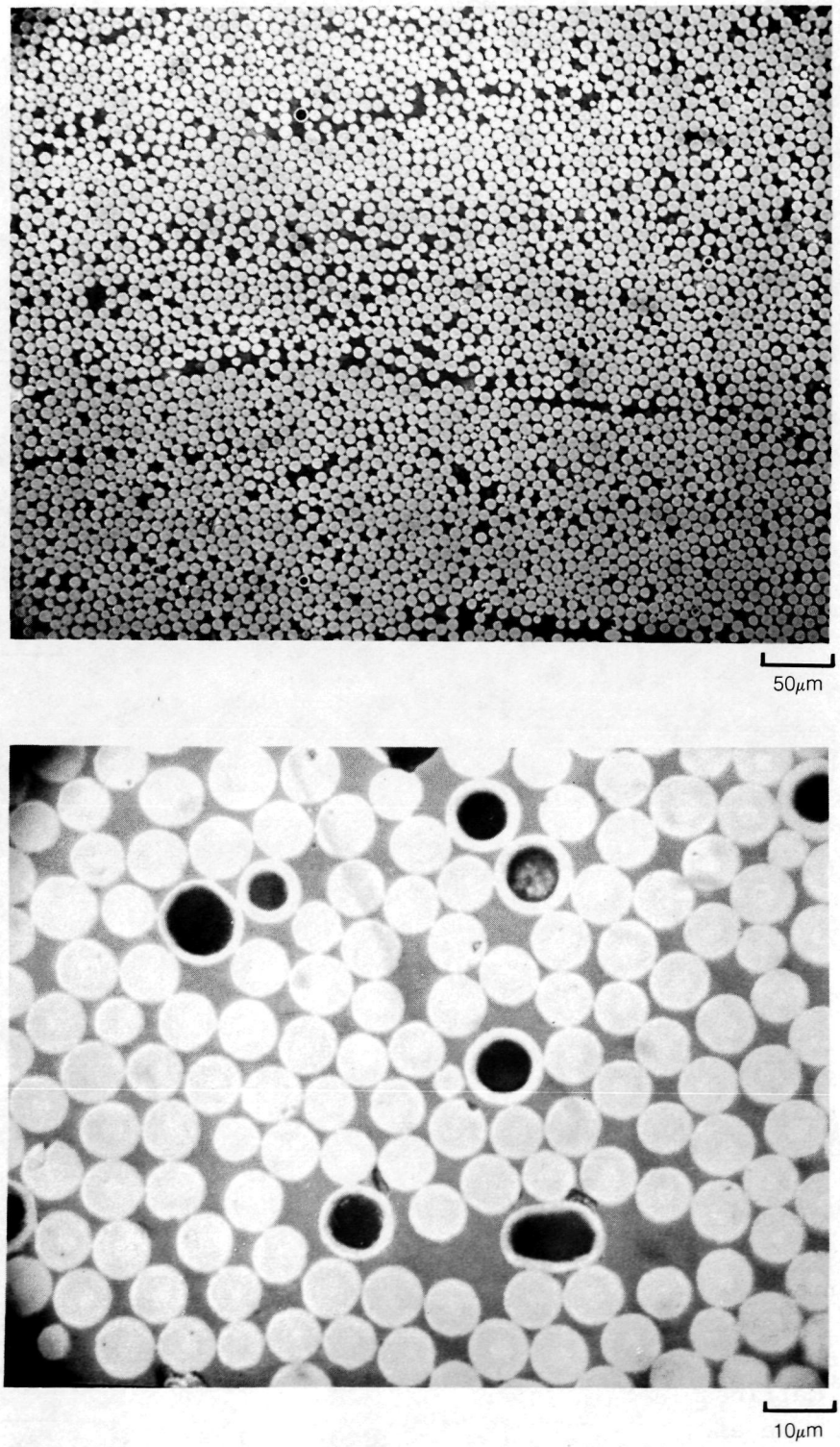

Fig. 89. HMS Fiber Reinforced MAS Consolidated at 1773K (2730°F) (GC948)

interesting point is that a few of the HMS fibers appear to have been hollowed out, Fig. 89 - bottom. The region shown in the figure has a much higher concentration of these fibers than the overall structure, however, despite their rather infrequent nature they provide an interesting new feature that has not been evident with any of the other fiber matrix combinations.

Composite 949, consisting of HMS fiber reinforced 774M borosilicate glass, was fabricated to provide a strength comparison with the MAS matrix composites which use the same fiber spool. The borosilicate glass matrix composite is clearly much stronger even though it is reinforced with a lower fiber content.

The axial three point flexural strength of HMS fiber reinforced MAS was measured as a function of test temperature, Fig. 90. In the as-fabricated condition the composite exhibited a maximum in strength at 973 K (1292°F) followed by a rapid decrease in strength at higher temperatures due to excessive deformation of the matrix. The specimens tested at 1173 K (1652°F) simply deformed under load. It should also be noted that all other specimens tested failed by an interlaminar mode rather than tensile fracture on the specimen surface. Thus, the flexural strengths reported are lower than the actual flexural strength of the composite.

The decrease in strength at elevated temperature was due to the retention of glassy material in the matrix after hot pressing. To eliminate this several composite specimens were put through a heat treatment cycle consisting of a 1 hr nucleation step at 1088 K (1562°F) followed by a 1 hr crystal growth step at 1423 K (2102°F). This procedure completed the crystallization of the matrix so that composite elevated temperature strength was markedly improved. Specimens tested at 1173 K (1652°F) and 1273 K (1832°F) exhibited strength values equivalent to composite strength at room temperature. Once again, however, composite failure occurred by interlaminar shear rather than tensile fracture. This failure mode also typified the heat treated specimens which were tested at room temperature. The heat treatment apparently caused an increase in matrix thermal stability, however, at the expense of composite interlaminar shear strength. Composite elastic modulus is shown as a function of temperature in Fig. 91 where it can be seen that heat treatment also caused a decrease in observed elastic modulus, probably also because of the decrease in interlaminar shear strength.

The thermal expansion behavior of uniaxial HMS reinforced MAS that has been heat treated is presented in Figs. 92 and 93. The axial thermal expansion curve, Fig. 92, of this system retains the general features of other HMS fiber reinforced glass matrices in that the composite initially contracts upon heating and then, at some elevated temperature expands at a more rapid rate. The axial coefficient of thermal expansion (CTE) at room temperature is approximately -5.5×10^{-7} K^{-1} (-3.0×10^{-7} $°F^{-1}$) which is in rather close agreement with the value for HMS/7740, Table XXI. The axial CTE decreases rapidly with increasing

temperature so that at approximately 373 K (212°F) the value of CTE is approximately zero. It should also be noted that there is very little hysteresis in the thermal expansion curve over the entire temperature range tested. The curve shown in Fig. 92 is the second thermal cycle of the specimen in the dilatometer; however, even the first thermal cycle showed very little evidence of hysteresis.

The transverse thermal expansion curve, Fig. 93, exhibited two distinctly different regions of expansion. The room temperature CTE for this orientation is approximately 10.6×10^{-6} K^{-1} (5.9×10^{-6} $°F^{-1}$).

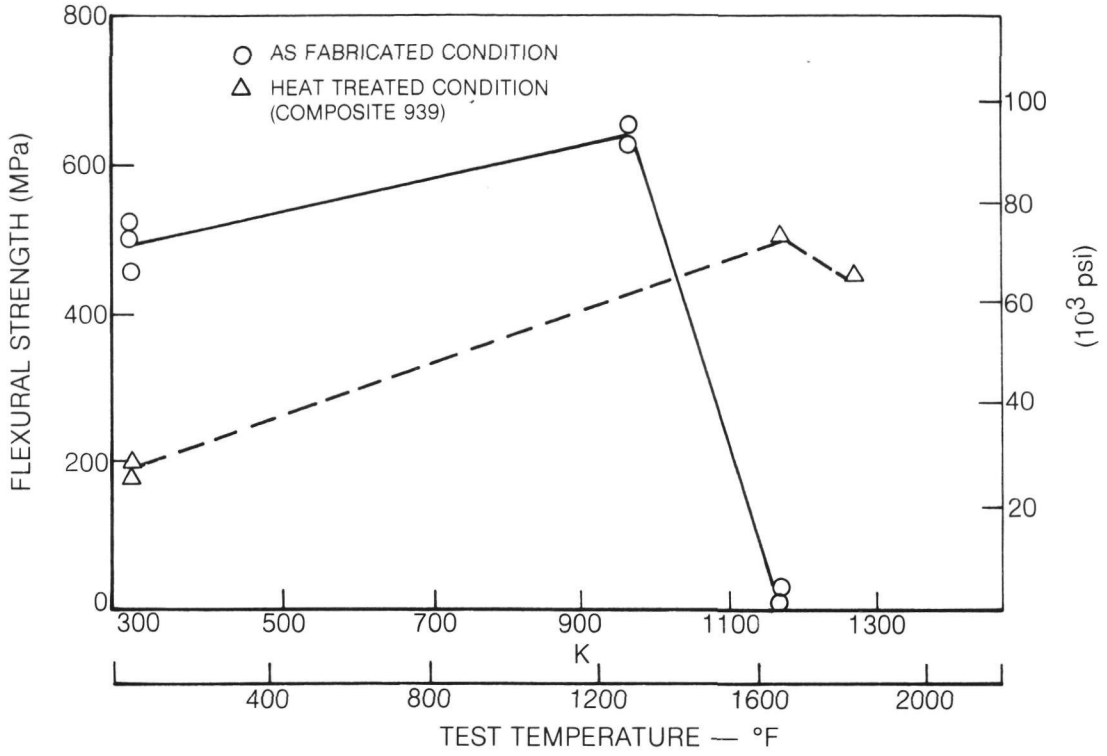

Fig. 90. Three Point Flexural Strength of 0° — HMS Reinforced MAS as a Function of Test Temperature (Tested in Argon)

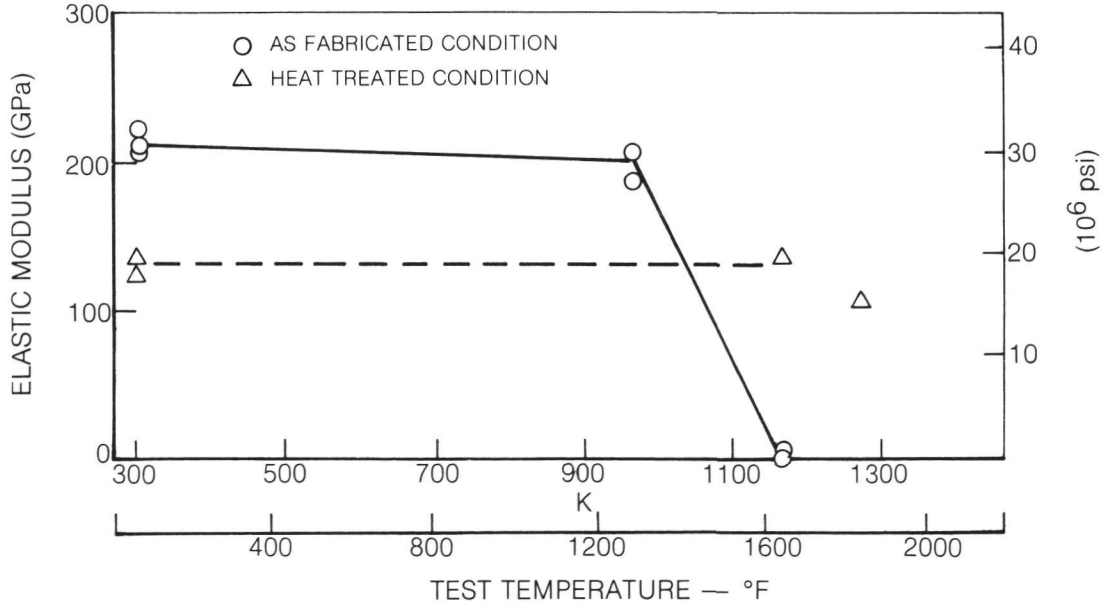

Fig. 91. Flexural Elastic Modulus of 0° — HMS Reinforced MAS as a Function of Test Temperature (Tested in Argon)

81—2—100—9

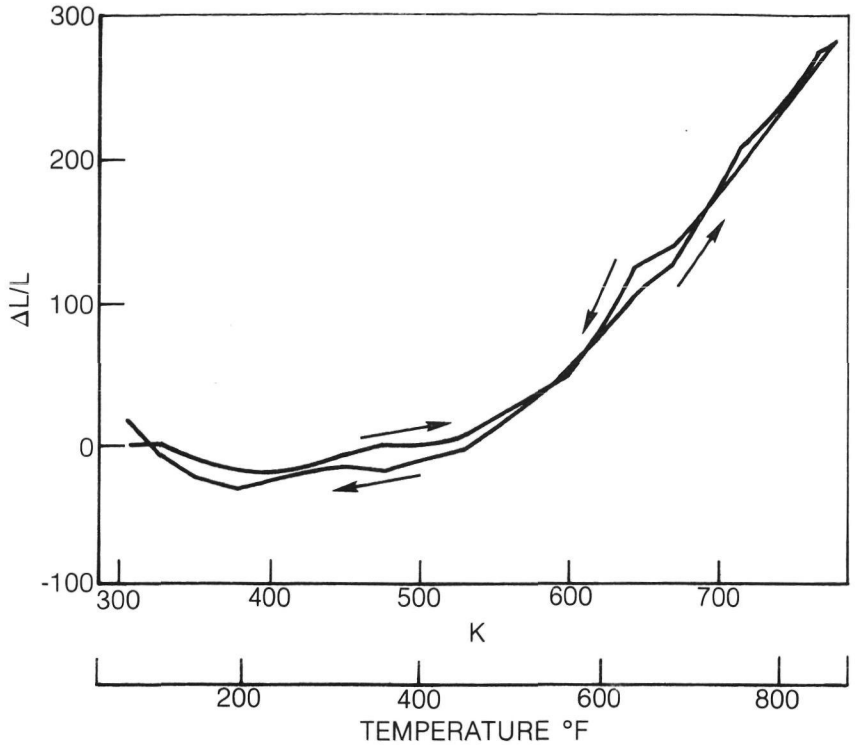

Fig. 92. Axial Thermal Expansion of Unidirectionally Reinforced HMS/MAS (Heat Treated) (GC959)

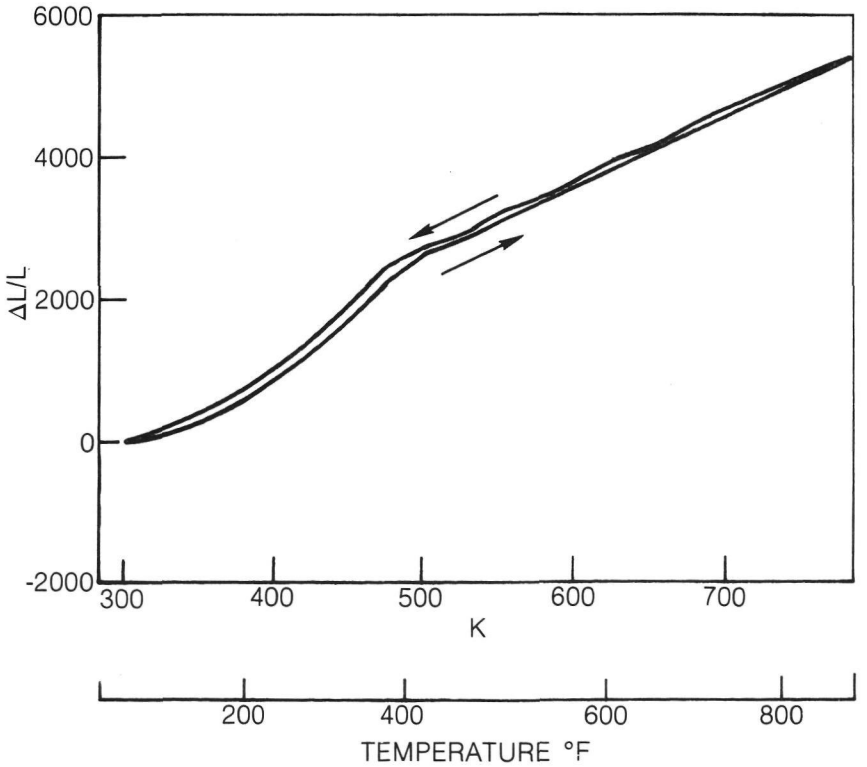

Fig. 93. Transverse Thermal Expansion of Unidirectionally Reinforced HMS/MAS (Heat Treated) (GC959)

81–2–100–12

V. SUMMARY AND CONCLUSIONS

The herein described program has demonstrated the exceptional potential of graphite fiber reinforced glass matrix composites for structural and nonstructural applications. Combinations of properties have been achieved which are superior to other fiber reinforced composite systems. Low density, high strength, high stiffness, dimensional stability and retention of performance up to high temperatures have all been achieved in a manner not possible in resin or metal matrix composite technology. The following points summarize some of the more important accomplishments of the program.

- A broad group of fibers and matrices have been combined to create a wide range of composite properties. Fibers with elastic moduli ranging from 234 GPa to 654 GPa have all been used successfully along with matrices including several glasses and a glass ceramic.

- Composite fabrication procedures have been developed which readily permit the fabrication of flat plate and shaped composites without the need for elaborate equipment.

- Limited secondary forming and joining procedures were developed to demonstrate the fabrication of structural shapes.

- Composite mechanical properties were measured under a wide range of test conditions. Tensile, flexure mechanical fatigue, thermal fatigue, fracture toughness, and fatigue crack growth resistance were all evaluated.

- A modified borosilicate glass was shown to be the best matrix for composites whose intended use temperatures are below 800 K. This matrix is compatible with a wide variety of graphite fibers and does not soften significantly below this temperature. At higher temperatures the limiting factor in composite performance was shown to be the oxidation of the graphite fibers.

- Inert atmosphere testing conducted at higher temperatures demonstrated that a 96% silica glass and an MAS glass ceramic could both be used as matrices to achieve composites which retained their properties up to 1300 K.

- Composite thermal dimensional stability was measured and found to be excellent. Composite thermal expansion behavior was primarily controlled by the fiber type used and then, secondly, by the matrix used. Values of composites coefficient of thermal expansion (CTE) as low as 1×10^{-7} K^{-1} were measured at 300 K. At higher temperatures CTE values of zero were also obtained due to the unique shape of the thermal expansion curves.

The above characteristics should make graphite fiber reinforced glass a candidate for space structure applications which require the combination of environmental and dimensional stability not available in other materials.

REFERENCES

1. Sambell, R. A. J., D. H. Bowen, D. C. Phillips: Carbon Fibre Composites with Ceramic and Glass Matrices, Part, I, Discontinuous Fibres Journal of Materials Science, 7 (1972) pp 663-675.

2. Sambell, R. A. J., A. Briggs, D. C. Phillips, and D. H. Bowen: Carbon Fibre Composites with Ceramic and Glass Matrices, Part II, Continuous Fibres Journal of Materials Science, 7 (1972) pp 676-681.

3. Phillips, D. C., R. A. J. Sambell, D. H. Bowen: The Mechanical Properties of Carbon Fibre Reinforced Pyrex Glass, Journal of Materials Science, 7 (1972) pp 1454-1464.

4. Levitt, S. R.: High Strength Graphite Fibre/Lithium Aluminosilicate Composites, Journal of Materials Science 8 (1973) pp 793-806.

5. Bacon, J. F., K. M. Prewo: Research on Graphite Reinforced Glass Matrix Composites, NASA Contract Report 145245, June 1977.

6. Bacon, J. F., K. M. Prewo and E. R. Thompson: Research on Graphite Reinforced Glass Matrix Composites, NASA Contract Report 158946, June 1978.

7. Prewo, K. M. and E. R. Thompson: Research Services on Graphite Reinforced Glass Matrix Composites, NASA Contract Report 159312, February 1980.

8. Prewo, K. M. and J. F. Bacon: Glass Matrix Composites-I - Graphite Fiber Reinforced Glass, Proc. of the 1978 International Conference on Composite Materials, AIME, 1978,

9. Prewo, K. M., J. F. Bacon and D. L. Dicus: Graphite Fiber Reinforced Glass Matrix Composites, SAMPE Quarterly, Vol. 10, No. 4, July 1979.

10. Brown, W. F. and J. E. Srawley: Plane Strain Crack Toughness Testing of High Strength Metallic Materials, ASTM-STP 410, 1966, p 13.

11. Konish, H. and T. Cruse: Experimental Investigation of Fracture in Advanced Fiber Composites, J. Comp. Materials, Vol. 6, (1972) p 114.

12. Damage Tolerant Design Handbook MCIC-HB-01.

13. Larsen, D. C.: Property Screening and Evaluation of Ceramic Turbine Engine Materials, AFML-TR-79-4188, Oct. 1979.

14. Satellite Applications of Metal Matrix Composites, Interim Tech. Report LMSC-DG21612, May 1978, Contract F33615-77-C-5190.

15. Brennan, J. J.: SiC Fiber Reinforced Glass Matrix Composites, ONR Contract N00014-78-C-0503.